Thermal Modeling and System Identification of In-Situ, Through-Ventilated, Industrial DC Machines

THERMAL MODELING AND SYSTEM IDENTIFICATION OF IN-SITU, THROUGH-VENTILATED, INDUSTRIAL DC MACHINES

BY

ISAAC M. JACKIW, B.Eng.

A THESIS

SUBMITTED TO THE DEPARTMENT OF MECHANICAL ENGINEERING

AND THE SCHOOL OF GRADUATE STUDIES

OF MCMASTER UNIVERSITY

IN PARTIAL FULFILLMENT OF THE REQUIREMENTS

FOR THE DEGREE OF

MASTER OF APPLIED SCIENCE

Master of Applied Science (2018) McMaster University

(Mechanical Engineering) Hamilton, Ontario, Canada

TITLE:	Thermal Modeling and System Identification of In-Situ, Through-Ventilated, Industrial DC Machines
AUTHOR:	Isaac M. Jackiw B.Eng., (Mechanical Engineering) McMaster University, Hamilton, Canada
SUPERVISOR:	Dr. James S. Cotton
NUMBER OF PAGES:	xxi, 127

For Kevin

Abstract

Concerns of the impact of greenhouse gasses (GHG) are leading heavy industry users to explore energy reduction strategies such as the conservation of electricity use in ventilated machines by the use of variable-cooling systems. For these strategies to be implemented, a thermal model of the system is required. This study focuses on the thermal modelling of through-ventilated, industrial, electric machines that employ a variable-cooling strategy, using only on-line data collected during regular machine operation. Two empirical thermal models were developed: a first-order model, and a second-order model which was extended from the first-order based on its performance.

By means of an energy-balance, the first-order model was able to define an estimation of the motor temperature based on only a single variable, and thus was able to be fit directly to complete process-cycle data to determine the parameter. Over the 18 process-cycle samples, this parameter was found to vary by as much as $\pm 10\%$, therefore, when a generalized model was proposed using the median value of the parameter, the maximum error seen over the process cycles was 9.0 $^{\circ}C$, with a maximum average error over a process-cycle of 4.2 $^{\circ}C$. An effort was made to determine the effects of reduced cooling on the model by performing reduced-cooling experiments during machine cool-downs, however the thermal-time constant, which directly relates the heat-transfer rate to the system capacitance, was found to vary by as much as 47%, suggesting that the system's capacitance was changing, and that the

first-order model was not accurate enough to distil these effects. A key obervation of the performance of the first-order model was that in heating it would under-predict the machine temperature, and in cooling would over-predict, suggesting that an additional heat-transfer path existed to the cooling air through some additional thermal capacitance.

In an effort to include higher-order effects so that reduced-cooling effects could be established, a second-order model was developed by adding an additional lumped-node to the system, introducing the supposed additional conduction/capacitive path, where the heat-generating node was considered analogous to the motor's armature, and the additional node was considered as a thermal-sink. This model was then numerically fit to the cool-down data for both maximum and reduced flow-rate cases in order to identify the system's main heat transfer parameters, however, once again, a large variance in the parameters was found. Through model simulation, this was determined to be the result of the system not starting at a steady-state temperature distribution, which resulted in the parameter estimation under-predicting the true values. As such, the upper-limits of the parameter spreads were used to identify the model. Assuming the system's heat generation was due to Joule-losses only, the second-order model was found to perform marginally better than the first-order model, with a maximum error of 8.6 $^{\circ}C$, and a maximum average error of 3.3 $^{\circ}C$ over the process-cycles. Though the second-order model typically performed better than the first-order model in cooling, it was found that the model would vary between over-predicting and under-predicting the machine temperature, indicating that additional and higher-order core losses may play a role in the heating of the machine.

Although the first-order model was found to be slightly less-accurate than that of the second-order, the first-order model has a much simpler and far less intrusive identification scheme than that of the second-order model with a relatively low loss in

accuracy. As a result, it would be possible to to use the first-order model for on-line temperature monitoring of the machine by performing tests during operation where the cooling rate is reduced to identify the change in the model parameter. However a sufficient factor of safety ($\approx$10 $^{\circ}C$) would be required to account for the under-estimation that occurs in heating. For the second-order model to be implemented, more controlled testing is required in order to properly discern the effects of reduced cooling from the effects of the initial temperature distribution. Additionally, the inclusion of core-losses in the machine heat generation term should be investigated to improve model performance.

Acknowledgements

Firstly, I would like to extend my gratitude to my supervisor, Dr. James Cotton, for providing the opportunity of this experience.

To (soon-to-be Dr.) Sarah Nangle-Smith (A.K.A. "Nangles"), for her persistent pushing to make me a better academic and person.

To Dr. Vick Lackhian, for helping me develop my Python code, despite not really getting anything out of it, and to the rest of the TMRL team, for providing the requisite technical, social, and emotional support.

A big thank you is owed to (future Dr.) Elizabeth Rowan, whose guidance at the end of this project helped me understand the field on a much deeper level.

To my other friends and family, for their support, motivation, and patience. I'm sure you all think I'm crazy for doing this all over again for a Ph.D.

To Fairweather Brewery, without whom this past year would have been un-hopped.

This work was made possible thanks to our industry sponsor, Arcelormittal Dofasco (AMD), with out whom this project would not have come to fruition, and to the Ontario Centres of Excellence (OCE) for providing additional project funding.

A special thank you to Kevin Hunt, the industry contact at AMD, for helping me get all of the data, for escorting me through the plant, and for the countless iced-teas.

Nomenclature

Acronyms

AC Alternating (electrical) Current

AMD ArcelorMittal Dofasco

CFD Computational Fluid Dynamics

CPI Consumer Price Index

DC Direct (electrical) Current

EMF Electro-Magnetic Frequency

FEM Finite-Element Modelling

FFT Fast-Fourier Transform

FTHME Rockwell FactoryTalk Historian ME

GHG Greenhouse Gas

HTC Heat Transfer Conductance

IR Infrared Radiation

NEMA National Electrical Manufacturers Association

RTD Resistance Temperature Detector

TCU Thermal Capacity Used

TMEIC Toshiba Mitsubishi-Electric Industrial Systems Corporation

VFD Variable Frequency Drive

VSD Variable Speed Drive

Symbols

$\dot{m}$ Mass flow rate $[kg/s]$

$\dot{Q}$ Heat flow rate $[W]$

$\dot{q}$ Heat per unit area $[W/m^2]$

ϵ Surface emissivity

γ thermal saturation parameter

$\hat{T}$ Estimated temperature $[^\circ C]$

σ Stefan-Boltzmann constant, 5.67x10^{-8} $[W/m^2.K^4]$

τ Time-constant $[s]$

A Area $[m^2]$

Bi Biot Number $Bi = \frac{L_C k}{h}$, $L_C = \frac{V}{A}$

C Thermal Capacitance $[J/K]$

c Specific heat capacity $[J/kg.K]$

F View-factor between radiating bodies

h Specific enthalpy $[J/kg.K]$

I Current $[A]$

k Thermal conductivity $[W/m.K]$

L Length $[m]$

N Sample size

p Pressure $[kPa]$

Q Heat energy $[J]$

R Resistance $[\Omega]$

RH Relative Humidity

T Temperature $[^{\circ}C]$

t Time

U Heat transfer coefficient $[W/m^2.K]$

UA Heat transfer conductance $[W/K]$

V Air-flow velocity $[m/s]$

Subscripts

Air Air

Air, Ave Average between inlet and outlet air

Arm Armature

C Characteristic Length

$Cond$	Conduction
$Conv$	Convection
E	Electric
f	Final
i	Initial
in	Inlet
J	Joule
M	Motor/machine aggregate
out	Outlet
p	Constant pressure
Rad	Radiation
$Sink$	Thermal Sink
SS	Steady state
Th	Thermal
Tot	Total or overall machine/motor

Contents

List of Figures

Chapter 1

Introduction

In recent years, increasing concerns about the impact of greenhouse gases (GHG) on climate change have led to substantial efforts to curtail worldwide GHG emissions. In an effort to incentivize innovation in the reduction of GHG emissions, especially those pertaining to carbon (carbon-dioxide) emissions, governments have begun employing carbon-pricing systems wherein an additional tax is imposed upon the emitters of GHGs (1). Since in many regions electricity generation is often tied directly to carbon-emitting fuels such as coal or natural gas, carbon-pricing initiatives have led to increased costs of electricity for residential, commercial, and industrial consumers. Additionally, efforts to reduce carbon emissions in the electricity sector such as the commissioning of new infrastructure have resulted in high electricity costs in regions such as Ontario and are only expected to increase due to carbon pricing (2). Figure 1.1 shows how electricity costs in Ontario have increased over the past 30 years by comparing the consumer price index (CPI) of electricity to that of all items. From the dramatic increase in the CPI of electricity as compared to other commodities in the past decade, it is clear that electricity has become much less affordable.

Today, the combination of the social push for reduced carbon emissions and the

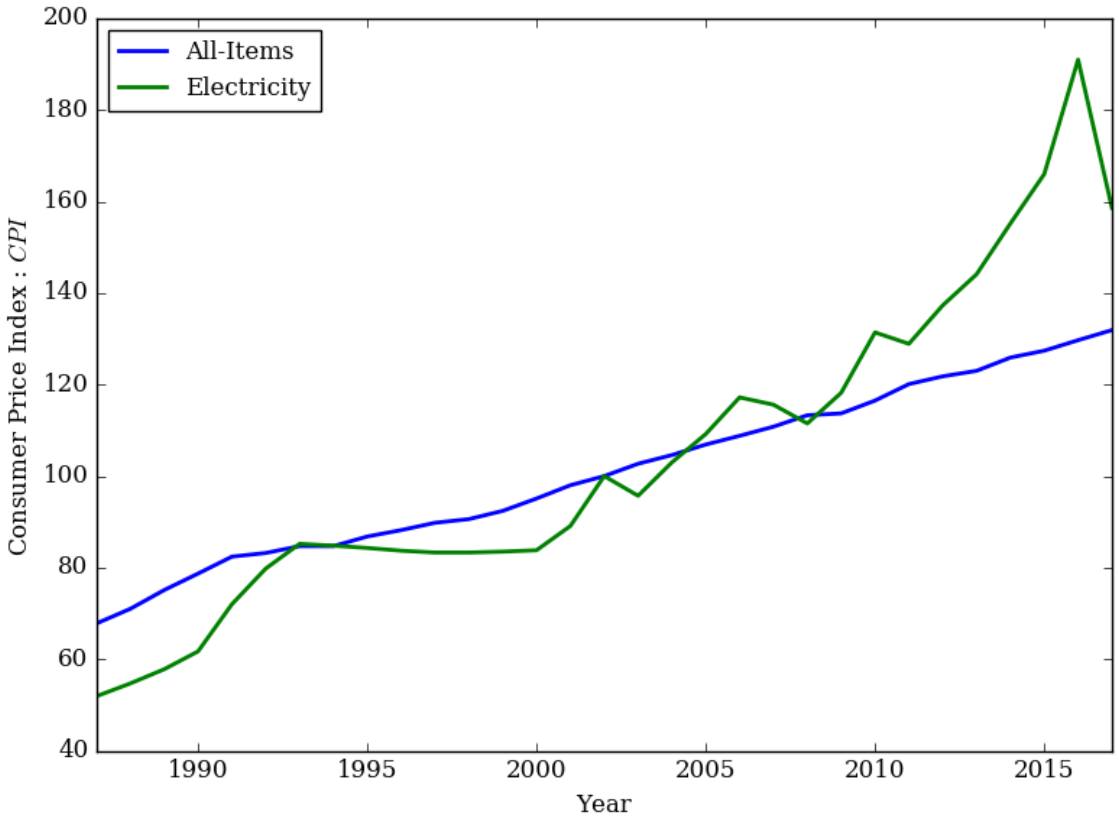

Figure 1.1: Consumer Price Index (CPI) of Electricity and All-Items in Ontario, 1987-2017 (3)

increased costs of electricity has allowed for an economic climate in which conservation initiatives may be highly profitable, and thus many industries are seeking out methods to reduce their electricity consumption (4). In a 2003 study performed by Almeida et al, motor systems were found to be responsible for 69% of the electricity consumed by industrial activities in Europe (5). Of these motors, 16% were found to be used in the driving of fans used for cooling and ventilation, and since the required power of the centrifugal fans typically used in these applications is approximately proportional to the cube of the air flow-rate through the fan, small reduction in air flow rate will correlate to large reductions in fan motor power consumption (5). The study also identified that the second largest electricity consumption related to motors in the

steel sector is the use of cooling and ventilation fans.

One of the largest applications of cooling fans in steel-mills is for the cooling of rolling-mill drive motors (6). The cooling of these motors provides great opportunity for energy reduction, as the cooling fans are typically run continuously at their maximum speeds, regardless of the motors loading (6). Furthermore, since the motors which drive the fans are typically relatively large motors themselves, (>75 HP) their efficiency remains nearly constant at reduced loads, therefore reducing the fan speed/load would not significantly reduce the motor's efficiency, as would be seen in smaller applications (7). Such cooling systems would be able to employ a variable frequency drive (VFD) or a variable speed drive (VSD) on the cooling fan of the drive motor, as per Figure 1.2 (6). This application would require the measurement of the machine temperature in order to inform the VFD/VSD control system of the cooling load required by the machine during its operation. Work done by Toshiba Mitsubishi-Electric Industrial Systems Corporation (TMEIC) found that using a VSD/VFD control in a steel mill consisting of six motors for a finishing mill and five motors on a roughing mill, energy savings of 7760 MWh/yr could be achieved (6). This is equivalent to the energy consumption of roughly 860 Ontario homes (8).

1.1 Motivation

In this thesis, the application of a variable-speed cooling system for the drive motors used by the industrial sponsor, ArcelorMittal Dofasco, (AMD) will be studied. Additional cooling opportunities exist for the mill motors at AMD as the company implements flexible manufacturing processes in an effort to meet the demands of Industry 4.0 (9). This results in highly dynamic loading of their steel mill as a large

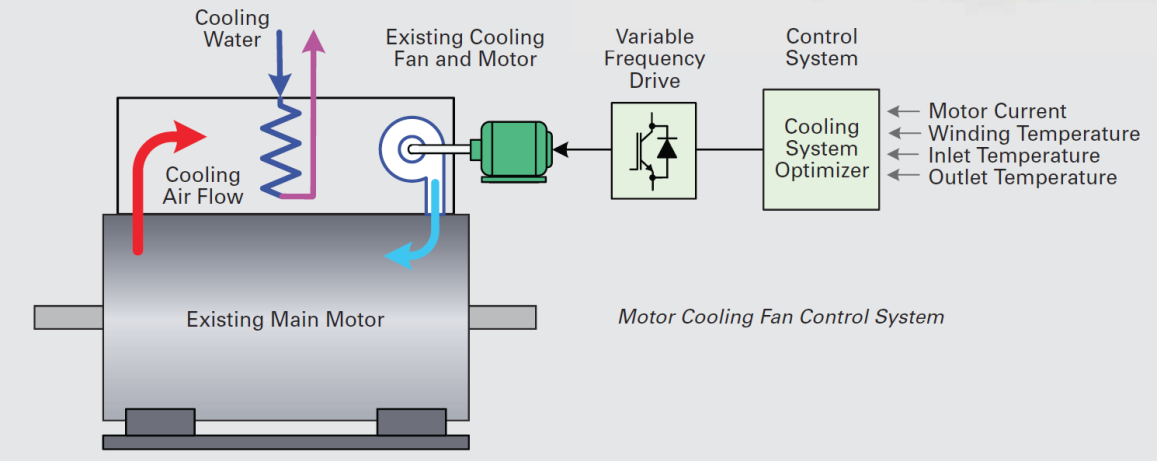

Figure 1.2: Schematic of a control system applied to the cooling loop of a motor used to drive a steel mill (6)

variation of products are manufactured, and thus varied cooling will be often applicable.

In a preliminary study by carried out by an automation vendor commissioned by AMD, it was identified that the fans used to provide cooling ventilation to the large electric motors used in the finishing area of the Hamilton hot-mill could be reduced by up to 20% for 75% of the year, leading to a potential savings equal to 15% of the associated annual energy bill. While the actual energy use and pricing of the partnered company is confidential and will not be published in this work, it is reasonable to expect significant savings, as the scale of the energy used by the cooling loops at the company are large and the systems are operated continuously through the year.

The application of a VSD control system for the thermal control of any system requires the measurement of the systems critical temperature. In DC machines, such as the mill drive motors, the critical temperatures within the machine are the temperature of the armature winding insulation, and the temperature of the stator magnets, or in the case of stator electromagnets, the stator winding insulation (10). For the

direct temperature measurement of these components, thermal sensors such as thermocouples have been implemented in the machines, including the armature windings which introduce the additional complication of having to transmit the sensor reading from a rotating, internal machine component.

If a reliable, on-line reading from these thermocouples could be obtained from outside the machine, then the fan control scheme for the temperature control of the armature would be relatively simple applying a fan curve that prescribes a certain air-flow-rate at a certain armature temperature. However, this data is not easily transmitted from inside the machine. Possible methods of on-line data acquisition include slip rings and radio transmitters. The retrofitting of these transmitters to in-situ machines is very costly, and the addition of extra components can interrupt the existing cooling air-flow behaviour, potentially reducing the effectiveness of the cooling. ArcelorMittal Dofasco implements an Accumetrics Telemetry system on the roughing mill at the facility, however these systems cost approximately $250 000/system, and have been found to be prone to failure and noise. Additionally, the radio transmitter equipment disrupts the flow path of the cooling air inside the motors.

In light of this, it was concluded that a real-time reading of the motor temperatures was not fiscally viable, and it is required that a thermal model of the motor, which can accept a continuous input of the motors current as well as the inlet and outlet cooling air temperatures, be developed for this application.

1.2 Objectives

The objective of this thesis is to develop a transient thermal model of through-ventilated DC machines. The model will be developed based on the first-order thermal

model typically used in industry for the thermal modelling of electric motors, and efforts will be made to improve the accuracy of this method in transient operation by extending the model to a second-order to include the effects of a more distributed system. Data collected from in-situ, DC electric motors used in a steel finishing mill by the partnered company, ArcelorMittal Dofasco, will be used to characterize and validate the model. Additionally, a methodology will be presented for the on-line characterization of the model for both standard operation and operation at reduced cooling air flow rates to allow the model to perform with controlled cooling for the purposes of energy consumption reduction.

1.3 Scope of Work

The model is expected to be used to provide a control temperature of large, through-ventilated electric machines given only on-line data collected from the cooling air, though real temperature data of the critical components will be required for the model identification. This control temperature, as well as the model, is required to develop a control scheme for the cooling of the machines so that only the required cooling may be applied. The outcome of such a control scheme would be increased energy savings via the reduction of the use of the cooling fan motors.

Chapter 2

Background and Literature Review

This chapter outlines the basic understanding of DC machines that is required for their thermal analysis. The standard temperature monitoring methods for DC machines will be discussed, and the applicable method, thermal modelling, will be reviewed in detail. Within this review, the fundamental principles of heat generation and transmission in DC machines will be discussed, as well as both the numerical and analytical modelling methods. These methods, as well as the additional approaches of analysis, will be discussed in the context of their applicability to the current work: the on-line thermal modelling of in-situ, industrial DC machines.

2.1 DC Machine Fundamentals

In general, all DC machines exhibit the same thermal behaviour: heat is generated primarily in the windings, with some excess generation occurring in the magnets and supporting structures, and is transmitted through the other motor components by conduction, convection, or radiation. The fundamental difference between the thermal behaviour of AC and DC machines is the current density and frequency,

which affects the current flow behaviour and thus the heat generation, although the heat generation mechanisms are ostensibly the same. Additionally, from a thermal perspective, electric motors and generators exhibit the same heat generation and transmission mechanisms.

In its most basic form, a DC machine consists of two components; one which is stationary, and one which rotates. The stationary component is termed the stator, while the rotating component is termed either as the armature (DC) or rotor (AC), which for this work will be considered interchangeable. Depending on the type of machine, one of these components will have permanent magnets, while the other has windings through which a controlled current flows, and thus creates a magnetic field which interacts with the magnetic field of the permanent magnets to generate torque. Insulation exists between winding loops in the machine to electrically isolate them from each other and the surrounding components. These components must be supported by a structure, typically composed of steel, which will function as a heat sink for the heat generating components which they support. The stator and armature windings are where most of the heat is generated, thus it is necessary to monitor their temperatures in order to provide thermal protection to the machine. Multiple methods of cooling are used for DC machines, including natural or forced external ventilation of the machines casing using a cooling fluid, forced internal convection through the machine using air, (typically termed blow-through) and forced internal convection of machine components using a fluid flowing through cooling channels in the machine (11).

The primary mode of thermal failure in the armature or stator of a DC machine is the failure of the insulation. The National Electrical Manufacturers Association (NEMA) provides standardized insulation class ratings based on the temperature for which the insulation is rated, i.e. the temperature under which no reduction in the

expected lifetime of the insulation will occur. If the rated temperature of the insulation is exceeded, the expected lifetime of the insulation dramatically decreases. When the insulation fails, short-circuiting between adjacent winding loops will occur, leading to a sudden decrease in the resistance between the loops which will cause the winding current to rapidly increase, further increasing the heat generation in the windings until they fail completely by melting (10). Figure 2.1 shows the expected insulation lifetime versus operation temperature for various NEMA classes of insulation. Under the rated temperature of the insulation, the expected lifetime is 100% of the nominal expected lifetime. Past the rated temperature, the expected lifetime of the insulation drops exponentially.

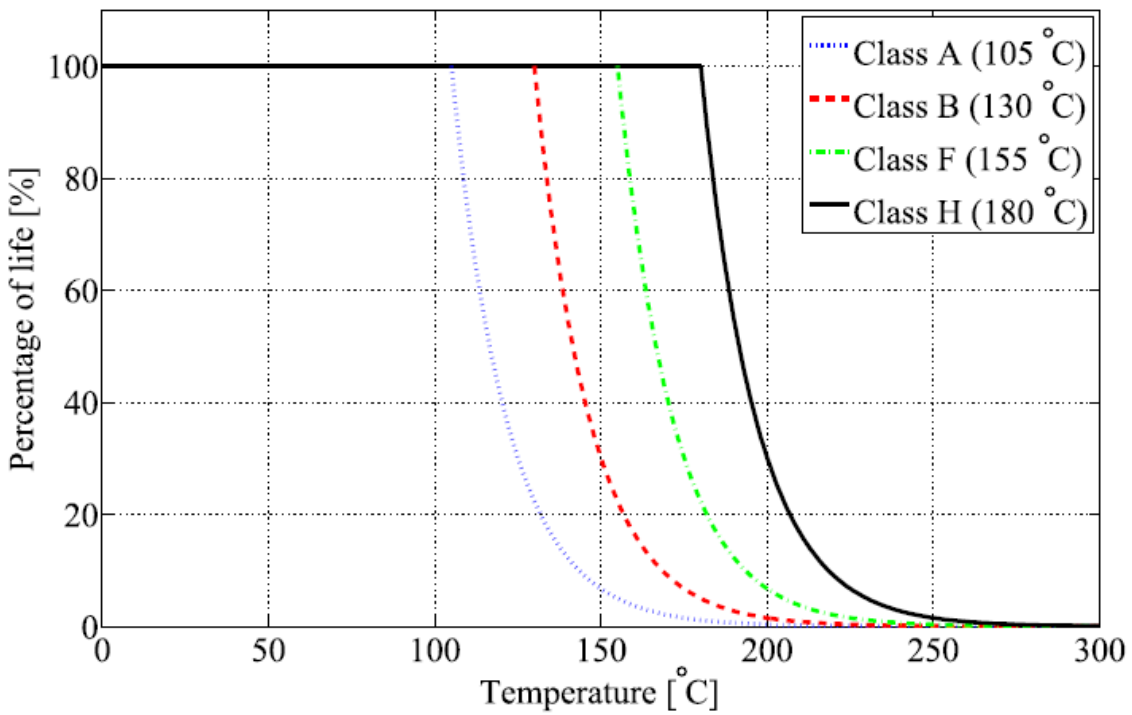

Figure 2.1: Motor winding insulation life for NEMA class insulation (12)

2.2 Motor Temperature Monitoring

In cases where the cooling of DC machines needs to be controlled, it is imperative that the relevant control temperatures be known or estimated. DC machines have two components where most of the heat is generated; the armature/rotor and the stator. It is generally understood that the armature is most susceptible to overheating in machine stall, while the stator is most susceptible during machine operation, (13) therefore it is typically preferred that both armature and stator temperatures be measured.

The difficult aspects of component temperature measurement are the presence of local "hot-spots", the presence of large amounts of electro-magnetic-frequency (EMF) noise and interference, and the installation of invasive probes in rotating components. Hot-spots occur where the local heat removal is low and/or the local heat generation is high due to anisotropies in materials or non-uniformity in machine design, leading to localized regions where the temperature may spike. Since the thermal protection of the machines is dependent on the highest temperature in the machine, these hot-spots are the critical points within the machine. As hot-spot locations are difficult to predict, it is infeasible to measure the hot-spot of the machine, thus it must always be considered that any measurement of the machines temperature may underestimate the actual critical temperature (14).

The most direct method of machine temperature monitoring is the use of sensors, such as thermocouples, thermistors, resistance temperature detectors (RTDs), and infrared (IR) sensors. For the fixed, external components of the machine, these methods are typically as accurate as the measurement device implemented, given that a good contact is made between the sensor and the component. However, for the rotating components in the machine, the on-line transmission of the readings can

be problematic. The transmission of these readings is either by use of slip-rings or radio-transmission. The retrofitting of these transmitters to in-situ machines is often very costly, and the addition of extra components can interrupt the existing cooling air-flow behaviour, potentially reducing the effectiveness of the cooling.

Alternatively, electrical temperature modelling methods, as used in (13; 15), use the machines windings as a RTD, which requires the determination of the resistance and the thermal coefficient of resistance of the windings of the specific machine in order to estimate the temperature of the machine from the resistance through the windings. This requires the accurate measurement of the winding resistance at multiple winding temperatures, which is often performed by applying a DC voltage through the windings, allowing them to heat up to the desired temperature.

The final method used for the temperature modelling of DC machines is thermal modelling, which is the approach investigated in the current work. Thermal modelling involves the development of a model of the heat generation and transfer in the machine, such that the temperature of the machine may be calculated based on the integration of the input current and the heat transferred through the machine to the cooling media. Thermal modelling is often used in motor temperature monitoring, as it can be used as a predictive method, in addition to the on-line monitoring of the machine. Furthermore, it can be used to better understand how the machine may react to varying conditions, such as changes to the cooling. Though thermal modelling is often used in the design process of modern machines, the motors examined in this work were commissioned before a thorough understanding of motor thermal modelling was developed, and as such no basis for the model exists from the manufacturer.

2.3 Motor Thermal Modelling

In the literature, there are three approaches to the thermal modelling of DC machines; numerical, semi-empirical, and analytical. Though there are differences in these methods, the considered heat transfer phenomena are the same.

2.3.1 Modeled Phenomena

2.3.1.1 Heat Generation

The least well-understood factors in the thermal modelling of DC machines is the heat generation within the machine due to electro-mechanical losses. In general, the current understanding of DC machine losses can be considered as four main components: (16)

1. Copper losses
2. Hysteresis losses
3. Eddy current losses
4. Stray losses

Copper losses are the most well-understood of these components, where heat is generated due to Joule-heating, $\dot{Q}_J$, as a result of a current, I, flowing through the conductive media with some electrical resistance, R_E, which may vary with temperature (Eq. 2.1).

$$\dot{Q}_J = I^2 R_E(T) \tag{2.1}$$

Hysteresis losses occur primarily in the ferromagnetic components of the machine due to the energy required to repeatedly switch the polarity of the magnetic domains

within the material. Since the rate of hysteresis loss is a function of how frequently the polarization of the domains are switched, it is directly proportional to the phase frequency of the windings, which is considered directly proportional to machine rotational speed. Eddy current losses occur as the electrically conductive material moves through a magnetic field. As this occurs, the magnetic flux through the material at any given point is changing, and due to Faradays law of induction, eddy currents are produced in the material. As these eddy currents are flowing through a resistive material, heat will be generated due to Joule heating, as in the copper losses. Eddy current are proportional to the square of the phase frequency, and thus the machine rotational speed.

The hysteresis and eddy current losses are often grouped under the term, core-losses or iron-losses, as they typically relate to the losses due to the electromagnetic behaviours in the iron cores of the machines. At high frequencies, additional effects may begin to take place and may affect both the copper and eddy current losses. As the core losses are a function of the motor speed, they are typically only dominant in highspeed machine operation.

Stray losses are those not accounted for in the previous three components and are often neglected.

Figure 2.2 shows a loss distribution diagram typical of DC machines, outlining the copper and core loss terms for both the stator and armature, (rotor) as well as the stray and mechanical losses which do not significantly contribute to the heat generated in the machine.

The standard methods for determining these losses are outlined in IEEE standard 112 (17). These methods use resistance measurements to determine the copper losses of the machine. The other machine losses, both those that generate heat and those that do not, are determined based on the relationship between the total input electrical

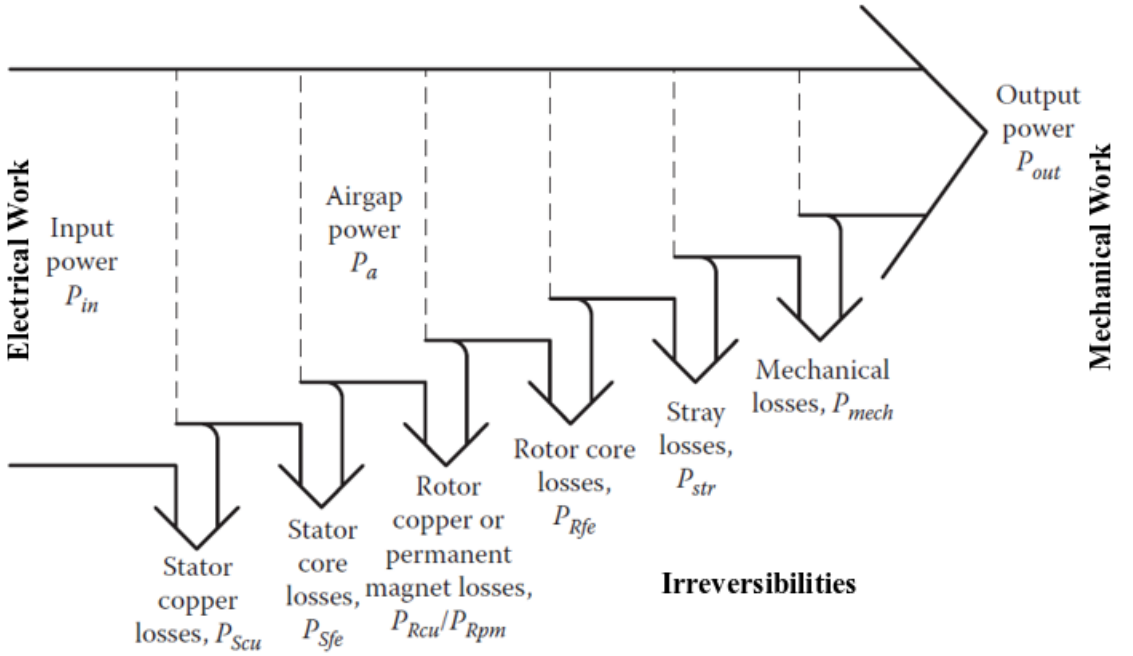

Figure 2.2: Loss-diagram of the losses in a DC motor, adapted from Emadi (16)

power, the measured mechanical power, and the predicted copper losses of the machine at various test conditions; both load and no-load motor operation at multiple motor speeds so that the motor-speed effects on losses such as core-losses may be included.

2.3.1.2 Heat Transmission

The thermal modelling of DC machines considers three modes of heat transmission:

1. Conduction through/between solid bodies
2. Convection to/from a fluid
3. Radiation between solid bodies

Heat transfer by conduction is given by:

$$\dot{q}_{Cond} = \frac{kA}{L}\Delta T \tag{2.2}$$

where k is the material conductivity, A is the flux area, L is the length over which the heat is conducted, and ΔT is the temperature difference over which the heat is transferred. In DC machines, conduction occurs through the components, such as through the winding copper, winding insulation, and core steel of both the stator and the armature.

Heat transfer by convection is given by:

$$\dot{q}_{Conv} = U_{Conv} A \Delta T \tag{2.3}$$

where U_{Conv} is the convective heat transfer coefficient, A is the heat flux area of the body exposed to the cooling fluid, and ΔT is the temperature difference between the body and the fluid. Both natural and forced convection are considered in much of the literature, where appropriate correlations for U_{Conv} are used. The correlations for the convective heat transfer coefficient are typically dependent on the body geometry, fluid properties,(viscosity and thermal conductivity) and the flow speed. For externally ventilated machines, forced convection occurs only on the exterior motor casing, whereas for blow-through machines, forced convection may occur on all components that are visible to the cooling air.

In most analyses, the conduction and convection heat transfer equations are written in terms of an equivalent resistance, R_{Th}, or overall heat transfer conductance, $UA = 1/R_{Th}$.

$$\dot{q} = UA\Delta T, \qquad UA_{Cond} = \frac{k}{L}A, \qquad UA_{Conv} = h_{Conv}A \tag{2.4}$$

These types of generalized heat transfer conductance are also used to describe the contact resistances between components, where the conduction from one body to

the next will depend upon how well the two bodies are in contact, such as bolted connections between supporting components.

Heat transfer by radiation for a grey body is given by:

$$\dot{q}_{Rad} = \epsilon \sigma F A (T^4 - T_\infty^4) \tag{2.5}$$

where ϵ is the surface emissivity, σ is the Stefan-Boltzmann constant, F is the view-factor between bodies, A is the heat flux area, T is the temperature of the body from which heat is being radiated, and T_∞ is the temperature of the body to which heat is being radiated. Since the machine windings are where most of the heat is generated, and thus will be the hottest components, radiation is most likely to be dominant in these components. In some early works, an attempt is made to account for radiation by applying correction factors to the convective components, while more recent approaches include it explicitly. Though sometimes considered as a significant mode of heat transmission, especially for motors cooled by natural convection, many works neglect it due to the added complexity where the non-linearity and complex view-factors within machines are concerned. Some researchers argue that radiation may be neglected due to the relatively low temperatures, the low emissivity of the metals used in the machines (copper and iron), and due to the low view-factors between most of the components (i.e. the components that are the hottest, the copper windings, have dominant view factors to their neighbouring windings, thus the bulk winding component radiates to itself (18)).

2.3.2 Thermal Modelling Methods

2.3.2.1 Numerical Modelling Methods

The numerical modelling methods used in this field include both finite-element (FEM) and computational fluid dynamics (CFD). In most early FEM, such as in (19), heat flow by conduction is solved through the solid bodies, where the boundary conditions are given by the convective heat transfer correlations. Other attempts use CFD to solve for the flow behaviour around the bodies, which is coupled to the FEM solutions to the conduction problem (20; 21; 22). The results produced by the numerical methods are highly dependent on accurate body geometries and correlations or turbulence model employed, as well as the assumptions that consider where and how the heat is generated. Additionally, these methods are very computationally expensive. Because of this, numerical modelling methods are unsuitable for the on-line measurement or control of DC machine heat transfer, nor is it suitable for applications where the machine geometry and flow behaviour is not extremely well-defined (23). Since these methods are typically only employed to gain a better understanding of how changes to machine design will affect its thermal performance, the estimation errors of the models are seldom discussed. In the work of Rajagopal et al, (19) the errors of the model varied depending on the component modeled, where for some components errors were as low as 2 $^{\circ}C$, while for others it was as high as 10 $^{\circ}C$. Numerical methods are therefore typically used in machine design as a way to predict how the machine will behave, or to model particular local behaviours in order to develop analytical models of individual components that may be solved less expensively.

2.3.2.2 Semi-Empirical Modelling Methods

The first-order model, or fully-lumped model, is the simplest model that may be applied to DC machine thermal systems, wherein only a single, homogeneous body or point-source is considered with a single external heat transfer coefficient, and a single thermal capacitance that exists at a uniform temperature. The thermal characteristics of this type of model are well-defined by the thermal time-constant, τ, which can be determined experimentally. Though first-order modelling of electric machines is not prolific in the literature and is widely considered as an inaccurate modelling technique for most machine protection applications, the first-order model is often the standard for electric machine thermal modelling in industry due to its simplicity (11). In these methods, the system time-constant is typically found by using cooling data in conjunction with the time-constant definition: the time required for the body to reach 36.8% of its initial temperature in cooling. Figure 2.3 shows how the thermal time-constant is found based on this definition for four different lumped-body time-constants.

There is limited literature that is based on the first-order model, possibly due to unpublished research done in industry. The literature that is availble focuses on the identification of the machines time-constant. Noodleman (25) considered the armature windings as the critical component to be modelled. It was shown that the two relevant model parameters, a time constant and a derating constant which accounts for variations in the heat generation, could be found by performing step-tests based on the motors duty cycle, where the time constant may be alternatively taken as the time required for the body to reach 63.2% of its initial temperature difference in heating. Pawlis et al (12; 26) performed the same analysis, however instead of calculating the time-constant based on its definition, the first order model

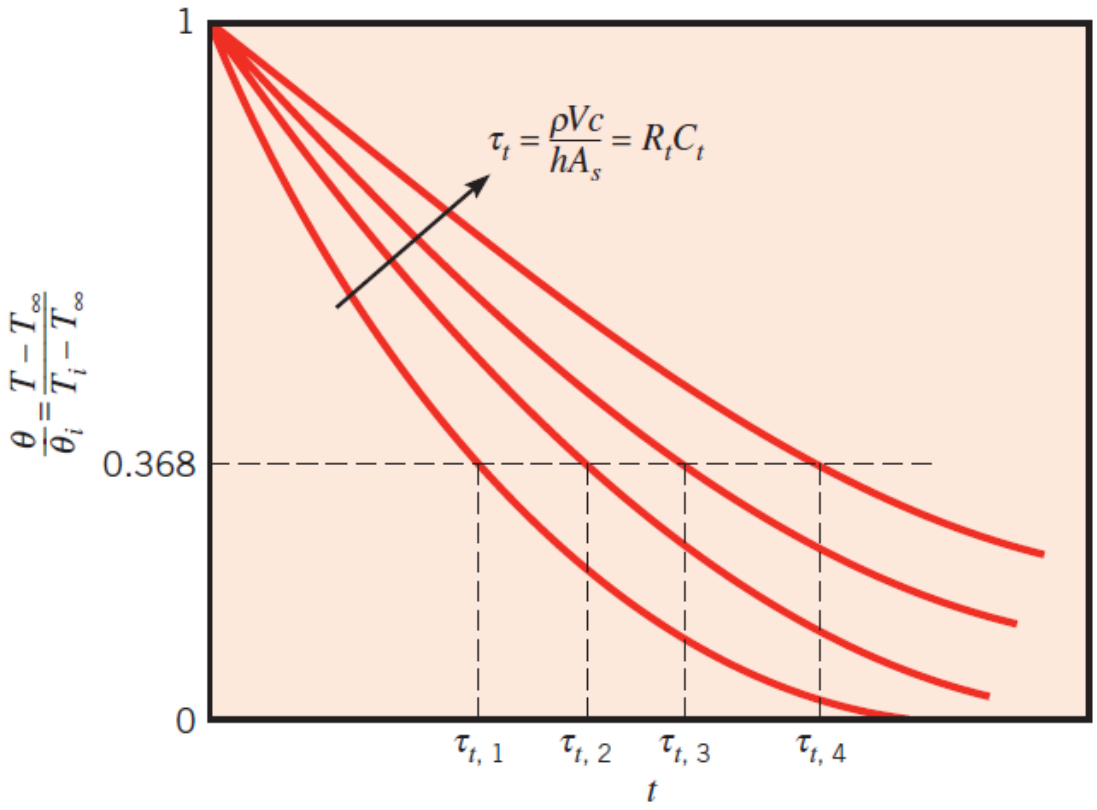

Figure 2.3: Plot of exponential decay showing the definition of the thermal-time-constant based on fall-time. (Incropera (24))

equation was numerically fit to the duty cycle data, with the assumption that all heat generation was due to Joule losses. Both groups found that the lumped model would under-predict the motor temperature in heating and over-predict the temperature in cooling, indicating higher order effects due to the system not truly being lumped which was not captured by the approach. Since higher order effects are shown to be present in the machines behaviour, the determination of the time-constant may be subject to error, as the machine will cool differently depending on the state of the higher order terms at the onset of the test.

As a step towards a more accurate thermal model, several attempts have been made at including a second lumped thermal node, resulting in a second order model.

Some basis for the assumption of two dominant nodes exists, where it is typically found that machines exhibit two-time constants: one in fast transients found in heating, and one in slow transients found in cooling, which was expected to correspond to an additional, larger thermal mass in the motor (27). Though not explicitly a second order model, Venkataraman et al (27) applied the knowledge that a longer time-constant for the motor exists to inform a relay algorithm which evaluates the time required to reach the critical temperature based on the current motor load and thermal state, based on an additional term, Thermal Capacity Used (TCU), which is essentially a correction based on the type of motor loading and the motor time-constants. The focus of this model was to better identify the thermal characteristics of electric machines during start-up to determine whether the machine was at risk of overheating. Though their goal was sufficiently realized, the scheme is not suitable for temperature estimation, as it only considers how long the motor will take to reach failure levels at the current trajectory and accumulated TCU, not the actual component temperature. Additionally, under repeated cyclic loading, the accuracy of the TCU method decreases, as it does not account for changes that occur in the TCU after start-up.

Gao (28) formulated a second order hybrid electrical/thermal model wherein the rotor and stator were considered as separate lumped states coupled by the thermal resistance of the air-gap between the components, and the rotor temperature was determined by the electrical modelling method described in section 2.2. The heat generation terms used in this model were assumed to be due to Joule-heating only in both the armature and stator. Gao (28) used a complex space vector representation of the motor, for which the model parameters were solved using several algorithms to correlate to the experimental data. Though the resultant model followed the motor behaviour closely with a maximum error of 5 $^{\circ}C$, Gao noted that the biggest challenge

to the estimation of the parameters was noise in the current measurements used for the electrical component due to non-linearities of the current behaviour in an DC machine.

The second-order model proposed by Moreno et al, (29) also considered that the motor rotor and stator were the critical components for thermal modelling of the system. The developed model considered heat generation due to Joule-heating, varying with component temperature, as well as hysteresis and eddy current losses. Heat transmission by radiation was assumed to be negligible, while the convection and conduction terms were lumped into thermal conductances dependent on the motor speed for both the interchange between the components, as well as to the cooling air. The model parameters were extensive, including the thermal conductances, conductance variation coefficients, stator and rotor hysteresis and eddy current loss coefficients, and the thermal capacitances. Methodical testing was performed to identify most of the model parameters using steady state tests, while the capacitances were determined with transient tests. To isolate the effects of motor and phase speeds, the tests included a locked-rotor condition, to isolate any effects related to motor-speed, as well as tests at multiple motor speeds in order to identify how the additional effects vary with motor-speed. The results of this model and identification technique were able to predict the actual motor temperature within 1 $^{\circ}C$. The extensive testing required in this method is potentially unpractical in an industrial environment due to risk of motor failure during the locked-rotor tests as well as the required down-time to perform the steady-state testing.

A third-order model developed by Milanfar (30; 31) supposed that the armature and stator windings were responsible for the fast-transient system behaviour, while the motor core and magnets were responsible for the slow transients. A three-state thermal model was developed, with one state for the windings, and two states for the

motor core and magnets, where heat transfer to or from the states was considered to be exclusively conduction or convection. The heat generation terms that were included were those which were determined to be the three significant sources of heat in the analyzed machine: Joule losses, iron losses, and eddy current losses, where the latter two are dependent on motor speed. The parameters of the model were identified using a state-space representation of the model solved with duty-cycle experimental data at varying motor speeds. Though this method produced results within 2 $^{\circ}C$, the identification of the model required accurate measurements of each of the three model-state components, as well as controlled testing in heating and cooling at multiple motor speeds.

Boglietti et al (32) constructed a fourth-order model concerning only the motor stator temperature, completely independent from the rotor, and the starting condition, as the topic of interest was thermal model-order performance under the fast-transient conditions. The model considered four components: the stator windings, the stator winding insulation, the rotor teeth, and the rotor yoke. The capacitances and resistances used were claimed to have been empirically determined by the authors through a test campaign conducted on several totally enclosed fan-cooled industrial DC machines of different manufacturers. The actual methodology used to find these parameters was not discussed. The fourth-order model was reduced to third, second, and single order analogues by progressively amalgamating the capacitances of components which had the smallest thermal resistances between them within each successive model. The third-order model combined the rotor teeth and yoke, while the second-order model further combined the stator windings and insulation, and as such the second order model considered the rotor and stator as the critical components. The fourth-order model was found to be the most accurate at estimating the stator temperature during the starting of the motor with a maximum deviation of 1

$^{\circ}C$, with each of the successive reductions being slightly less accurate than the previous. This is shown in Figure 2.4, where the motor temperature is plotted against time for each of the four proposed thermal models, as well as the actual temperature measured during the experiment. It can be seen that though each model follows the measured motor temperature well for the first two-thirds of the test, larger deviations are seen in the final third.

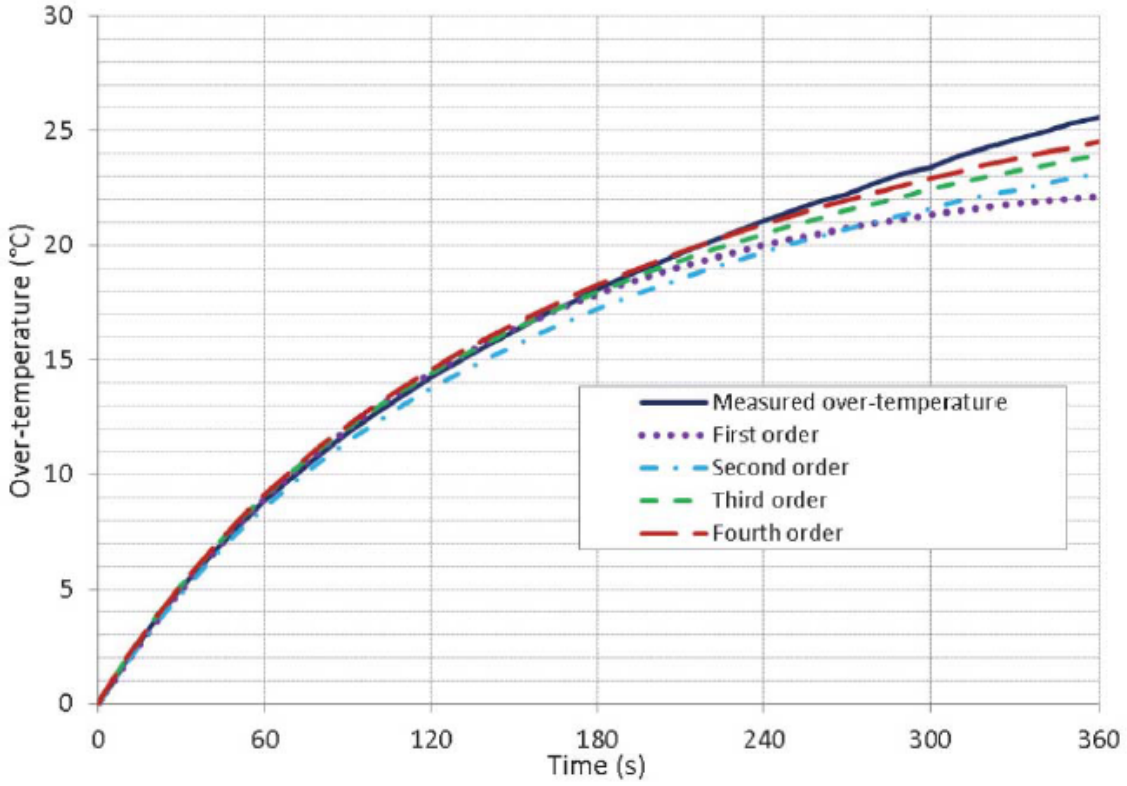

Figure 2.4: Plot of the motor over-temperature against time for the performance of four motor thermal models of differing orders compared against a measured value. (Boglietti (32))

Though it is possible that the simpler models are less accurate due to their inability to capture the higher order physics of the machine, it is reasonable to assume that the superior performance of the fourth-order model is due to the parameters used having been identified explicitly for the fourth-order model, whereas the lower order model

parameters were not identified, but rather wrought from the simplification of the fourth order model. Boglietti et al concluded that the higher order models would be more suitable for theoretical analysis of motor design, as their higher computational effort and more difficult identification scheme makes them less suitable for online measurement of in-situ motors, while the simpler models provide satisfactory results for most control applications with relative ease.

While semi-empirical models can provide relatively good results for most applications with relative ease, the main flaw shared between all of the identification methods discussed above is that they require tuning via controlled experiments where the motor is run continuously until it is fully heated the amount of time required to reach thermal-saturation may be great, or where the motor is run while locked-out, which, even when done conservatively, could risk rapid over-heating and failure of the motor when there is not good understanding of the motors response. These tests pose the problems of requiring expensive and substantial production down-time, as well as the risk of motor damage which in addition to being extremely expensive to repair would lead to even more production down-time while the machine is repaired. Since the larger the machine is, the longer the tests will take and the more expensive possible repairs will be, and since the machines studied in this thesis are very large, 5000 HP, and are critical to the production process at AMD, it is not possible to perform these tests.

2.3.2.3 Analytical Modelling Methods

As the order of the semi-empirical thermal models is increased, such as including additional components and/or multi-dimensional heat transfer, determination of the parameters by experimental correlation becomes impractical. As such, the parameters of higher-order models are most often calculated based on assumed geometries and

heat transfer correlations. Much of the early work on this was done using steady-state analyses to work out the thermal resistances between the included components, however Perez and Kassakian (33) were the first to include transient behaviour in these models by adding capacitance terms. Mellor and Turner (14) developed on the work of Perez and Kassakian by modelling the individual components of the machine more simply as concentric cylinders, instead of the complex geometries used earlier, which are reduced into an equivalent thermal-circuit analogue. Heat capacity and generation are assumed to be uniformly distributed through the cylinders, where Joule losses are considered in both the armature and stator windings, and the iron and eddy losses are lumped together as a core loss term within the appropriate bodies. Heat transfer between bodies is modelled by appropriate conduction resistances, while heat transfer to the air is modelled using convective resistances developed from standard heat transfer correlations for air-flow over cylinders as appropriate for the assumed flow paths in totally-enclosed, fan-cooled machines. The thermal resistance network, now known as the lumped parameter thermal network, developed by Mellor and Turner is considered to be one of the standard approaches for simple modelling of DC machines. However, as the solution to the model parameters depend on heat transfer correlations which require detailed knowledge of the machine geometry, and more critically an understanding of the flow in aspects such as local flow speeds and directions. For relatively simple designs (i.e. where the flow is entirely axial or across), these quantities can be reasonably assumed, however for the more complex flow geometries found in industry (combination axial-cross flow, with potential for flow through components, as well as non-axisymmetric components), these correlations will not hold.

Much work has been carried out by researchers such as Boglietti and Stanton (34; 35; 36; 37) in attempts to improve the Mellor and Turner model, including efforts to

both reduce to the model complexity for in-situ applications, as well as increasing the model complexity to allow more accurate modelling of more complex phenomena. The culmination of these efforts was the development of software such as MotorCAD, (23) a product of Statons company, Motor Design Limited, in which most of the modelling specifics, such as geometry relationships and heat transfer correlations, are stored in the software back-end, while the user has only to input the geometric parameters of the model. Though this software can often produce accurate thermal models for DC machines, it is still limited by the main constraint of many of the other models discussed: it requires that the input geometries be detailed and accurate, that the assumed geometric relationships between components be consistent for the analyzed machine, and that the air-flow through the machine matches the air-flow assumed by the software. Furthermore, manufacturing tolerances and material variations may lead to inaccuracies in the model between identical machines. Because of this, this software is most often used in motor design in an effort to understand the behaviours of components critical to the design, rather than as a method of on-line machine temperature estimation.

2.4 Chapter Summary

The thermal modelling of electric motors is a critical part of machine protection. Due to the high computational effort of numerical solutions to DC machine thermal behaviour, these methods are not suitable for the on-line estimation of motor temperatures, though they are well suited to process of designing new machines. Because of this, high-order analytical models often provide more tractable models for thermal control of the machine design, as the relevant components are simplified into a more finite number of parameters. Additionally, high-order analytical models may also be

simple enough to be used for on-line estimation of machine temperatures, for which the numerical methods are far too computationally expensive. When the machine geometries are well-known, both numerical and high-order analytical methods produce accurate results, however, if the machine is not well-defined, as is the case with in-situ machines that predate these estimation methods, the assumptions and correlations used in the modelling do not hold. As such, for these purposes, low-order analytical models which are identified by experimental methods are required for applications, where a model is to be developed for a machine for which the physical and flow geometries are not known a priori.

Since the topic of this thesis focuses on the on-line modelling of an in-situ industrial DC machine, where the machine design drawings as well as any manufacturer test data is not available, numerical and higher-order analytical modelling methods are excluded from the analysis, as most of the required model inputs are not available. Therefore, this thesis will consider the low-order approach to thermal modelling of a large DC machine.

Chapter 3

Experimental Methodology

3.1 Introduction

The facility offered for study by the industrial partner, ArcelorMittal Dofasco, was a large, DC electric drive motor implemented in the companys finishing area of the Hamilton, Ontario hot-mill. The aim of the study was to identify a model of the machine that could be used to predict its instantaneous operation temperature based on externally monitored values of the cooling air and motor current input. It was therefore important to have online monitoring of the air temperatures at the inlet and outlet of the cooling air ducting, the cooling air flow rate, and the motor current input. As the safeguarding of the motor against extreme humidity had to be considered, the humidity of the air was also an important measurement. For the identification of the model parameters, as well as the model validation, measurements of the armature winding temperature was required. Additionally, the isolation of particular operational conditions, such as cooling with no heat input, was necessary to the model identification procedure as this allows for model reduction.

3.2 Experimental Facility

The experimental facility is comprised of two main systems as shown in figure 3.1; the motor and its cooling loop. The motor is the main system to be modelled in this study via its coupling to the cooling loop. Heat is generated in the motor during mill operation due to the motor losses discussed in section 2.3.1.1. The motor is cooled by the cooling loop, which uses a fan to draw cooled air from a reservoir in the basement of the facility to cool the motor internally by forced convection. A telemetry system was implemented to monitor the air-flow, while a data logger was used to record the temperature measurements inside the motor. Production data that gives the motor current input was measured to complete the models inputs.

3.2.1 Drive Motor

The machine analyzed in this study is a shunt-wound, blow-through, 5000 HP electric motor, approximately 3.75 m in diameter and 2.5 m long, manufactured by General Electric Canada. It is important to note that all measurements concerning the motor presented in this section are very approximate as access to the motor design drawings was not available to AMD, and dismantling of the machine to measure the components more accurately was prohibited. The motor consists of 3 major components:

1. Armature
2. Stator
3. Commutator

The armature of the motor is approximately 2.5 m in diameter and 1.25 m long. It is comprised of three components; the armature windings, the spider, and the shaft.

The armature windings are conducting copper bars covered in a layer of insulation which is intended to electrically isolate each bar from its neighbour to prevent shorting of the circuit. The insulation class used on the armature windings is Class F, which is rated to 155 $^{\circ}C$. The spider consists of an outer ring which holds the copper windings, and a radial framework which supports this structure to the shaft. Both components are made of steel, and are bolted together. The shaft of the motor is made of steel, roughly 1 m in diameter and 4.3 m long, and transmits the torque generated by the armature and stator to the rollers used in the mill. A second drive motor is coupled to the studied motor by the shaft. The whole armature assembly weighs approximately 50 000 kg, and is supported on either side by large, grease-filled bearings.

The motors stator is copper-wound, having a fin-like geometry supporting the magnets, and is similarly insulated with class F insulation. The stator is an annulus around the armature, with a gap of approximately 2 cm, and a thickness of approximately 60 cm. It is approximately the same length as the armature.

The motor armature and stator are housed in a fiberglass compartment which confines the cooling air flow through the motor. The whole motor sits on a concrete foundation. At the front of the motor (opposite of the commutator), a grating exists in the concrete foundation which allows airflow from a cooling fan on the level beneath; the basement cooling air reservoir. Under the back side of the motor, there is another grate which allows some of the airflow to be returned to the basement air reservoir. When rotating, the motor itself adds additional pumping power to the cooling air, however it is found that the increase in mass flow rate of the cooling air during motor operation is typically only 2% of the nominal flow rate.

The commutator is comprised mainly of copper and is roughly 1.75 m in diameter and 20 cm thick. It is connected directly to the shaft of the motor; however, it is housed in a separate compartment.

The critical component of the motor is the stator and the armature windings insulation, as the stator and armature windings are where most of the heat is generated, thus the winding insulation is most likely to melt resulting in catastrophic motor failure. As a safety measure, the partnered company has imposed that the maximum desired temperature of the winding insulation not exceed 80% of the insulations rated temperature; approximately 120 $^{\circ}C$.

3.2.2 Cooling Loop

The drive motor is cooled by a 75 HP fan which draws from a basement reservoir and blows through the motor. Using the basement of the facility as the cooling air reservoir allows the thermal mass of the facility's foundation to be used as a sensible heat sink in the early warm days of spring and summer, as the basement will still be cool from the winter, to help keep the reservoir air temperatures low. After the air has passed over the armature and stator of the motor, approximately $2/3^{\text{rds}}$ of the air is returned to the basement reservoir, while the rest is used to cool the commutator in an adjacent compartment before being exfiltrated to the room where the motors are kept (Power House). The air that is returned to the basement is passed by a chiller to keep the reservoir air cool. The fan was retrofitted with a VSD in order to allow for the control the cooling air flow rate through the machine required in this study. A schematic of the cooling loop implemented is presented in figure 3.1.

In the summer, the basement reservoir is supplied by several fans which draw air from the roof of the facility. In the winter, the air exfiltrated to the Power House is recirculated to the roofs supply fans instead of the make-up air being drawn from the much cooler and drier environment outside in an effort to maintain a suitably humid environment for the operation of the motors commutator. For SA45 grade commutator

brushes, the acceptable range of absolute humidity for proper brush operation is 4.6 to 16 g_w/m^3 (38).

As air flows through the motor, it first comes up from the grate in the concrete foundation, then turns and travels through the armature spider. The air then flows radially outward through the armature windings and is returned to the basement reservoir through the grate beneath the back of the motor. The commutator compartment receives cooling air by intentional exfiltration from the main motor compartment, approximately $1/3^{rd}$ of the total flow, and vents this air through two outlet vents in the commutator compartment.

3.2.3 Internal Measurement Equipment

In the manufacturing of the motors, seven type K thermocouples were imbedded into the winding insulation of the armature to ensure the motors insulation was evenly baked (the process by which the winding insulation is applied). Six of the thermocouples were placed along one side of the armature in the axial direction, while the seventh was placed on the opposite side of the armature. Unfortunately, it is unclear where each thermocouple actual is from where the sensor leads are accessible, thus it is not possible to conclude with confidence exactly which local temperature each thermocouple is reading. Additionally, the quality of the contact between the thermocouples and the winding insulation is not known, thus large differences in the temperature readings is expected.

Though they were not intended to be used in the on-line measurement of the armature winding insulation temperatures, the seven thermocouples were connected to a MicroEdge Instruments SITE-LOG LPTM-1 data logger that can be accessed from inside the machine during shutdowns, allowing for monthly data acquisition.

The data logger provides an additional channel measurement of the thermistor that is used as its cold-side junction. Since the logger box is mounted to the front of the armature (i.e. it sees the inlet flow, directly), this reference channel (channel 0) is expected to closely follow the inlet air temperature. Due to the memory limitations of the data logger, the sampling period of this data is 20 seconds.

Figure 3.2 plots the measured temperature versus time of the seven armature channels for an example process-cycle, the duration of which was 45 hours, with very dynamic production using the raw data as measured by the sensor. Figure 3.3 shows the same, however the data has been smoothed by the method outlined in section 3.4.2. Referring to figure 3.2, it is of note that the noise present in the thermocouple readings occurs only while the machine is being operated, and not while the motor is cooling-down. (i.e. there is current flowing through the machine or motion)

3.2.4 External Measurement Equipment

A Rockwell FactoryTalk Historian ME (FTHME) data acquisition system was used to record and store data from multiple temperature, humidity, pressure, and airflow sensors. The full list of sensor equipment used in this system can be found in table 3.2. Figure 3.1 indicates where each of these are measured in the system.

3.2.5 Mill Production Data

In addition to the temperature data collected from the internal and external telemetry systems, the mills production data was also acquired. These records keep data for each work piece that passes through the mill, and includes the start time of the roll, the roll time duration, and the maximum total current input to the motor over the duration of the roll, which were used in this study.

The current profile of a typical roll duty-cycle is shown in figure 3.4, where the percent-maximum-duty-cycle current is plotted against the roll duration, which is typically on the order of about 60 seconds. At the start of the roll, the current is set to 80% of the maximum current for that roll for 2% of the roll duty-cycle in order to start the rotation of the rollers as well as forming of the piece. The current is then reduced to 65% of the maximum roll current, and ramped up to the maximum current at 90% of the duty cycle as the piece is accelerated through the roll. The current is finally rolled off to 85% over the remaining 10% of the duty-cycle, as the roll of the piece is finished. From figure 3.4, it can be seen that the current is most often below the recorded peak current during the roll. Because of this, the production data must be manipulated such that a more accurate current profile may be provided for the input current data. For this analysis, the approximate current loading profile during a roll that will be assumed is annotated in figure 3.4.

3.3 Experimental Procedures

Since the machine being studied is used in a major production facility, any controlled testing that could have caused production delays or pose any risk to the machines life or function was strictly forbidden, thus machine operation data could only be obtained for the dynamic operation of the mill, and during mill shutdowns.

3.3.1 Process-Cycles

As the motor being studied is used in a production environment, much of the data obtained corresponded to dynamic production operation. During production, work pieces are processed one at a time through the mill, with short gaps between pieces.

During a typical process-cycle, the machine is only processing a piece for approximately 50% of the cycle duration, where the machine is on only for the piece rolls, and off for the gaps between them. Due to this varied operation, the mill never appears to reach a steady state, thus this data is not useful in the identification of the steady-state operation of the system. However, this data is important for the validation of any method that attempts to model the system behaviour. Where dynamic operation conditions were considered, the analysis used complete process-cycle samples of the motors operation. An example of such a process-cycle is presented in figure 3.5, where the motor temperature, (left axis) as measured by channel 3, and the motor current, (right axis) are plotted against process-cycle duration. As expected, regions in which the motor current is large results in the rise in temperature of the machine as heat is generated due to losses as discussed in section 2.3.1.1, and regions in which there is no current results the decrease in temperature of the machine as it cools. Using the method outlined in section 3.4.1, 18 process-cycles were isolated from the available data.

3.3.2 Cool-Downs

Samples of data through which the motor was being substantially cooled in between long mill off-times (typically >1 hour) were isolated from the data sets. Cool-down data was of interest since all data sets exhibit much less noise and fewer fluctuations when the motor is not operating. Additionally, only the internal and external data sets would have to be correlated to obtain a solution over these domains, allowing for a simpler solution, rather than having to include the additional terms which would correspond to the heat generation due to motor losses. Using the method outlined in section 3.4.1, 135 cool-downs were isolated from the data.

3.3.3 Controlled Cool-Down Tests

In some instances of motor cool-down, the cooling fan speed was reduced in a specified manner in order to acquire data from which the cooling air speeds effect on the convective heat transfer could be determined. Since the fan control system has not yet been automated, an AMD employee was responsible for manually setting the fan speed during these times. Due to the dynamic environment of the mill, reducing the fan speed at the onset of the cooldowns was difficult, and in many instances the fan speed was not reduced until 10-15 minutes into the cool-down, at which point most of the cooling had already occurred. Additionally, due to other mill shutdown procedures, these samples were not able to reach the determined "fully-cooled" state, and thus all are categorized as "partially-cooled". As there were only a few controlled tests performed, these tests were isolated manually based on the known-times at which they occurred. Six controlled cooling tests were successfully performed at 85%, 80%, 75%, 70%, 65%, and 60% of the nominal (maximum) fan speed.

3.4 Experimental Data Processing

3.4.1 Data Isolation

Since the internal data sets exhibit very high amounts of noise during motor operation, and since no controlled testing of the cooling fan speed was allowed to be performed during motor operation, the most important data samples required for the analysis method presented in this thesis are regions through which the motor is solely cooling. To isolate these samples, a program was written in Python which identifies suitably large gaps in the production data ($>$ 1 hour) and isolates the sample using the start and end times of the production gap. These times were then matched to the internal

and external data sets to isolate the relevant data for the cool-down samples. The cool-down samples were then manually resized to ensure that as much of the cooling data for which there was a significantly reduced amount of noise was captured in the sample as possible, and that any unphysical noise was removed. Due to un-logged motor operation, there were occasionally disruptions in the cooling where the motor was run without the current to the motor being logged, thus these samples occasionally had to be manually retrimmed, to ensure that no heat input was present, or else the samples had to be rejected. Due to the varied operation of the machine, the lengths of these samples was between 1 hour to >10 hours. As such, various degrees of cooling are achieved, which is expected to affect the energy balances performed on this data as the excess internally stored heat is not accounted for, therefore these samples are further categorized as fully-cooled (>5 hours) and partially-cooled (<5 hours) so that all of the data may be presented with the omission of potentially skewing effects. This threshold was determined by visually examining the samples and observing the elapsed time at which all of the samples show no more cooling to be occurring.

For the validation of the presented models, as well as the identification of the remaining parameter in each model, complete cycles proceeding from fully-cooled to regular-operation and back to fully cooled are required. For this, process-cycles were isolated where, as with the cooldown isolation discussed previously, sufficiently large gaps in the production data (>5 hours) were identified by a developed program in Python, and the process- cycles were selected as the times between the end of the previous production gap, (when the machine was initially fully-cooled) and the end of the subsequent gap (when the machine was finally fully-cooled after the process-cycle). An additional hour was added to the start of these samples so that the starting temperature of the models could be set based on a fully-cooled state, providing a known initial temperature that could be assumed uniform. Since the isolation of

the process-cycles used a much longer production gap to identify the breaks between cycles, it is expected that the machine starts and ends at a fully-cooled state.

3.4.2 Data Filtering

Since the internal telemetry is subject to a large amount of noise during operation, it is seldom useful in identifying the true temperature of the system at any given point. Conventional data filtering algorithms such as the Fast-Fourier-Transform (FFT) or high-pass filters are not applicable for this data set since the sampling rate is so low (20s) compared to the noise contributors, therefore Savitsky-Golay filtering was used to smooth the data such that realistic comparisons and estimations may be drawn. In the Savitsky-Golay filtering algorithm, a polynomial of a specified order is fit over a specified window-size and the data points are shifted to lie closer to the fitted polynomial. The window is then shifted, and the process is repeated, thus smoothing the data. Care must be taken in the selection of both the polynomial order and the window-size to ensure that physical fast-transients in the data are not obscured. For the Savitsky-Golay filter used in this study, a 6th degree polynomial was used over a window size of 30 minutes (91 points for the internal telemetry). The 6th degree polynomial was selected as it provided a sufficient fit to the data during rapid cooling. Figure 3.6 Shows the effect of varying the polynomial degree on the smoothing of the data during a sample cooldown with a window-size of 30 minutes. The 30-minute window was selected as this time-scale was found to be relatively short with regard to the observed total cooling times, thus any data smoothing applied over this window size should have minimal effect on the observed cooling dynamics. Figure 3.7 shows the effects of varying window-sizes on the smoothing of the data over a sample cooldown. Since the external telemetry sampling rate is still relatively low ($1s$) with respect to

the theoretical contributors of noise in the data, the Savitsky-Golay filtering method will also be applied to the external data sets, with a polynomial degree of 6 and a window size of 30 minutes (1801 points).

3.5 Uncertainty Analysis

3.5.1 Internal Sensor Uncertainty

The internal data collection which measures the armature temperature uses 7 type K thermocouples, which are recorded by the Site-Log LPTM module by MicroEdge Instruments, as well as the cold-side compensation temperature (CH0) read by an on-board thermistor. Though the expected error of the thermocouples by themselves is relatively low (as tabulated in table 3.1), it is noted that the accuracy of these readings is highly dependent on a good thermal contact between the sensor and the measured body, a good electrical contact between the thermocouple and the data acquisition system, and low ambient electrical interference. It has been noted in the operation of the machine that significant and often unphysical fluctuations (such as negative temperature readings) occur in the data. It is believed that this is either due to poor contact resistance between the thermocouple and the armature winding insulation due to degradation over time, poor electrical contact with the data acquisition system due to movement in the fittings, or electromagnetic interference from the large fluctuating electromagnetic fields that exist in the machine due to its operation. The best evidence seen of any of these possibilities is that on occasion, one or multiple channels of the data acquisition system would, over the course of a month, become unplugged from the unit, or the contact would become slightly loose such that the increase in the electrical contact resistance would cause the reading to be much higher than reality.

Table 3.1: Sensor list for internal data acquisition system measurements

Measurement	**Device**	**Error**
Cold-Side Temperature (CH0)	MicroEdge Site-Log LPTM on-board thermistor	$\pm.2\ ^{\circ}C$
Armature Temperature	Type K thermocouple (unknown)	$\pm.75\%$ or 2.2 $^{\circ}C$ (Standard Type K)

3.5.2 External Sensor Uncertainty

The external data collection equipment, which collects data from sensors reading the air flow rates, temperatures, and humidity, feeds the FTHME data acquisition system which provides a real-time measurement of the quantities. The data was stored by the system in a databank from which it was later acquired for the analysis. Figure 3.1 shows the location of the sensors used in the external data set, and table 3.2 summarises the sensor manufacturer, as well as the associated error of the sensors.

3.5.3 Air-Property Calculation Uncertainty

The relevant calculations using air properties in this analysis were the air mass flow rate, and the change in enthalpy of the cooling air. The air properties in this analysis were calculated using the CoolProp Humid Air package (39) in Python for humid air properties, which calculates psychrometric data based on ASHRAE-RP1485, assuming that the pressure was constant, atmospheric ($p = 101.325\ kPa$) and equal at the measurement locations, since the actual pressures were not successfully measured.

To calculate the propagation of the sensor uncertainty in these calculations, the Monte Carlo method was used to simulate $N = 10e6$ samples for three humidities, 25,

Table 3.2: Sensor list for external data acquisition system measurements

	Measurement	**Device**	**Error**
T_1	Inlet Air Temperature	Thermo Kinetics T-PAC type K thermocouple	$\pm.4\%$ or 1.1 $°C$
T_2	Return Air Temperature	Thermo Kinetics T-PAC type K thermocouple	$\pm.4\%$ or 1.1 $°C$
T_3	Commutator Vent Temperature	Thermo Kinetics T-PAC type K thermocouple	$\pm.4\%$ or 1.1 $°C$
F_2	Return Air Flow Speed	Ebtron GTC116-PC (4 probes)	$\pm 3\%$
F_3	Commutator Vent Flow Speed	Ebtron GTC116-PC (4 probes)	$\pm 3\%$
RH	Commutator Relative Humidity	Omega HX92AC-D	$\pm 2.5\%$ at 22 $°C$ $+0.18\%$ RH/$°C$

50, and 75 %RH, and for air temperature rises ranging from 4 to 12 $°C$ where an inlet temperature of 20 $°C$ is prescribed. The nominal return air and commutator vent velocities were taken as 3.3 m/s and 4.6 m/s, respectively, which were assumed to be constant across the flow areas of 3.43 m^2 and 0.412 $m^2/each$. The flow temperature and humidity ranges and the speeds chosen were found to accurately capture the more extreme limits of the flow in order to assess the maximum possible error of the calculations over the use of the machine. Random sensor noise following a normal distribution as governed by the uncertainty of each sensor, as tabulated in table 3.2, was added to each of the measurements in order to study their propagation into the air-property calculation carried out by the CoolProp Humid Air package. The results of the Monte Carlo analysis are presented in figure 3.8 and figure 3.9, which show the percent error in the mass flow (figure 3.8) and enthalpy rise (figure 3.9) calculation

to a 95% confidence interval over the array of RH and temperature rise of interest.

From these results, it is evident that the error incurred from the mass-flow calculation is relatively low, only about 1.3%, while the error on the enthalpy-rise calculation is much higher, especially at low temperature differences; as high as nearly 16% at temperature rises of approximately 4 $^{\circ}C$. However, it is noted that during typical machine operation, which is the range over-which the calculation is of more critical interest in the estimation of the machine temperature, the air-temperature-rise is higher than 8 $^{\circ}C$ and thus the error of the enthalpy-rise should typically be less than 8%.

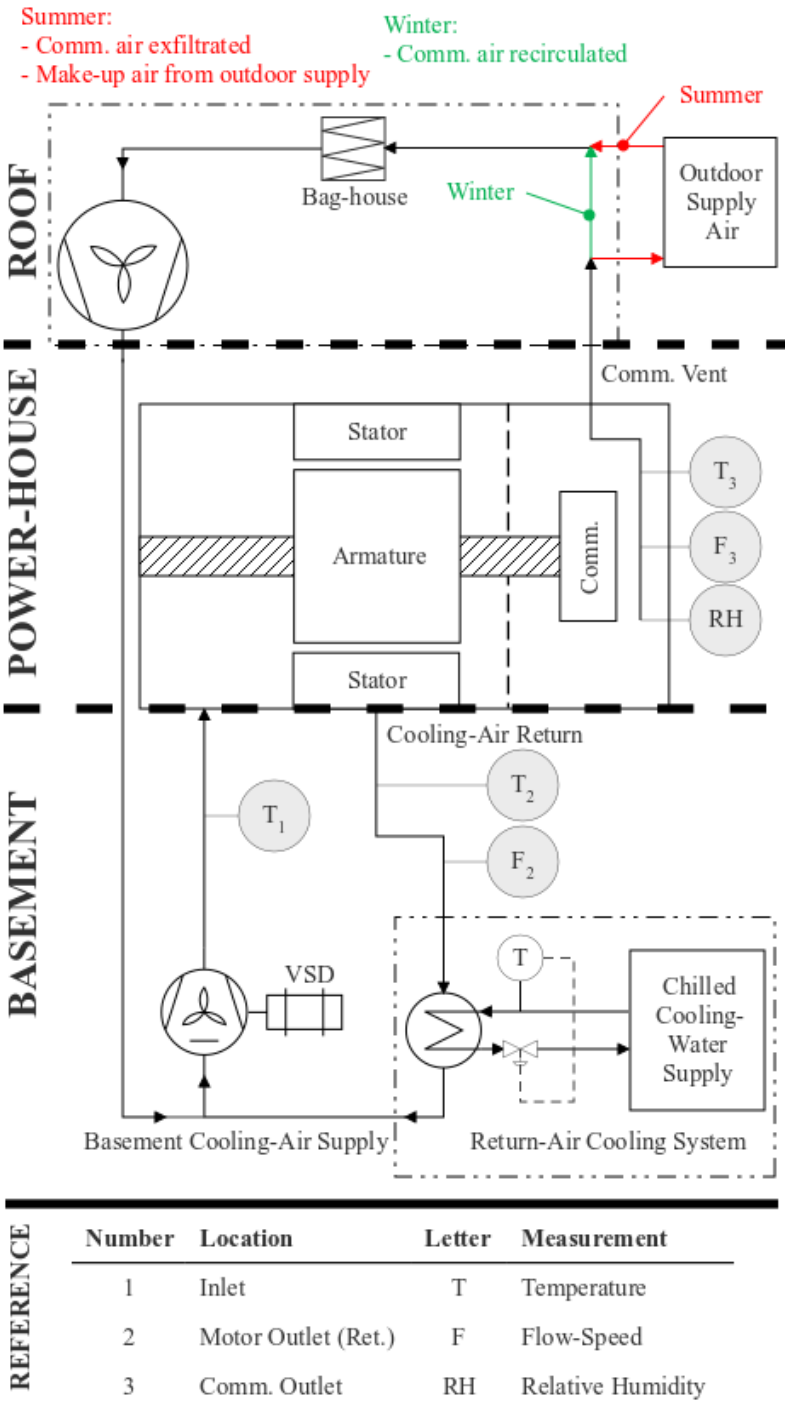

Figure 3.1: Schematic of the cooling-loop implemented in the cooling of the drive-motors at AMD. The abbreviation "Comm." refers to the motor's commutator.

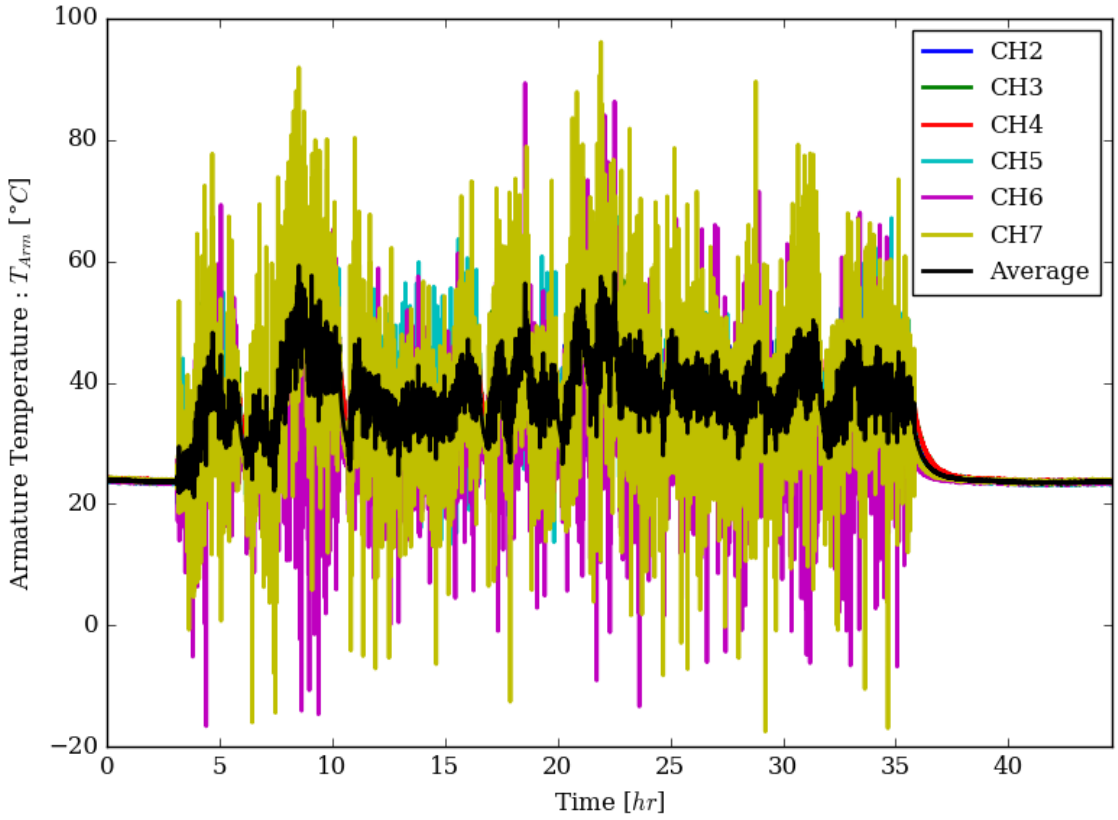

Figure 3.2: As-measured temperature measurements of the seven thermocouples embedded in the winding insulation. Large amounts of noise are visible on all channels while the machine is running.

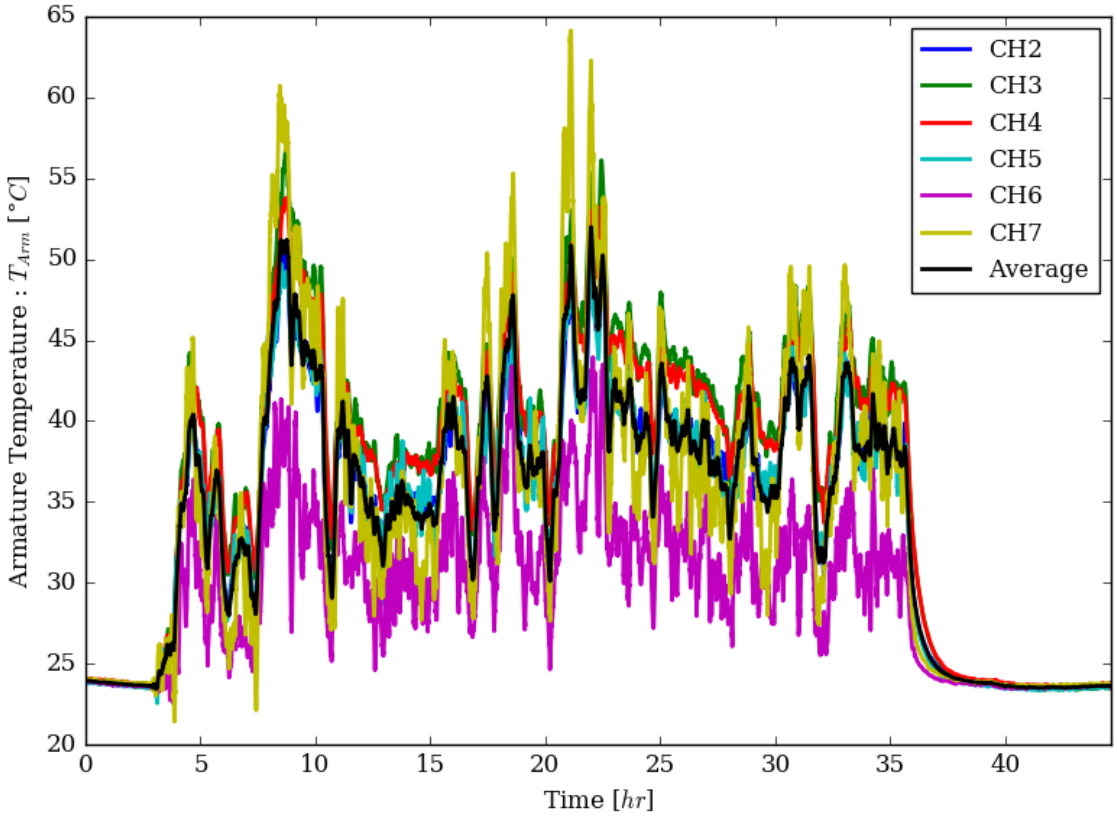

Figure 3.3: Temperature measurements of the seven thermocouples embedded in the winding insulation, smoothed by the method in section 3.4.2. Large amounts of noise are visible on all channels while the machine is running.

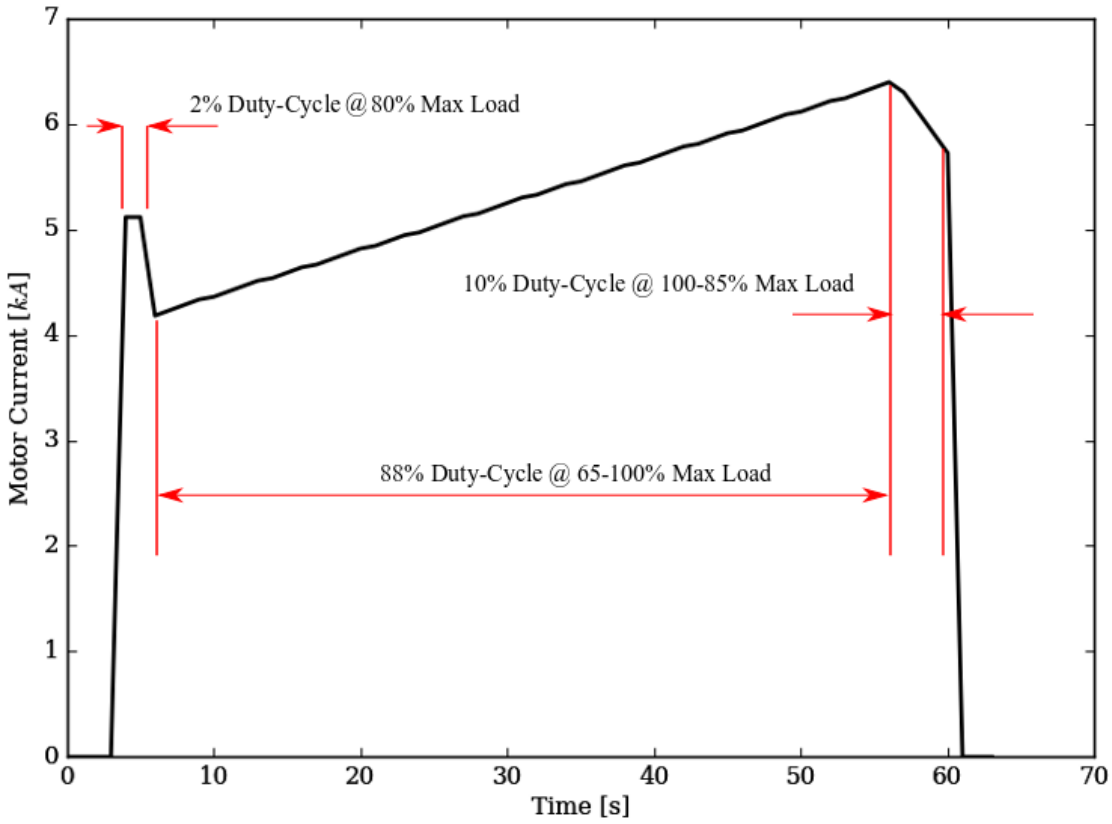

Figure 3.4: Profile of the drive-motor current for one roll duty-cycle

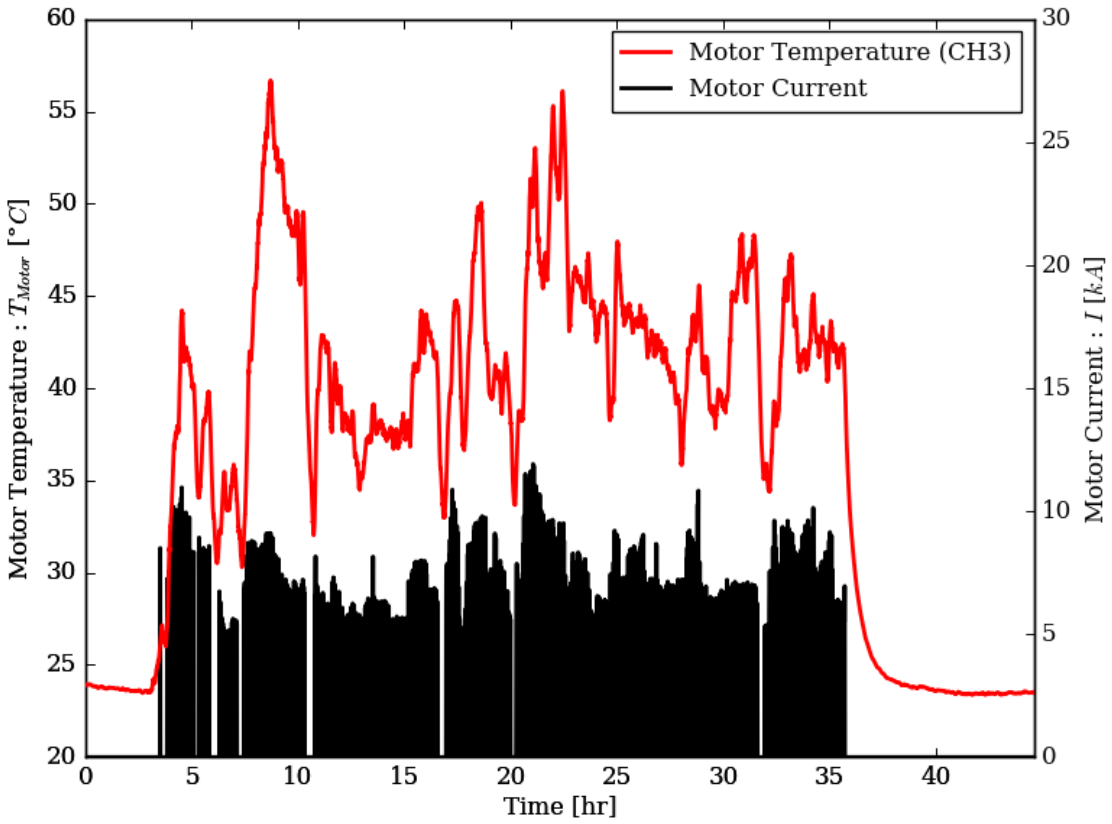

Figure 3.5: Measured motor temperature (left axis) and motor current (right-axis) for one process-cycle

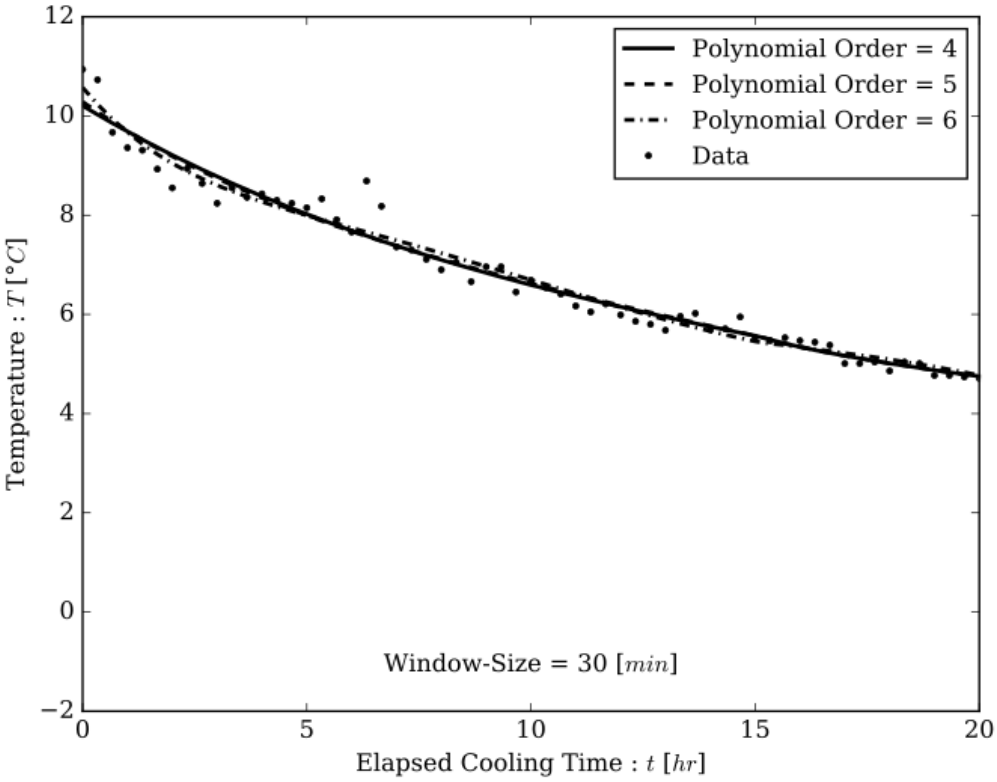

Figure 3.6: Effect of polynomial order on Savitsky-Golay data-smoothing algorithm.

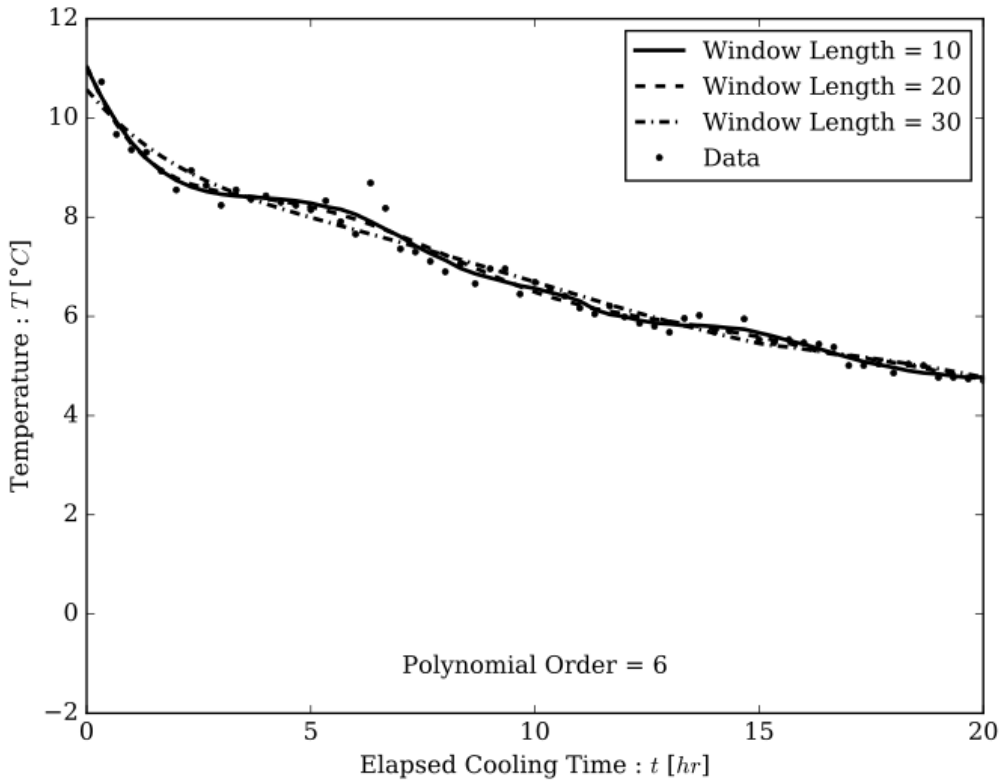

Figure 3.7: Effect of window-size on Savitsky-Golay data-smoothing algorithm.

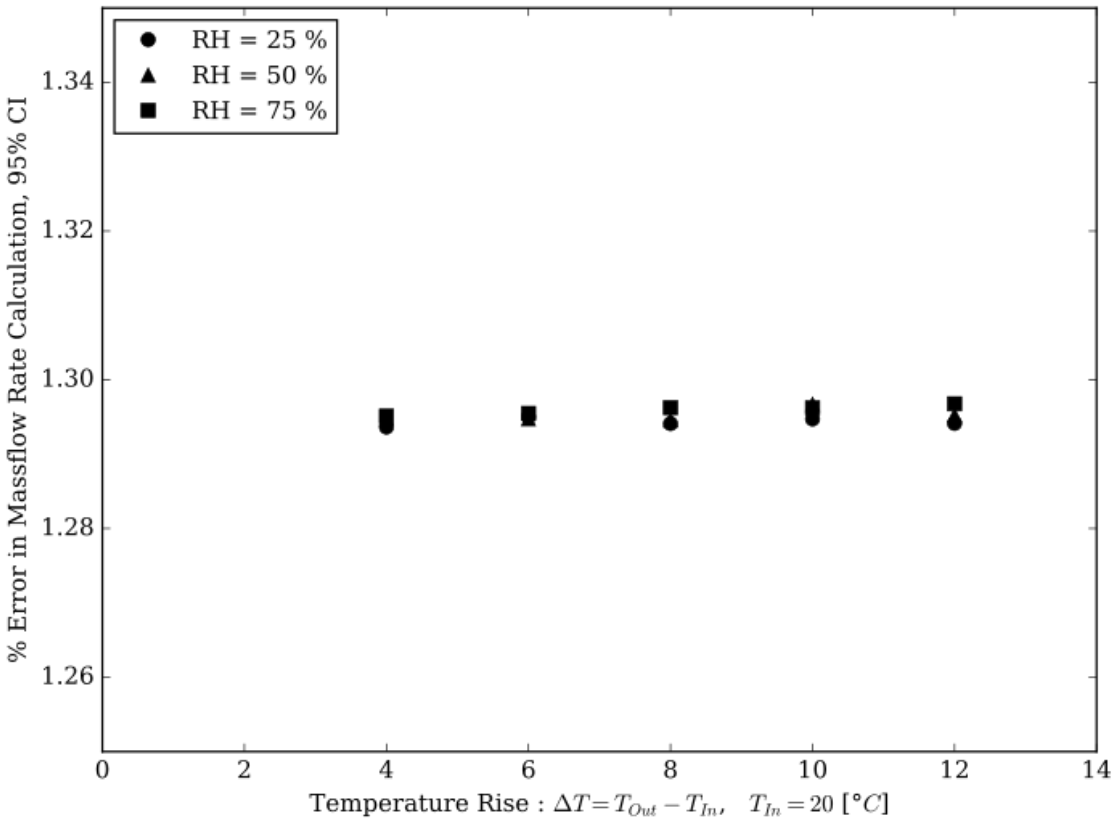

Figure 3.8: Error on air mass flow-rate calculation found by of Monte-Carlo analysis performed on calculations using CoolProp (39) air-properties

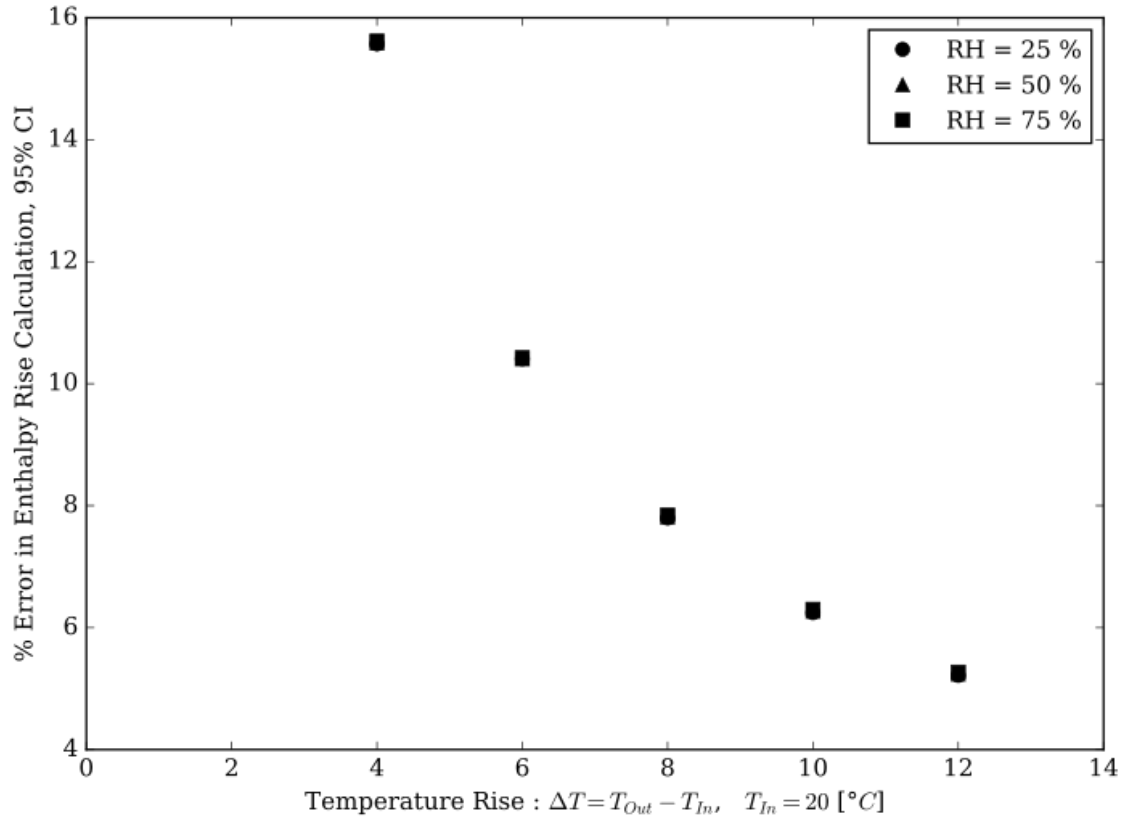

Figure 3.9: Error on air enthalpy-rise calculation found by of Monte-Carlo analysis performed on calculations using CoolProp (39) air-properties

Chapter 4

First-Order Model and Identification Methodology

4.1 Introduction

In the machine, heat is generated by a combination of Joule losses in the armature and stator windings, as well as core losses in the armature spider. Since the speed at which the motor typically operates is low, it is likely that the core losses will not be significant in the machine with respect to the Joule losses. Any heat generated in the machines bearings is considered to be external to this analysis, as these bearings lie outside of the ventilation compartment, over which the control volume is drawn. As such, all heat is assumed to be generated by the Joule losses in the armature and stator windings, from where it must be conducted through the winding insulation. The heat generation is assumed to be uniform throughout the winding bars.

Once the heat has left the windings through the insulation, there are three heat transfer paths through which it may flow: conduction through other machine components, forced convection to the cooling air, and radiation to other components. It

Table 4.1: Biot numbers for major machine components, as calculated in Appendix A

Component	Bi
Stator	$0.18 - 1.8$
Armature Windings	$0.01 - 0.13$
Armature Spider	$0.18 - 1.8$
Armature Shaft	$0.1 - 1.0$

is assumed that all components of the machine are visible to the cooling air, and that radiation to other components may be neglected as the interacting temperatures are sufficiently low and the machine sufficiently encased that any radiation present would be minimal and to nearby components whose surface heat transfer would also be dominated by the forced convection, as shown in (18). As such, all components are assumed to have a heat transfer path by convection to the cooling air in addition to conduction to any adjacent components. In the stator, by the same assumptions as in the armature, heat is generated by Joule losses in the windings and is conducted through the winding insulation. The heat is then either transferred directly to the cooling air by convection or is first conducted to the supporting steel structure before being convected to the air.

An approximate analysis of the validity of the lumped assumption for the components of the machine was performed, as shown in Appendix A. Table 4.1 presents the approximate Biot number ranges calculated for the main machine components, assuming hollow concentric-cylinder geometry for each component as in the Mellor and Turner model (14). The stator, spider, and shaft were assumed to be composed of steel, while the armature windings were assumed to be composed of mostly copper. The heat transfer coefficient used in the calculation was taken as the typical range for forced-convection to a gas of 25-250 W/m^2K (24).

From table 4.1, it is evident that the validity of the lumped assumption for the components depends upon the true heat transfer coefficient between the cooling air and the component. However, it can also be seen that for the whole range of heat transfer coefficient, the armature windings are within the accepted range of Bi ($Bi < 0.1$) where the lumped assumption is considered valid. For the other components, where $Bi > 0.1$, the lumped assumption will be less accurate. Although some of the components may exhibit distributed behaviour, it is impractical to model the machine as such due to the minimal information and data available in this study, therefore the development of the model will continue by first assuming that the machine may be modelled as a first-order system. Should the model not function for the desired analysis due to the presence of higher-order effects, then additional terms may be added to approximate a more representative distributed model.

As the modelling techniques discussed in this thesis are based on a uniform motor temperature, the armature temperature that is, on average, the hottest measured (see figure 3.3) will be used to describe the armature temperature. Although an average would be more accurate to the lumped assumption, the threshold temperature that would be imposed on any control scheme with this machine would be based on the highest temperature, thus the hottest available armature temperature reading will give the most conservative estimate of the armature temperature, relative to the control scheme. Though channel 7 exhibits the highest peak temperature, the hottest temperature, on average, is read by channel 3, which is closely paralleled by channel 4. Thus, channel 3 will be considered as the motor temperature for this analysis, as it will provide the most conservative estimate of the actual hottest temperature measured for most of the machines operation. A factor of safety may then be applied to the model in order to provide a more conservative estimate of the critical machine temperature in case hotspots exist.

4.2 Transient First-Order Model

In the first-order thermal modelling approach for DC machines, the machine is considered to be a single, lumped-body at a uniform temperature, T, with some overall thermal capacitance, C_M, and an overall convective heat transfer conductance to the cooling air, UA. The convection rate to the air is then defined by:

$$\dot{Q}_{Conv}(t) = UA(T_M(t) - T_{Air,Ave}(t)) \tag{4.1}$$

Where $T_{Air,Ave}$ is the average cooling-air temperature, given by:

$$T_{Air,Ave}(t) = \frac{T_{in}(t) + T_{out}(t)}{2} \tag{4.2}$$

As previously discussed, the heat generation in the machine is assumed to be due to Joule losses, exclusively, thus the heat generation term in the lumped component is:

$$\dot{Q}_{Gen}(t) = I(t)^2 R_E \tag{4.3}$$

where I is approximated by the total motor current in Amps and R_E is the electrical resistance of the motors windings in Ohms, and is assumed to be constant.

A unique aspect of a system this large is that sufficient heat is rejected to the cooling air for the cooling air temperature rise to be measurable within uncertainty. Additionally, since the flow is confined, the heat transfer rate to the air, $\dot{Q}_{Conv}$, can be directly quantified from an energy-balance on the cooling-air using the cooling air enthalpy, h_{Air}, at the inlet and outlet of the cooling air. A schematic of the first-order model is shown in figure 4.1.

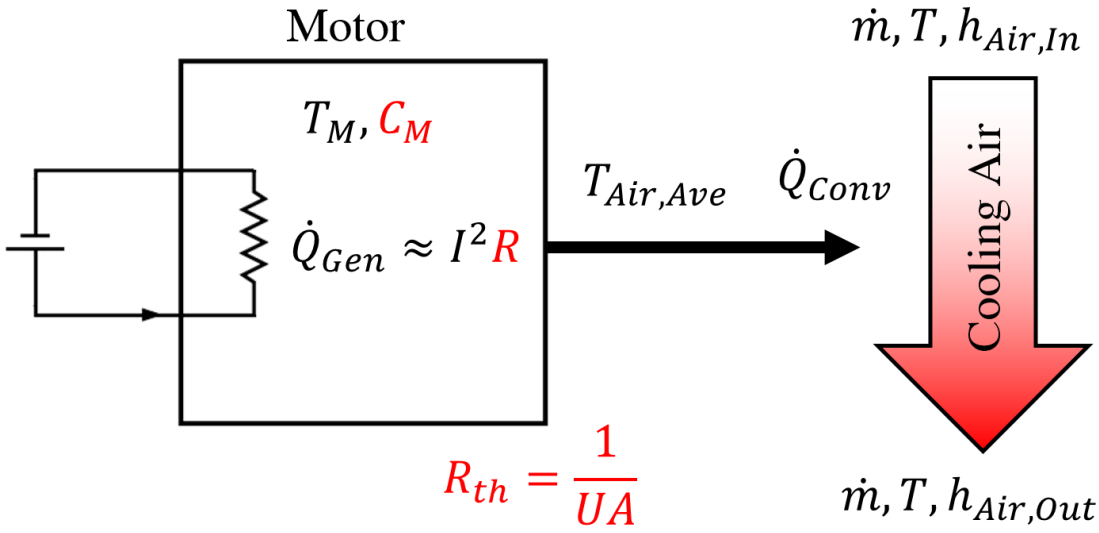

Figure 4.1: Schematic of the proposed first-order heat transfer model. Parameters shown in red text are the unknown parameters of the model.

4.2.1 Governing Equations of the First-Order Model

By performing an energy balance on the lumped-body shown in the previous section, the following ordinary differential equation is obtained:

$$\dot{Q}_{Gen} = \dot{Q}_{Out} + \dot{Q}_{Stored} \tag{4.4}$$

$$-\dot{Q}_{Stored} = \dot{Q}_{Out} - \dot{Q}_{Gen} \tag{4.5}$$

$$-C_M \frac{dT_M(t)}{dt} = UA(T_M(t) - T_{Air,Ave}(t)) - I(t)^2 R_E \tag{4.6}$$

Furthermore, by performing an energy balance on the cooling air passing over the machine, the following relationship is found:

$$UA(T_M(t) - T_{Air,Ave}(t)) = \dot{m}(t)\Delta h|_{Air}(t) \tag{4.7}$$

As the goal of this work is to achieve an online estimation of the motor temperature

from the monitored air properties, equation 4.7, which has only one unknown thermal parameter, UA, can be rearranged to give an estimation of the motor temperature, $\hat{T}_M(t)$, from the cooling air measurements alone, as shown in equation 4.8.

$$\hat{T}_M(t) = \frac{\dot{m}\Delta h|_{Air}(t)}{UA} + T_{Air,Ave}(t) \tag{4.8}$$

The mass flow rate; or more correctly, the local air velocity; of the cooling air is expected to impact UA, variations in the flow will need to be accounted for in the model. The accounting of the variations in flow during cooling fan speed reduction in VSD control of the cooling will be approached later in section 4.3.2. Variations in UA as a result of changes in air flow due to machine operation will be assumed negligible, as the airflow is only increased by 2% when the motor is rotating due to its pumping effects as mentioned in section 3.2.1, and as the motor is only rotating for approximately 50% of the process-cycle as discussed in section 3.3.1, thus any effect on the average UA over a process-cycle will be minimal.

In order to use equation 4.4 for the estimation of the lumped machine temperature, three parameters would have to be known: UA, C_M, and R_E, and the ODE would have to be solved given the continuous input and the temporal history of the model, as opposed to only the continuous input required by the estimation from 4.8.

4.3 First-Order System Identification

4.3.1 Fitting of the First-Order Governing Equations to the Data

As equation 4.8 provides an estimate of the motors temperature with only one unknown, UA, the output of this modelling approach can be fit to the data such that

the error between the estimated motor temperature, $\hat{T}_M(t)$, and the recorded motor temperature, $T_M(t)$, is minimized in order to solve for UA. The fitted value of UA for the isolated process-cycles is presented in figure 4.2, using a boxplot to show the distribution of the data. A jitter (random noise) is added to the x-axis of this graph so that the individual data points may be more clearly identified in cases where they may lie on-top of each other. The median, maximum, and minimum values of UA from the boxplot are shown in the figure textbox. From this analysis, the overall conductance was determined to be 11.4 $\pm$ 10% $kW/°C$

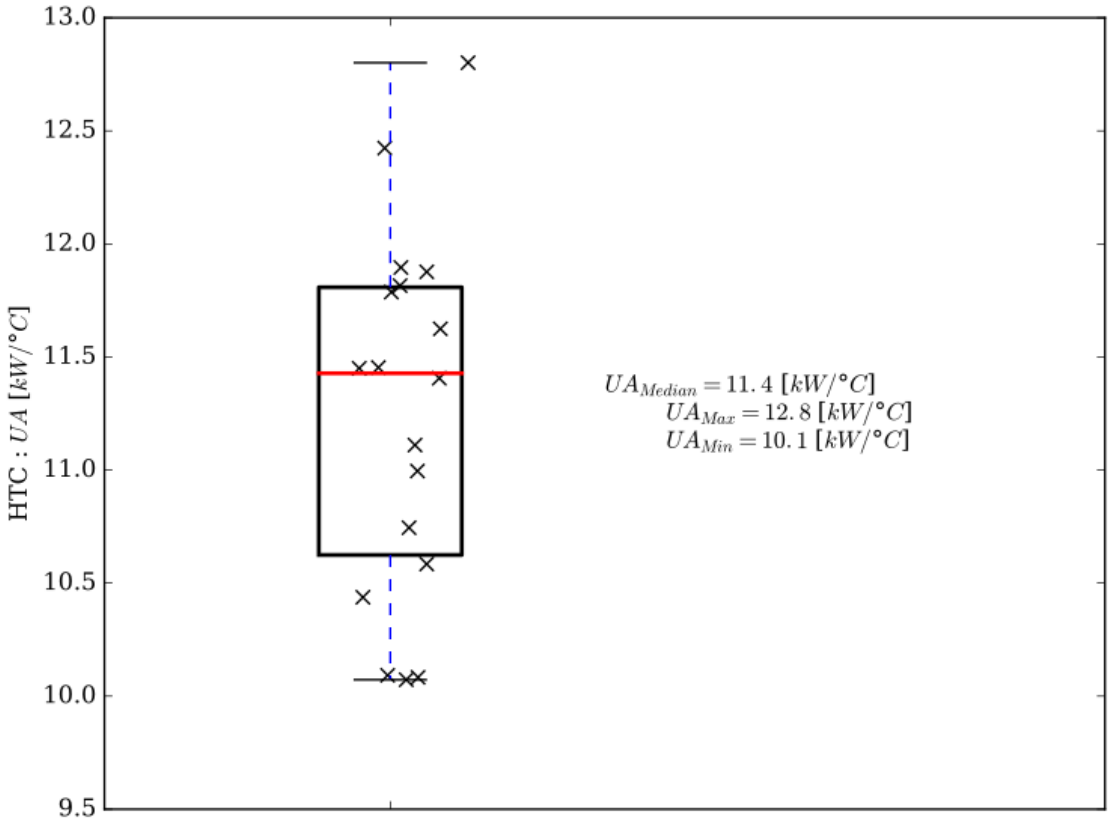

Figure 4.2: Values for UA for the 18 process-cycle samples, fitting equation 4.8 to the internal temerature data (Channel 3)

4.3.2 Identification of Reduced Cooling Effects in the First-Order Model

The problem that arises with this modelling method is that the aim of the model is to provide controllability based on the mass flow rate of the air from the fan speed, which would change the value of UA. Therefore, it is necessary to characterize how UA changes as the airflow rate is reduced.

The simplest way to do this would be to operate the fan at a reduced speed during a process-cycle and to find the UA at the reduced mass-flow-rate, as was done previously. However, since the degree to which UA will be affected is unknown there is the possibility of overheating the machine. Due to risk mitigation, this method is therefore not viable, as machine protection is paramount. This leaves cooling periods as the only periods in which controlled testing may be performed.

Since there is no current through the motor, and thus no heat generation during cooling, equation 4.4 reduces to:

$$-C_M \frac{dT_M(t)}{dt} = UA(T_M(t) - T_{Air,Ave}(t)) \tag{4.9}$$

which has the general solution of an exponential decay characterized by a time-constant, $\tau = \frac{C_M}{UA}$, for which the motor capacitance, C_M, should be constant as UA is changed, thus any changes in τ may be correlated directly to a change in UA, without necessarily needing to know the capacitance of the body.:

$$T_M(t) = T_{M,i} e^{-t/\tau} \tag{4.10}$$

Figure 4.3 shows an example of the first-order cooling model, equation 4.10, being fit to a sample cool-down, where the motor temperature is plotted against the elapsed

time of the cool-down. Both the real data points and the smoothed data to which the curve is fit are shown. As shown in B, smoothing the data using the Savitsky-Golay filter discussed in 3.4.2 does not significantly affect the fit. Smoothing is performed in this case to maintain similarity with the fitting process of the second-order model proposed in 5.3.1, which was found to require smoothing of the cool-downs in order to achieve appropriate convergence of the fit. The fitting process was performed using the rest of the 135 cool-down samples, as well as the 6 reduced-cooling cool-down samples, including both fully-cooled and partially-cooled samples, resulting in figure 4.4, which plots the determined cooling constant for each sample to the cooling-air mass-flow rate during the cool-down. Partially-cooled samples are included in this analysis as the cooling characteristic being fit still conforms to these samples and does not concern the overall energy balance which is not maintained in these samples (i.e. the main deficiency of these samples, that the remaining stored energy cannot be estimated, does not affect this particular analysis). A boxplot is imposed over the samples for which the cooling was not reduced to show provide a more clear visualization of the data distribution. The median, maximum and minimum values of the time-constant from this boxplot are shown in the figure textbox.

4.4 First-Order Model Validation

4.4.1 First-Order Modeling of Motor Temperature

Using the median value of UA from figure 4.2, equation 4.8 can then be used to estimate the motor temperature using only the continuous and on-line inputs of from the external measurement system. Figure 4.5 shows the measured and estimated motor temperature versus process-cycle duration, as well as the error (right axis)

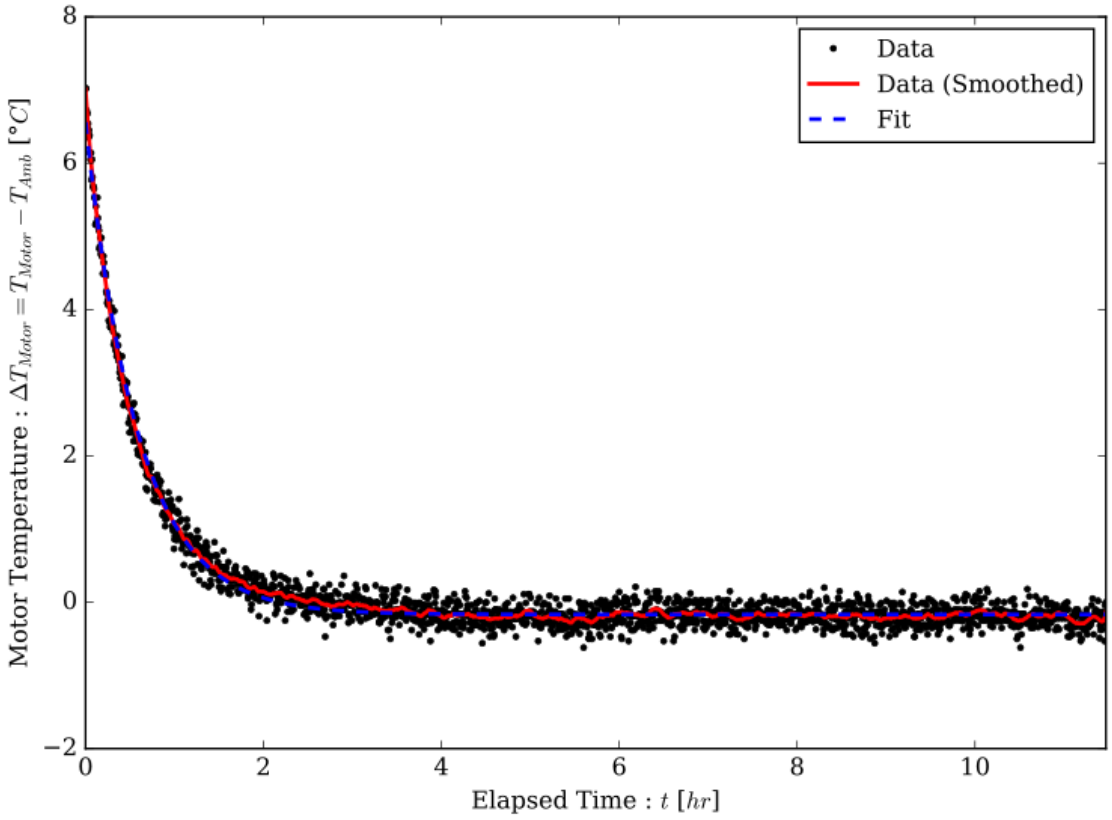

Figure 4.3: Motor temperature (channel 3) vs. elapsed cooling time for an example fit of equation 4.10 to a cool-down sample.

between them. This figure shows that the model performs the worst during fast transients such as heating and cooling.

The maximum and average errors in estimation using the first-order model for the 18 isolated process-cycles, in $°C$, are shown in 4.2.

From figure 4.5, it can be seen that the model generally follows the behaviour of the data. Since the median value of UA was chosen, it is expected that for some process-cycles, the model will over-predict, while others will over-predict. Over the 18 process-cycles, a maximum error of 9.0 $°C$, and a maximum average error of 4.3 $°C$ occur, as shown in table 4.2.

Table 4.2: Estimation error of the first-order model for 18 process cycle samples.

Sample	**Max** $[^{\circ}C]$	**Average** $[^{\circ}C]$
1	9.0	4.3
2	6.4	2.0
3	8.3	2.3
4	8.6	3.4
5	6.8	2.9
6	7.8	2.9
7	7.6	3.6
8	6.9	3.3
9	7.3	3.4
10	6.6	3.2
11	6.2	3.1
12	7.9	3.0
13	8.7	3.5
14	7.8	3.5
15	7.0	3.2
16	7.3	3.0
17	6.9	2.9
18	6.9	2.9
Max	**9.0**	**4.3**

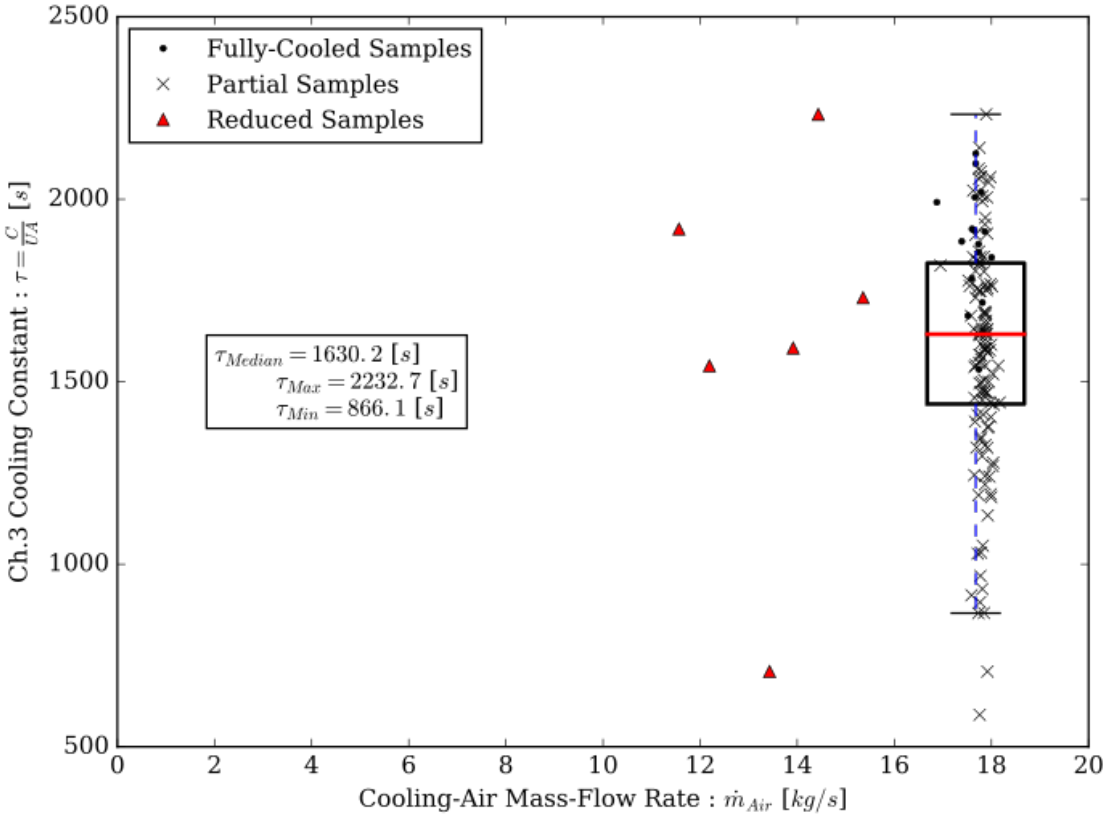

Figure 4.4: Cooling constant, τ, vs. mass-flow rate for all cool-down samples. Maximum flow-rate cases are presented with a boxplot to visually show their distribution. Reduced-flow-rate samples are presented separately.

4.4.2 Reduced Cooling Effects in the First-Order Model

By examination of figure 4.4, it can be seen that the degree to which the cooling constant is affected is within the range of variability of the cooling constants found for the maximum flow rate cases. Since the maximum variation in UA found from fitting the model to the process-cycle was $\pm 10\%$ (figure 4.2) while the variation in the cooling constant was $\pm 47\%$, between the median and the minimum values, it follows that the variation in the cooling constant is likely due to a changing capacitance, and not the variation of UA. Since the motors thermal capacitance is changing between samples more than the UA, the lumped assumption is insufficient to define the effects

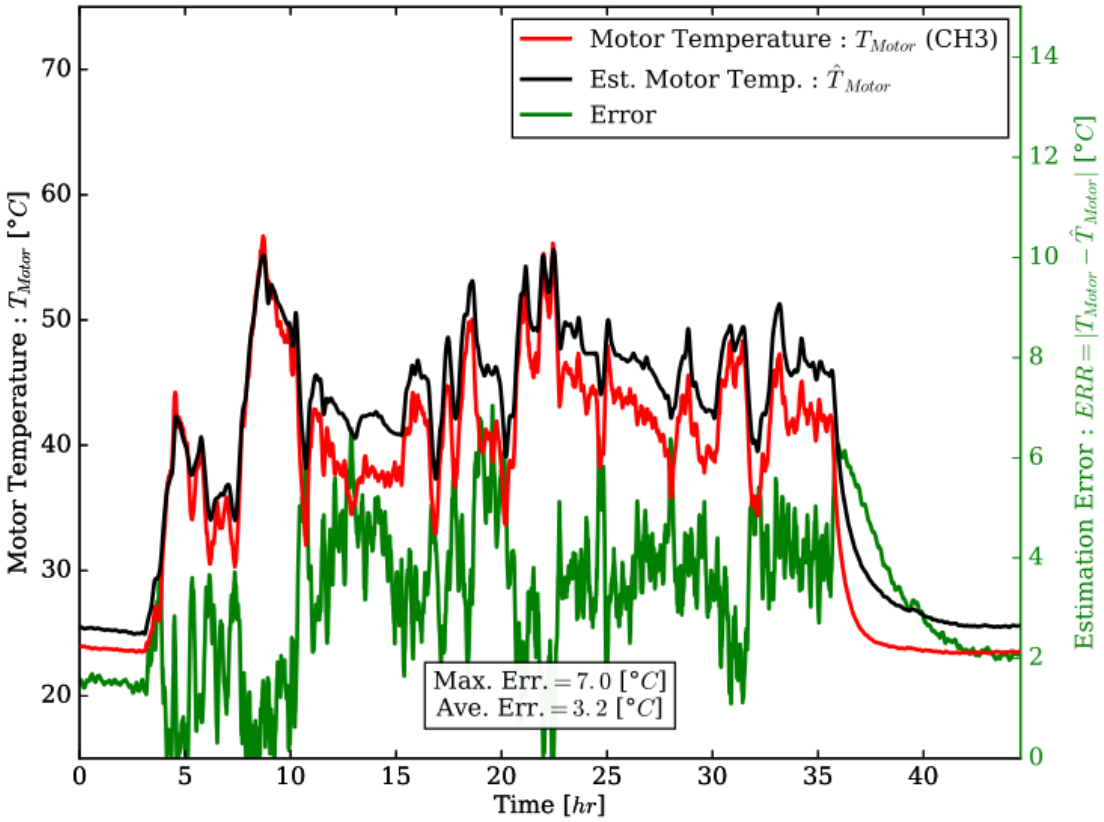

Figure 4.5: First-order model validation using median value of UA as shown in figure 4.2

of reduced airflow on the heat transfer dynamics, thus necessitating a higher order model.

To evaluate the capacitance of the thermal body that is interacting in the cooling samples, an energy balance may be applied over the duration of the sample, i.e. the energy of the body at the start of the sample must equal the energy of the body at the end of the sample plus the energy that has left the body over that period:

$$Q_i = Q_f \tag{4.11}$$

$$C_M T_{M,i} = C_M T_{M,f} + Q_{Out} \tag{4.12}$$

$$C_M = \frac{Q_{Out}}{T_{M,i} - T_{M,f}} \tag{4.13}$$

Where the energy that has left the body over the cooling period is given by the energy rejected to the cooling air:

$$Q_{Out} = \int_{t=0}^{t_f} \dot{m}\Delta h|_{Air}(t) = \sum_{t=0}^{t_f} \dot{m}\Delta h|_{Air}(t)\Delta t \tag{4.14}$$

If the energy removed during the cooling sample is plotted against the temperature difference between the start and end of the cooling sample, then the relationship between the two axes should be linear and increasing, with an intercept at the origin. By fitting a linear trend to the data, the slope of the trend will give the thermal capacitance of the body, as shown in figure 4.6. The fully-cooled data, as mentioned in section 3.4.1, is the subset of cool-downs for which the machine was able to fully cool, whereas the reduced samples are too short for the machine to have reached the same temperature as the cooling air. Since the relationship drawn between the energy removed and the motor temperature change that is used to estimate the machine capacitance requires that the all of the initially stored energy in the motor be released to the air, i.e. the motor be fully cooled to the cooling air temperature, only the fully-cooled samples are included in the linear fit.

While figure 4.6 shows that the data generally follows the trend, it is evident that the thermal capacitance that is interacting in the cooling regions is changing, as the deviation from the fitted line is as high as 100%. As such, it is not possible to quantify

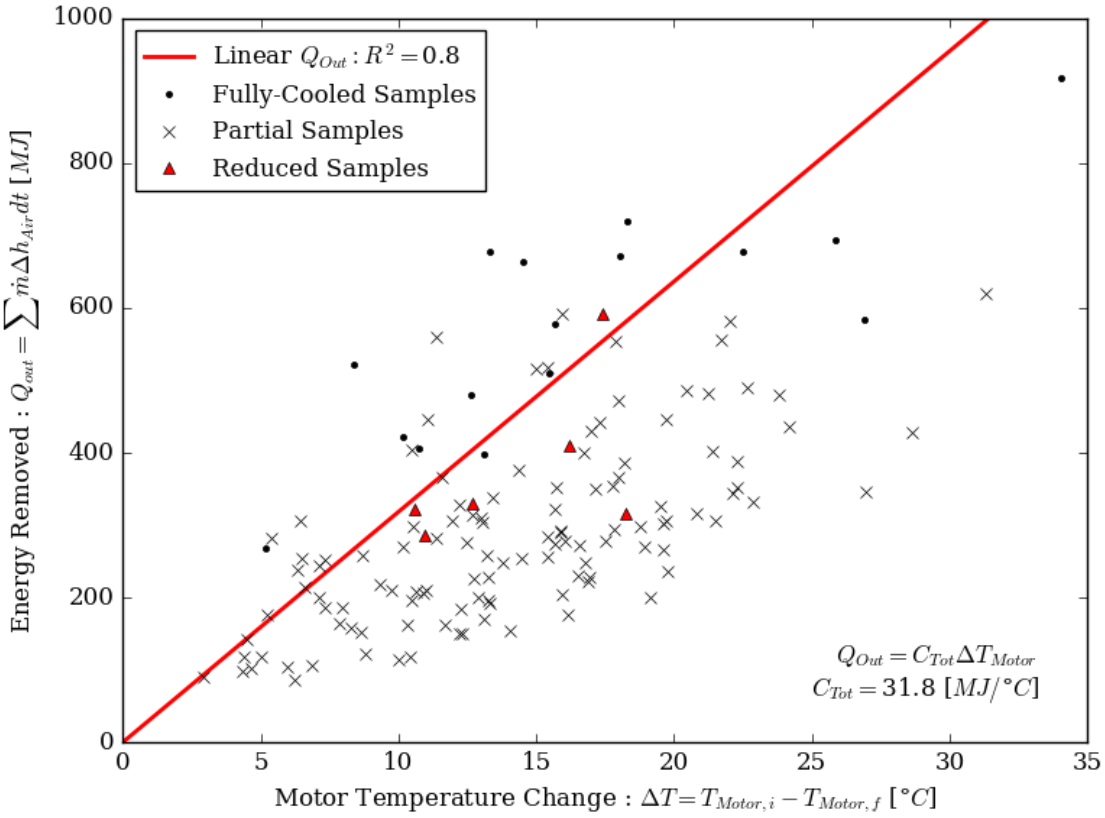

Figure 4.6: Energy removed vs. armature change in temperature. Linear relationship fit to data is expected to give first-order system capacitance by its slope.

the effects of reduced air-flow rate on the heat transfer of the motor given this data, and the first-order model of the motor is not appropriate for cooling-fan speed control.

4.4.3 Identified Deficiencies of the First-Order Model

The main deficiency of this approach identified was that the systems thermal capacitance was found to be changing, thus it can be concluded that the machine as a whole is distributed, where a changing level of thermal penetration affects the amount of thermally interacting volume, and thus a changing interacting thermal mass and capacitance. In this case, it is likely that the more distributed part of the system is

the armature spider, in which case as the thermal penetration front moves radially inward, additional interacting convective heat transfer surfaces will be exposed as well as additional thermal mass (figure 4.7). Modelling such a phenomenon would involve a much more detailed geometric model of the machine, as well as additional validation data of the temperature profiles of the machines other components, which is not available in this study. Furthermore, the solution would require the characterization of local convective heat transfer coefficients along the other interacting bodies, adding additional complexities to the solution. Though a fully distributed model is not a practical approach to this problem, the conclusion that the system is distributed may inform development of the model by allowing attempts to be made at including the effects additional thermal capacitance.

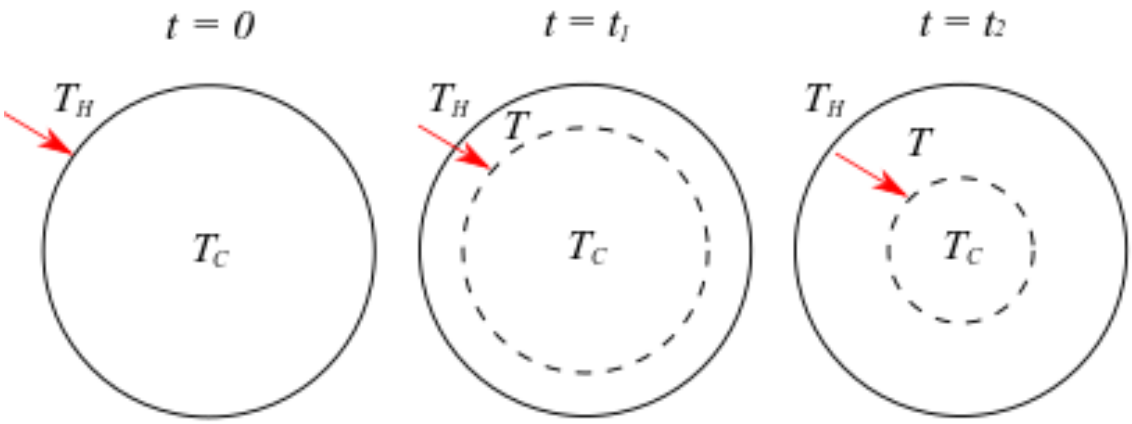

Figure 4.7: Schematic of the distributed conduction problem for a cylinder with a heat flux from the perimeter. The evolution of the conduction penetration-front is shown at times $t = 0$, $t = t_1$, and $t = t_2$.

Although the first-order thermal model for the machine was proven to be insufficient in characterizing the heat transfer in the system, particularly in determining the effect of varying the air flow rate, the performance of the model may be used to account for the interaction of non-lumped components to create a modelling approach

that may be more suitable. In order to identify the missing dynamics, the deficiencies of the first-order model must be identified, as well as which internal dynamics that were neglected by the assumptions may be causing these deviations to occur. So that the sample-to-sample variations in UA could be neglected, observations of the first-order model performance was considered using only the value of UA for which the error was minimized for the presented process-cycle, as shown in figure 4.8. Point A indicates a region of fast heating in which the model under-predicts, and point B indicates a region of fast cooling in which the model over-predicts. Additionally, it may be noted that for this value of UA, where the global error was minimized, the error in the model is typically much lower for the bulk of the machine operation, typically below 2-3 $°C$.

The combination of these effects suggests that there is an additional heat transfer path from the heat source, the armature windings, to the air via conduction to a thermal-sink (B) that also sees the cooling air. Heat is stored in the thermal-sink during rapid machine heating (A) and released directly to the cooling air during rapid cooling (B). This is supported by figure 4.9, which shows the motor and the inlet and outlet cooling air temperatures (y-axis) during a cool-down against the elapsed cooling time (x-axis). Figure 4.9 shows how during the cooling, after just under one hour, the outlet air cooling air temperature exceeds the measured motor temperature, which would not be possible unless heat is being transfered to the cooling air from a source with a higher temperature during that period. It is thus concluded that there is an additional heat transfer path from the measurement location of the motor temperature, the armature windings, and the cooling air through some additional thermal capacitance in the machine.

Given this conclusion, a higher-order model is proposed, for which there is an additional body that serves as a thermal sink and as a second heat transfer path

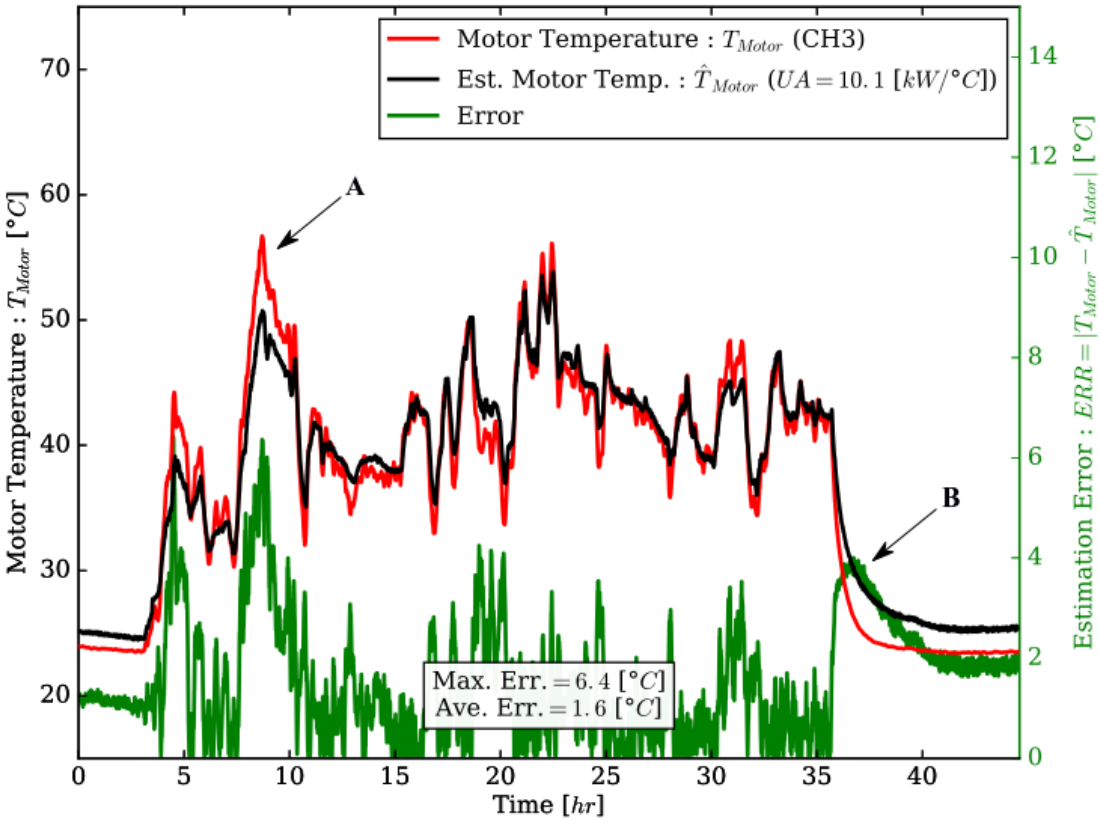

Figure 4.8: First-order model performance using the value of UA fit only to the modelled process-cycle. Point A indicates where the model under-predicts after being heated. Point B indicates where the model over-predicts during cooling.

through conduction from the armature windings to the convective heat transfer to the cooling air.

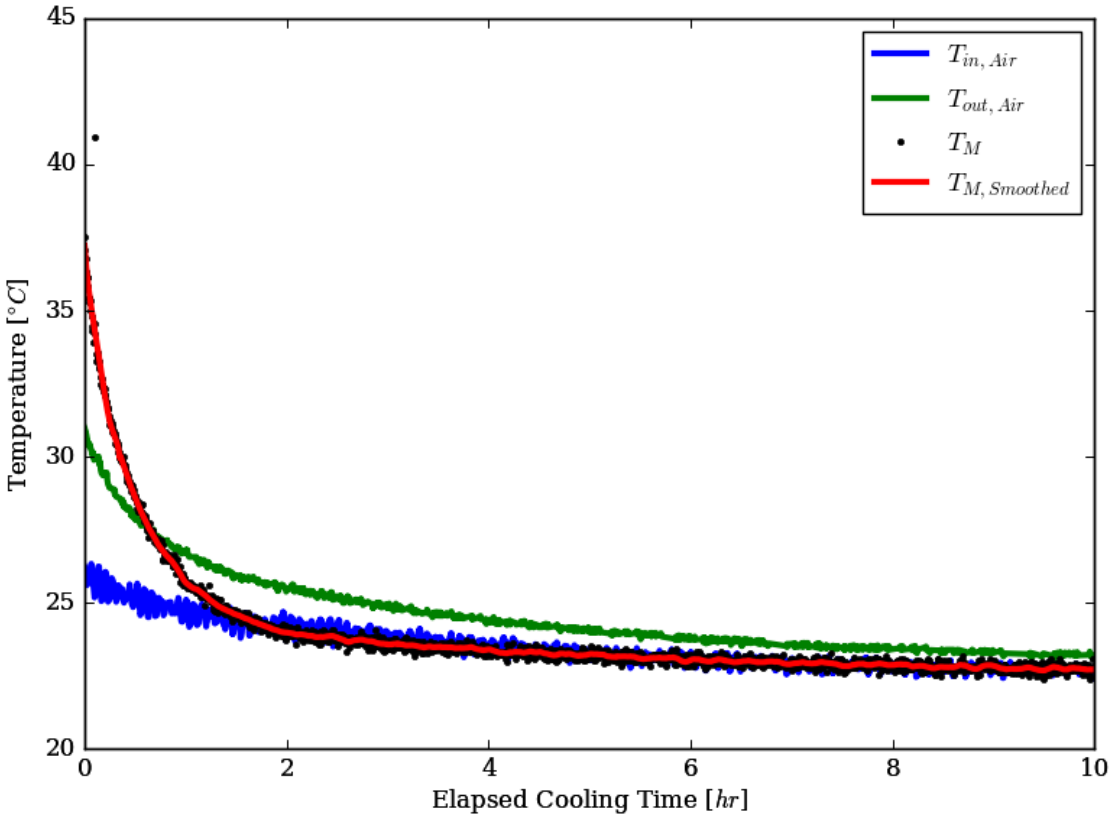

Figure 4.9: Motor and inlet and outlet cooling air temperatures plotted against elapsed time for a cool-down. The outlet cooling air temperature being higher than the motor temperature in the later stages of the cooling (past approximately 1 hour) emphasizes that there is a separate heat capacitance from which heat is being delivered to the cooling air.

Chapter 5

Second-Order Model and Identification Methodology

5.1 Introduction

The electrical machine thermal model proposed in this thesis attempts to consider the higher order (distributed) nature of large machinery by improving upon the lumped modelling approach currently used in industry. The proposed higher order model adds an additional lumped body, providing a conduction-convection path for the heat to be transferred from the heat generating body, the armature, to the cooling air, as opposed to the solely convection-based cooling of the first-order model. The additional lumped-body in this approach is intended to capture higher order system dynamics by providing a more accurate representation of the thermal behaviour of the machine in comparison to the first-order approach. This modelling approach was identified by first analyzing the system using the first-order model which suggested additional heat transfer paths which could account for regions in which the model was deficient.

The methodology presented for identifying the heat transfer parameters follows

three main analyses:

1. Data isolation

   (a) Identify and extract process-cycles from large dataset

   (b) Identify and extract cooling tests at 100% flow rate from large dataset

   (c) Identify and extract reduced flow rate tests from large dataset

2. System identification for the first-order model to inform initial guesses of second-order model:

   (a) Fit lumped model air-side energy balance to armature over process-cycles to determine the overall UA of the lumped model

   (b) Fit linear relationship between the energy removed by the cooling air and the motor temperature change over cooling test data to determine the overall thermal capacitance of the lumped model

3. System identification the second-order model:

   (a) Use overall UA and capacitance as determined in step 2 to inform initial guesses

   (b) Fit model results to cooling test data by minimizing error on the armature and outlet air temperature data to solve for the two thermal capacitances and the three thermal conductances of the model (C_{Arm}, C_{Sink}, UA_{Arm}, UA_{Sink}, UA_{Cond})

   (c) Characterize heat generation term by fitting the model to the process-cycle data

Table 5.1: Summary of heat transfer paths and parameters in the second-order model

	Armature	**Sink**
Heat Gen.	I^2R_E	None
Temp.	T_{Arm}	T_{Sink}
Capacitance	C_{Arm}	C_{Sink}
Heat Transfer	$\dot{Q}_{Conv,Arm}$ $\dot{Q}_{Cond}$	$\dot{Q}_{Conv,Sink}$ $-\dot{Q}_{Cond}$
HTC	$UA_{Conv,Arm}$ UA_{Cond}	$UA_{Conv,Sink}$ UA_{Cond}
ΔT	$T_{Arm} - T_{Air,Ave}$ $T_{Arm} - T_{Sink}$	$T_{Sink} - T_{Air,Ave}$ $T_{Sink} - T_{Arm}$

5.2 Second-Order Transient Model

The new thermal modelling approach for electric machines proposed in this thesis is an attempt to capture the higher order physics associated with a distributed model by approximating the distributed part of the system as a separate lumped thermal sink which interacts with a heat generating lumped body via conduction and with the cooling air via convection. This results in an additional path through which the heat generated in the armature windings may transfer to the air, as well as an additional thermal capacitance in which heat may be stored. A summary of the heat transfer that govern this model is presented in table 5.2. The schematic of this model is presented in figure 5.1.

5.2.1 Governing Equations of the Second-Order Model

Performing an energy balance on both the armature and thermal sink lumped-nodes results in two coupled ODEs: equation 5.2 (armature) and equation 5.4 (thermal sink).

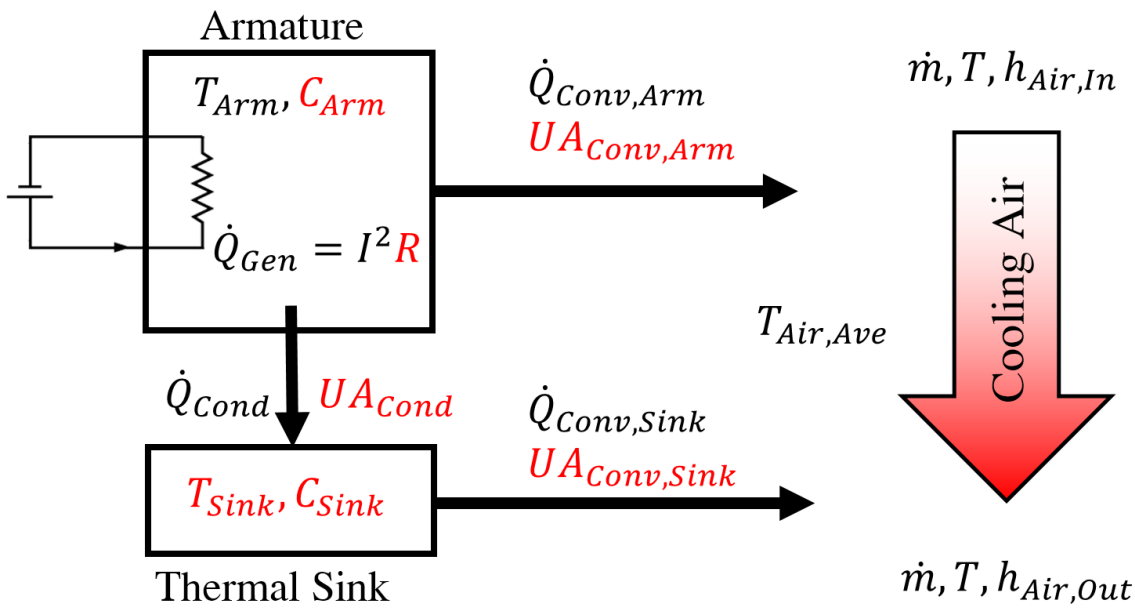

Figure 5.1: Schematic of the proposed second-order heat transfer model, including an additional heat transfer path to the cooling air from the heat-generating armature node through a thermal-sink, creating a second capactive node. Parameters shown in red text indicate the unknown parameters of the model.

$$-\dot{Q}_{Stored,Arm} = \dot{Q}_{Conv,Arm} + \dot{Q}_{Cond} - \dot{Q}_{Gen} \tag{5.1}$$

$$\begin{aligned} -C_{Arm}\frac{dT_{Arm}(t)}{dt} &= UA_{Conv,Arm}(T_{Arm}(t) - T_{Air,Ave}(t)) \\ &\quad + UA_{Cond}(T_{Arm}(t) - T_{Sink}(t)) - I(t)^2R_E \end{aligned} \tag{5.2}$$

$$-\dot{Q}_{Stored,Sink} = \dot{Q}_{Conv,Sink} + \dot{Q}_{Cond} \tag{5.3}$$

$$\begin{aligned} -C_{Sink}\frac{dT_{Sink}(t)}{dt} &= UA_{Conv,Sink}(T_{Sink}(t) - T_{Air,Ave}(t)) \\ &\quad + UA_{Cond}(T_{Sink}(t) - T_{Arm}(t)) \end{aligned} \tag{5.4}$$

Table 5.2: Second-order equation variables and their corresponding telemetries.

Variable	**Associated Telemetry**	**Real Time Acquisition**
Armature Winding Temperature : T_{Arm}	Internal data logger	No
Thermal Sink Temperature : T_{Sink}	N/A	N/A
Cooling Air Temperature : $T_{Air,Ave}$	External telemetry (calculated)	Yes
Cooling Air mass flow rate : $\dot{m}_{Air}$	External telemetry (calculated)	Yes
Cooling Air Temperature : Δh_{Air}	External telemetry (calculated)	Yes
Cooling Air Temperature : I	Production Data	Yes

Furthermore, by performing an energy balance on the cooling air passing over both components of the machine, equation 5.5 is found.

$$UA_{Conv,Arm}(T_{Arm}(t)-T_{Air,Ave}(t))+UA_{Conv,Sink}(T_{Sink}(t)-T_{Air,Ave}(t)) = \dot{Q}_{Out}(t) \quad (5.5)$$

Where:

$$\dot{Q}_{Out}(t) = \dot{m}(t)\Delta h|_{Air}(t) \quad (5.6)$$

The variables of these equations, as well as the data sets with which they associate, are tabulated in table 5.2.

5.3 Second-Order System Identification

5.3.1 Fitting of the Second-Order Governing Equations

For the application of this model, the six parameters must be identified: C_{Arm}, C_{Sink}, $UA_{ConvArm}$, $UA_{ConvSink}$, UA_{Cond}, and R_E. By observing cooling regions only, the heat generation term, R_E, may be omitted so that initially only the thermal capacitances

and HTCs must be solved. To solve for these parameters, the model equation solutions were fit to the real armature and outlet air temperatures, allowing for the simultaneous identification of all five parameters. Though another approach would be to use the process-cycle samples for the fitting of the model parameters, it was found that this is not practical for this model as convergence was not possible. This is suspected to be the result of a complex objective function, as the process-cycle behaviour is complex and non-monotonic, which impedes the ability of the parameters to be chosen such that the error may be minimized.

In order to fit the model solution to the outlet air temperatures, an estimated outlet air temperature based on the heat transfer in the estimated model was used. (Equation 5.7)

$$\hat{T}_{Out}(t) = \frac{\frac{((UA_{Conv,Sink}*(\hat{T}_{Sink}(t)-T_{Air,Ave}(t))+UA_{Conv,Arm}(\hat{T}_{Arm}(t)-T_{Ave,Air}(t))}{\dot{m}_{Air}(t)} + c_{in}(t)T_{In}(t)}{c_{out}(t)} \tag{5.7}$$

The least-squares method using the LMFIT (40) optimization tool in Python was used to minimize the objective function, given by equation 5.8. Since both internal and external data sets are used in this calculation, it is necessary for both input data sets to be at the same sampling rate, thus the external data set is down-sampled from $1s$ to $20s$, using the mean of the depreciated samples.

$$S = \sum_{i=1}^{n} r_i^2, \qquad r_i = |T_{Arm} - \hat{T}_{Arm}| + |T_{Out} - \hat{T}_{Out}| \tag{5.8}$$

5.3.2 Initial Condition to the Solution of the Governing Equations

While the initial value of the armature temperature can be easily taken from the data, the solution of these equations additionally requires the initial condition of the thermal sink. Due to the manner in which the ODEs describing the armature windings and the thermal sink are coupled, the temperature of the sink will depend on all three HTCs, as well as both thermal capacitances and the integration of heat transfer over the preceding process-cycle, unless the system is initially at steady state at the onset of cooling. In order to simplify the solution, it was assumed that at the onset of every cool-down, the machine was starting at a steady-state temperature distribution, which gives rise to the following initial condition to the thermal sink temperature:

$$T_{Sink_{i,SS}} = \frac{UA_{Cond}T_{Arm_i} + UA_{Conv,Sink}T_{Air,Ave}}{UA_{Cond} + UA_{Conv,Sink}} \tag{5.9}$$

The effect of using this steady-state start assumption in the analysis of cool-down samples for which the assumption does not hold (i.e. the machine does not start at a steady-state temperature distribution at the onset of cooling) is the underestimation of the model parameters. This effect is discussed in detail in appendix C1.

5.3.3 Initial Guesses of Fitting Parameters

To attain convergence, the fitting requires initial guesses of the parameters that are close in magnitude to the true values. Since the only information available about the heat transfer in the machine is that which was gathered from the first-order modelling attempt in section 4.3, the HTC and capacitance determined may be used to constrain the initial guesses of the overall HTC and capacitance of the higher order

model. From a circuit-analogue analysis, an overall HTC may be written in terms of the second order model HTCs, accurate only when the machine is at a steady-state temperature distribution, equation 5.10. Noting that the overall HTC of the second order model must be the HTC of the first-order model, equation 5.10 may be rewritten as equation 5.11 so that a more well-defined parameter, UA_{Tot}, may be used as a model input instead of one of the unknown additional HTCs.

$$UA_{Tot} = UA_{Conv,Arm} + \frac{1}{\frac{1}{UA_{Cond}} + \frac{1}{UA_{Conv,Sink}}} \tag{5.10}$$

$$UA_{Conv,Arm} = UA_{Tot} - \frac{1}{\frac{1}{UA_{Cond}} + \frac{1}{(UA_{Conv,Sink}}} \tag{5.11}$$

As an initial guess, all HTCs specific to the second order model will be set equal. Using the median value of UA_{Tot} found in section 4.3.2, 11.4 $kW/°C$, the specific second order HTC initial guesses are left to each be 7.6 $kW/°C$.

In order to use the knowledge gained from the first-order analysis performed earlier to inform the initial guesses of the second-order model capacitances, it is necessary to determine the relationship between the overall machine capacitance that was determined under the first-order assumption, and the two capacitances of the second-order model. If the cooling of a second-order system is to be modelled as an equivalent first-order system, then the change in stored energy over the cooling of each must first be equal.

$$\Delta Q_{Stored,First-Order} = \Delta Q_{Stored,Second-Order} \tag{5.12}$$

$$\Delta Q_{Stored,First-Order} = C_M(T_{M_i} - T_{M_f}) \tag{5.13}$$

$$\Delta Q_{Stored,Second-Order} = C_{Arm}(T_{Arm_i} - T_{Arm_f}) + C_{Sink}(T_{Sink_{i,SS}} - T_{Sink_f}) \tag{5.14}$$

Because the armature temperature is that which was used in the first-order approach earlier, it can be noted that the first-order motor temperature is equivalent to second-order the armature temperature. It will then follow that:

$$C_{Tot}(T_{Arm_i} - T_{Arm_f}) = C_{Arm}(T_{Arm_i} - T_{Arm_f}) + C_{Sink}(T_{Sink_{i,SS}} - T_{Sink_f}) \tag{5.15}$$

Considering the steady-state temperature of the sink as defined in equation 5.9 and assuming that the machine is fully cooled it will follow that $T_{Sink_f} = T_{Arm_f} = T_{Air,Ave}$. As an additional simplifying assumption, the average cooling air temperature throughout the cooling will be assumed constant, such that $T_{Air,Ave} = T_{Sink_f} = T_{Arm_f}$, which will then give that $T_{Sink_{i,SS}} = (T_{Arm_i} T_{Arm_f})$. Using this relationship for $T_{Sink_{i,SS}}$, equation 5.15 then becomes:

$$C_{Tot} = C_{Arm} + \frac{1}{2} C_{Sink} \tag{5.16}$$

To better understand the relationship between the first- and second-order models, as well as the effect of the steady-state start condition, a second-order model was numerically studied by generating simulated cool-down samples with varying initial temperatures of both the armature and the thermal sink (see appendix C1). This simulated data set was then analyzed using the energy-based capacitance estimation

from section 4.4.2, and it was found that if the steady-state start condition is met, the overall capacitance will be constant, i.e. plotting the energy removed against the armature temperature change will yield a linear relationship (figure 5.2). When the steady-state-start condition is not achieved, the data points will fall below the expected linear relationship (figure 5.3). Physically, this occurs because the initial sink temperature will actually be lower than the steady state value at the given initial armature temperature, which reduces the thermal sinks contribution to the total initial energy stored, resulting in a lower equivalent-lumped thermal capacitance.

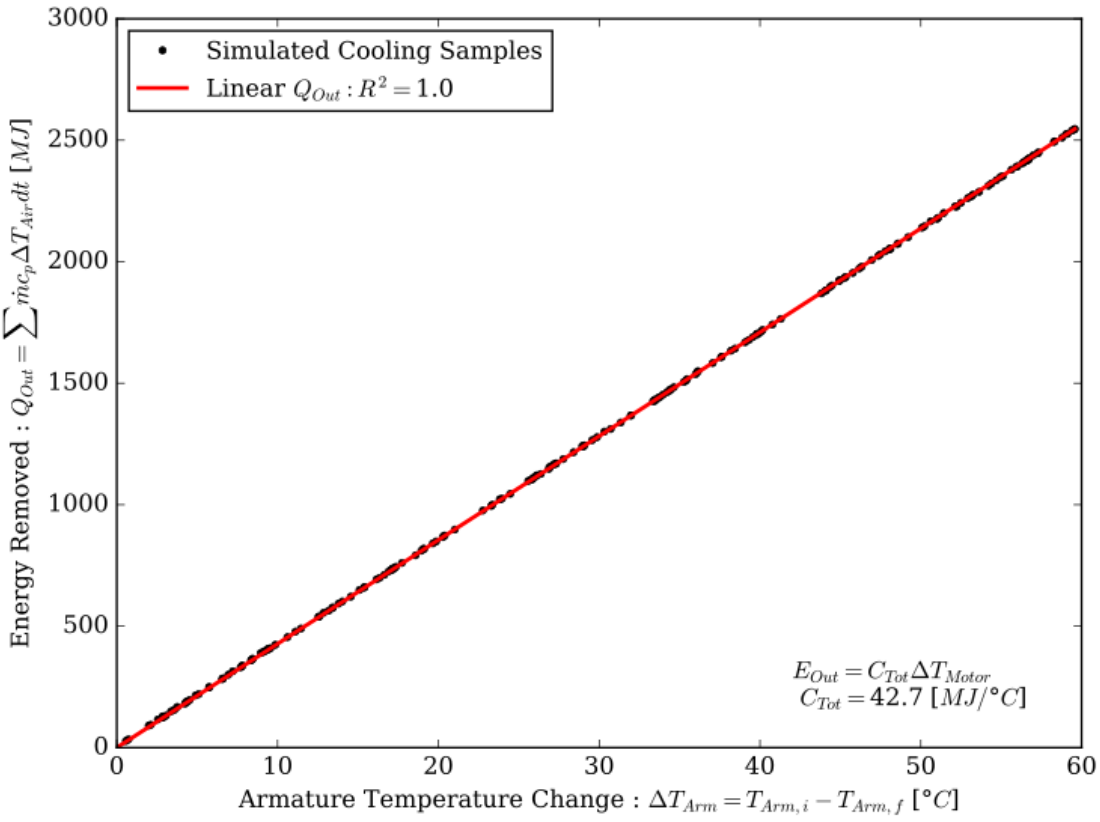

Figure 5.2: Energy removed by cooling air vs. armature temperature change for simulated, second-order, steady-state-start cool-downs.

As the existence of non-steady-state starts in the data results in the underestimation of the overall system capacitance, it is reasonable to assume that the highest

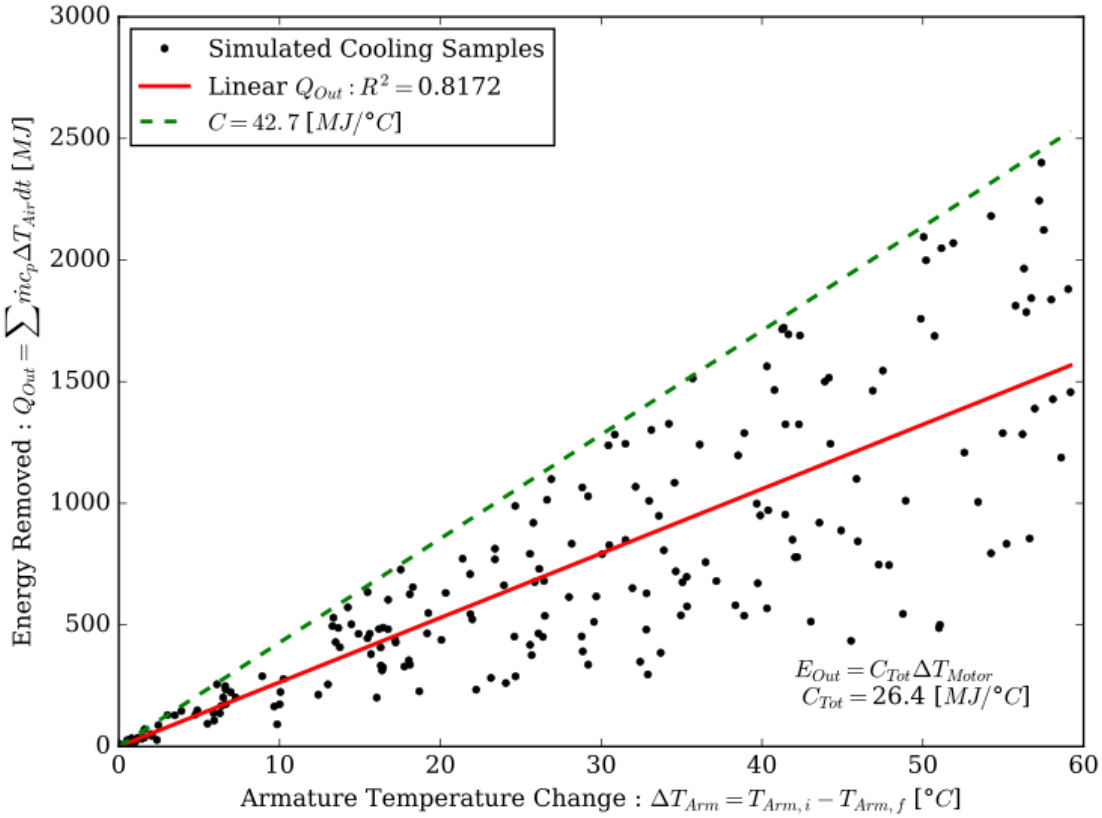

Figure 5.3: Energy removed by cooling air vs. armature temperature change for simulated, second-order, non-steady-state cool-downs.

possible value of the overall capacitance as determined in this method will be a more accurate estimation of the overall capacitance of the system. This is because the highest values of overall capacitance as determined in this analysis are expected to come from the analysis of samples that are the closest to meeting the steady-state start condition, thus for these samples, this analysis will be the most valid. The relationship shown in 5.16 can then be drawn between the lumped capacitance and two capacitances of the higher order analysis by equating the heat stored in both models for the same steady-state armature temperature at the onset of cooling, where C_{Tot} is the maximum value of the overall thermal capacitance, as shown in figure 5.4 which

presents the analysis performed in section 4.4.2 with the addition of the new understanding of the effect of the cool-down data not beginning at steady-state, which gives the line $C_{Tot} = 60\ MJ/°C$.

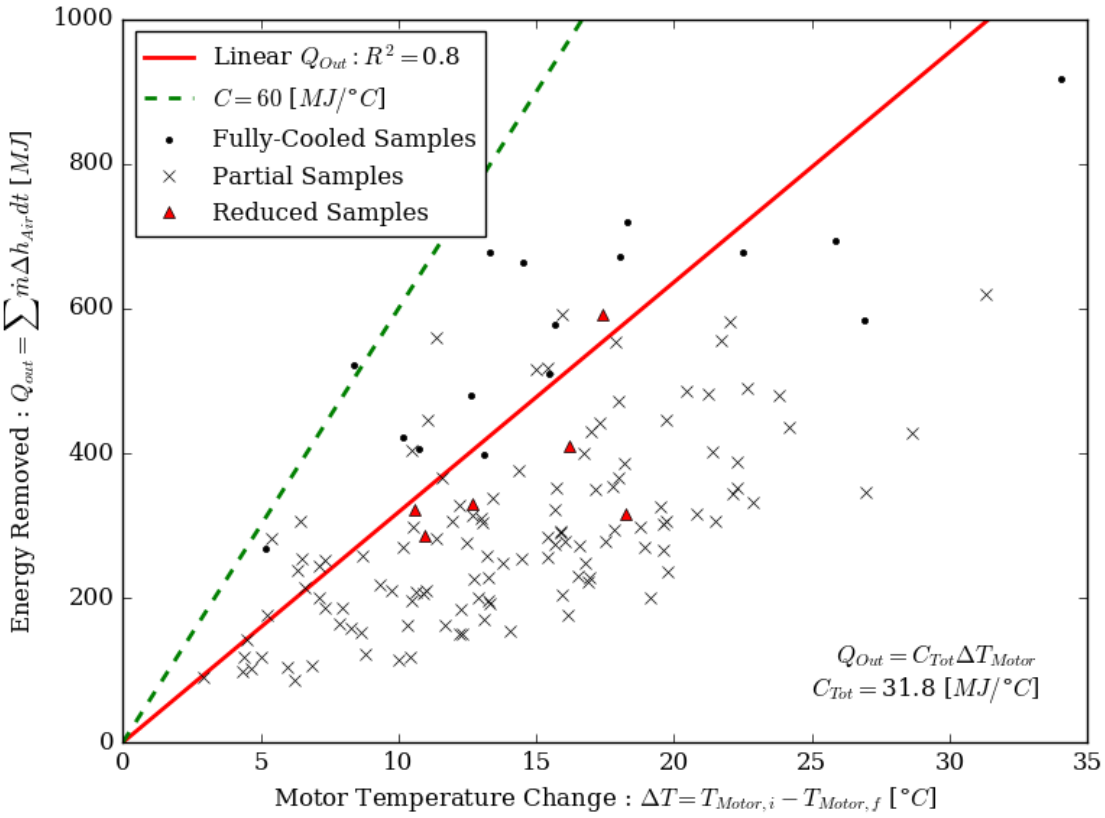

Figure 5.4: Energy removed vs. armature temperature for real cool-down data. Upper-limit of spread will more accurately identify the overall machine capacitance for non-steady-state-start cool-downs.

From the performance of the first-order model during cooling shown in figure 4.8, it is reasonable to assume that the capacitance of the thermal sink is much greater than that of the armature, as the measured armature temperature falls much faster than the estimated over-all machine temperature which is based on the total energy convected to the cooling air, suggesting that the additional body which is releasing energy to the cooling air has stored more energy than the armature. As an initial

guess, it was assumed that the sink capacitance was an order of magnitude (10x) greater than the armature capacitance, based on the approximate ratio of the total thermal capacitance of copper (of which the armature windings are composed) to steel (which comprises the rest of the machine). The initial guesses of the armature and thermal sink capacitance are then found to be 10 and 100 $MJ/^{\circ}C$, respectively.

5.3.4 Second-Order Fit Results

Since the program was unable to attain acceptable convergence on the first attempt, likely due to the presence of local minima in the objective function due to slight waviness in the smoothed temperatures, the algorithm was iterated so that better convergence could be reached. A discussion of the error function minimized in this approach, as well as a discussion on the method used to help reach convergence, is presented in Appendix C2. As the ranges of values achieved were very large, with some results being likely unphysical ($C_{Sink} \approxeq 0$), the data presented is that which lies within the 40-60 percentile range, excluding all other samples as outliers. The results of this analysis are shown in figure 5.5 and 5.6, where boxplots are used to show the distribution of the spread of the parameters determined from the samples. The figure text-boxes indicate the median values of these spreads, as well as their upper and lower limits.

A significant observation of the second-order model parameters identified is the wide spread of values over which they lie, particularly in the thermal sinks capacitance and convective HTC. This is similar to observations made in the discussion of the lumped-equivalent capacitance presented in section 4.4.3, where the spread of the determined parameters was found to be the result of the machine not being at steady-state at the onset of the cooling samples. The sample-sets simulated in

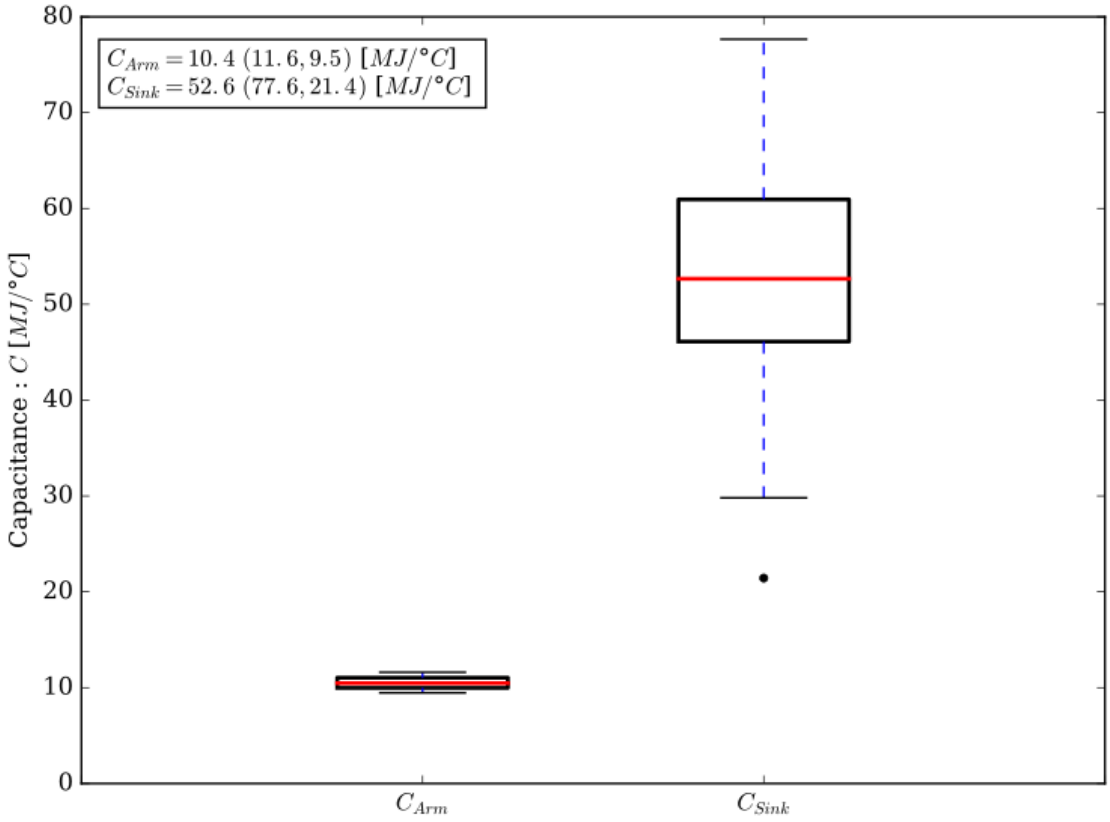

Figure 5.5: Second-order capacitances found from the fitting of second-order model to cool-down data. Boxplots are used to visually represent the spread of the data.

appendix C1 using both steady and non-steady state start conditions were then analyzed using the second-order system identification approach to determine the effects of the steady-state-start assumption on the identification results. It was found that for samples in which a steady state starting condition was not achieved, the heat transfer parameters were under-predicted. When a large set of results from various degrees of non-steady-state start conditions are amassed, the resultant distribution of the parameters will hold a wide spread, the shape of which is the result of the degree to which the samples were saturated. Thus, the median of the spread does not estimate the true value of the overall component capacitance. Since non-steady-state start conditions consistently skew the results downwards, it follows that the upper

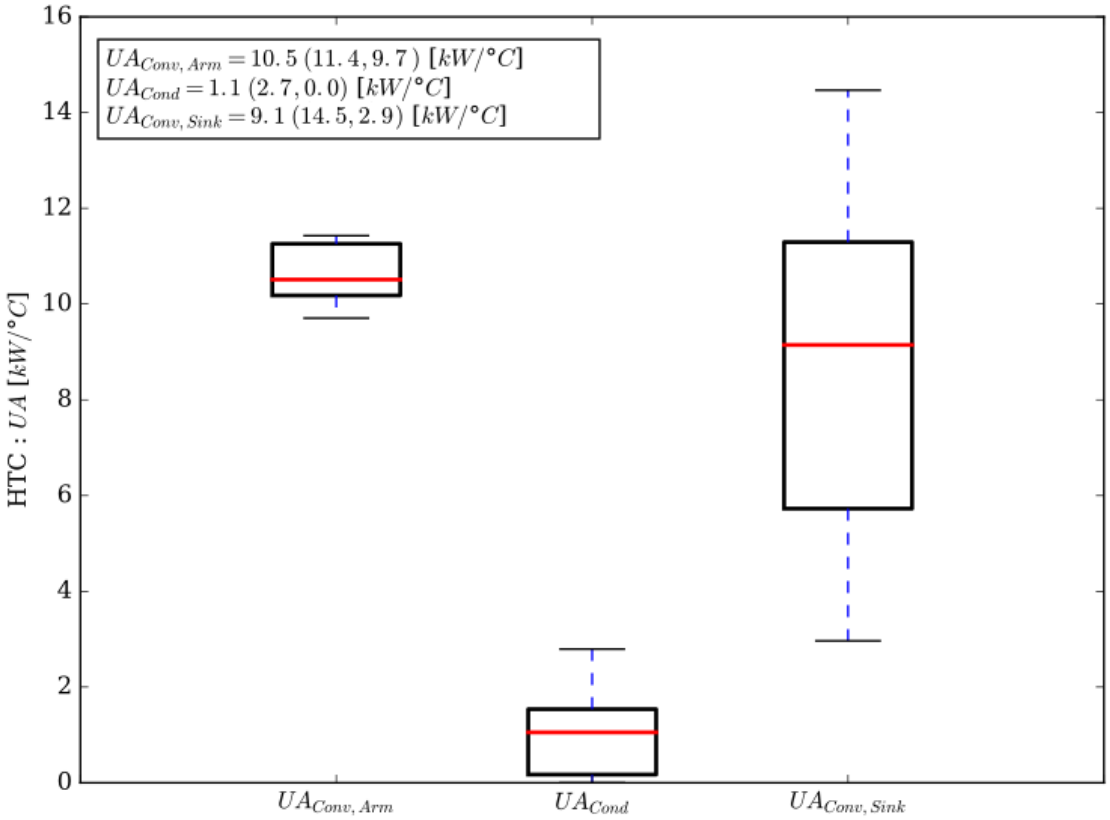

Figure 5.6: Second-order HTC's found from the fitting of second-order model to cool-down data. Boxplots are used to visually represent the spread of the data.

limit of the parameter spreads more closely estimate the true parameters. Therefore, from this analysis, it can be concluded that the effects of a non-steady-state start can be accounted for approximately by observing the distribution of parameters obtained from the fitting of many samples and using the higher values of the distribution as a the estimation of the parameters true value.

In order to assess the validity of fitted parameter values, approximate values of the machine component capacitances are compared. Based on the geometries shown in appendix A; with the copper and steel densities taken as 8933 and 7800 kg/m^3, and specific heat capacities of 385 and 434 $J/kg°C$ (24), respectively; the heat capacity of the armature windings (copper) and the stator (steel) were found to be 16 and 100

$MJ/°C$, respectively. As these calculated values are similar in magnitude to those of the fitted results, the parameter values found in this section are considered to be valid.

5.3.5 Identification of Electrical Resistance for Heat Generation

The first method attempted was based on the premise that the only significant energy input to the system was by Joule losses in the windings, and that the only significant removal of energy from the system was the cooling air. As it was found that the measured temperature change of the machine between the start and end of the process-cycles was typically below the error of the reading (2.2 $°C$), the change in sensible heat of the machine was neglected. Under this hypothesis, these energies were calculated by discretizing over the process-cycles, and summing the quantities:

$$
\begin{aligned}
Q_{in} &= Q_{out} \\
Q_{in} &= \int I(t)^2 R_E \rightarrow R_E \sum I(t)^2 dt \\
Q_{out} &= \int \dot{m} \Delta h|_{Air}(t) \rightarrow \sum \dot{m} \Delta h|_{Air}(t) dt
\end{aligned}
$$

This leaves only R_E to be determined, for which the energy balance may be rearranged:

$$
R_E = \frac{Q_{out}}{\sum I(t)^2 dt}
$$

This quantity was calculated over the isolated process-cycles, and are presented in figure 5.7, which displays the spread of the determined values of each process-cycle

in a boxplot overlaid upon the actual data, to which some x-axis jitter was added to improve readability. It is worth noting that while this analysis assumes that only Joule-losses are responsible for heating in the system, it would be expected that any additional losses be captured by the calculation of the energy removed, thus R_E, and the calculated heat input, would be corrected to approximately account for the average heat input by other losses previously neglected.

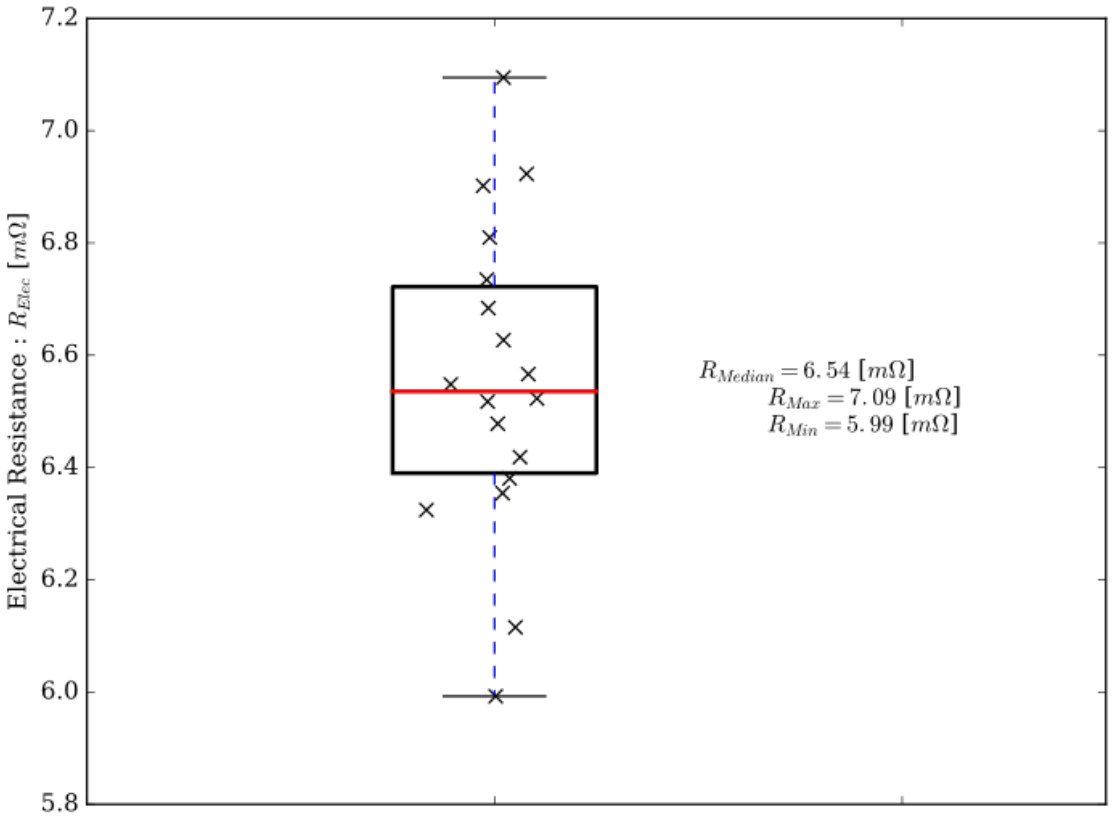

Figure 5.7: Motor winding electrical resistance as determined by the energy-balance method.

The resultant armature temperature estimation, using the median value of R_E from figure 5.7, is shown in figure 5.8, where the armature temperature, both measured and estimated, (left axis) is plotted against the duration of the process-cycle, as well as the error in the estimation (right axis). Both the maximum and the average error

over the process-cycle are indicated in the figure text-box.

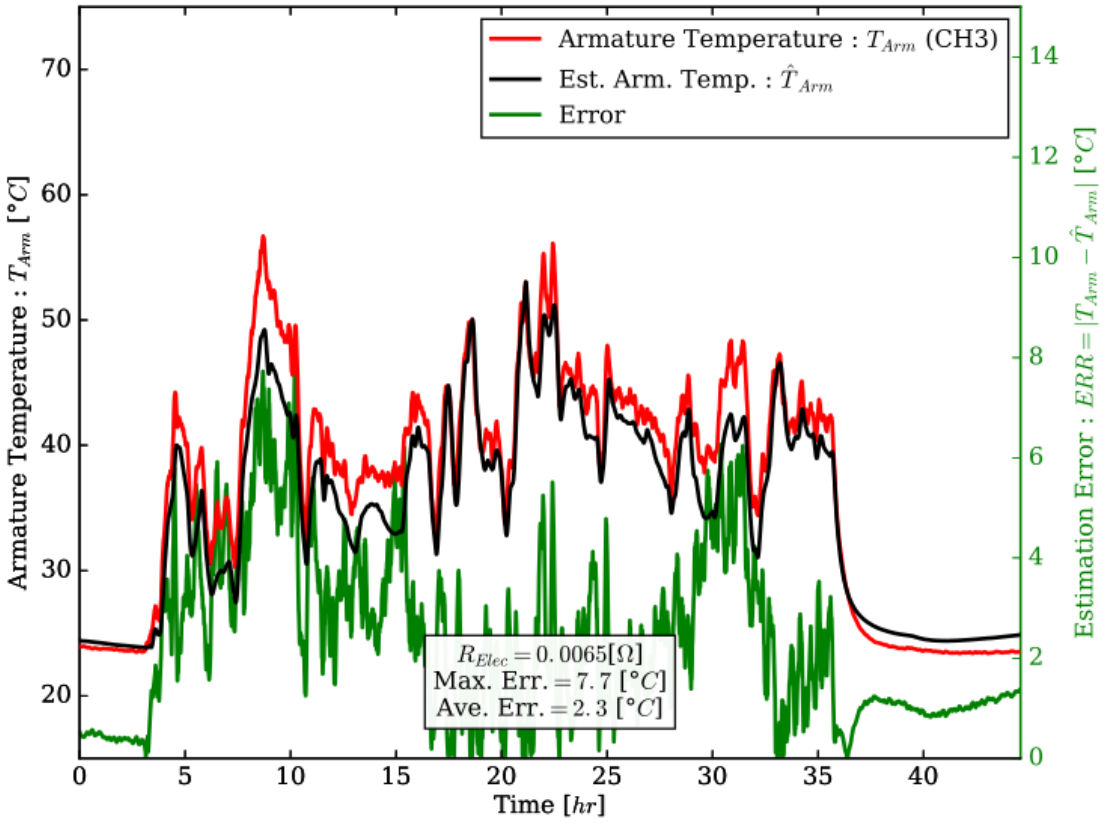

Figure 5.8: Plot of measured and second-order-estimated armature temperature (right axis) with estimation error (right axis)

5.3.6 Identification of Reduced Cooling Effects in the Second-Order Model

Once all of the heat transfer parameters are found for the base-case of 100% fan speed, the effect of reduced fan-speed and air mass-flow rate on the parameters must be determined. Since only the convection HTC parameters are expected to depend on the air mass-flow rate (speed), the thermal capacitances as well as the conduction HTC may be assumed constant. For the six reduced flow-rate tests, the fitting process

in section 5.3.1 was repeated with the estimated and constant values of C_{Arm}, C_{Sink}, and UA_{Cond}. The results of this analysis are presented in figure 5.9 and figure 5.10 for the armature and thermal sink respectively, where the determined HTC's are plotted against the cooling-air mass flow rate. The boxplot presented at the highest cooling-air mass flow rate (approximately 18 kg/s) shows the spread of the values determined from the maximum-flow-rate samples, as determined in section 5.3.

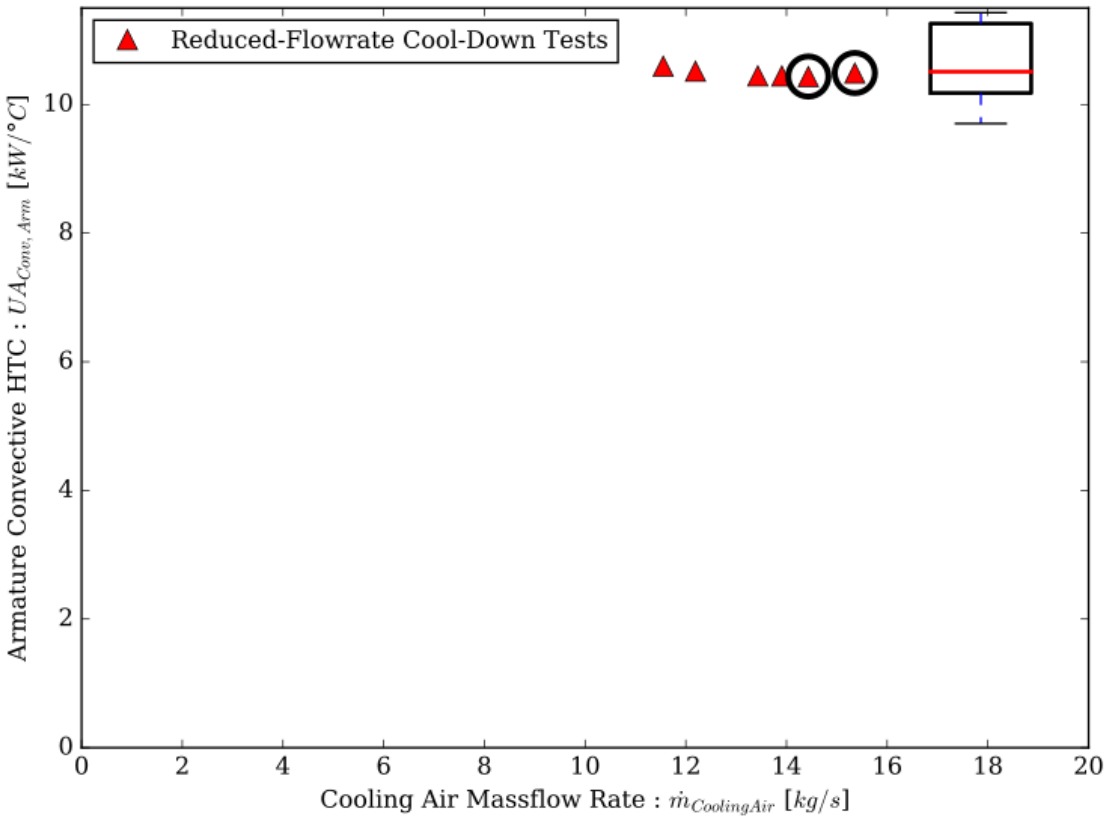

Figure 5.9: Armature convective HTC vs mass flow rate determined by the fitting of second-order model to the cool-down data. The distribution of the full-flow rate samples is represented by a boxplot. Reduced flow rate samples presented separately.

The circled data points on figure 5.9 and figure 5.10 indicate the samples for which an acceptable fit was achieved, such as the one shown in figure 5.11, for 80% fan speed. The other samples, such as the one shown in 5.12 for 60% fan speed did not achieve an

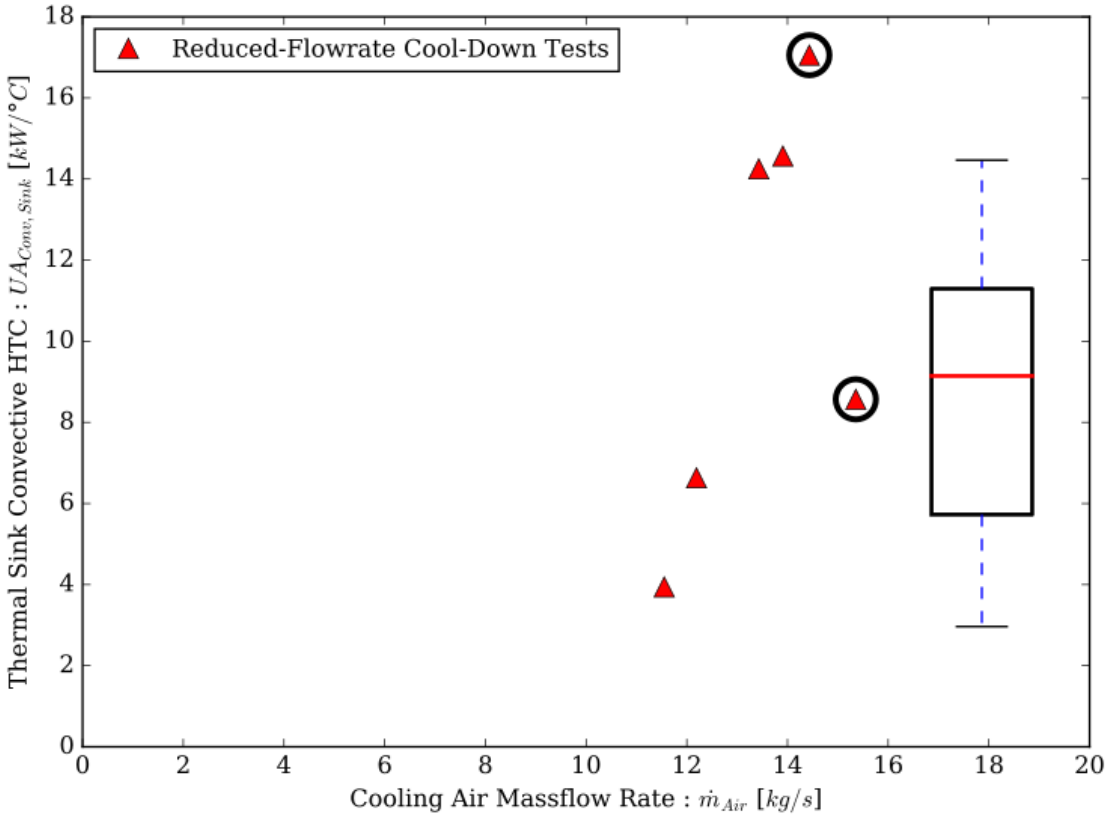

Figure 5.10: Thermal-sink convective HTC vs mass flow rate determined by the fitting of second-order model to the cool-down data. The distribution of the full-flow rate samples is represented by a boxplot. Reduced flow rate samples presented separately.

acceptable fit, as the flow rate was not adjusted until part-way through the cooling. Since the solved model assumed a fixed HTC during the sample, the change in mass flow rate mid-way through the sample due to the difficulties in planning the manual adjustment of the fan speed impedes the proper fitting of the model parameters, as the HTC undergoes a step-change with the mass-flow rate, which is not accounted for in the model when it is fit to the data. This results in potentially large errors in the determination of the HTC and capacitances.

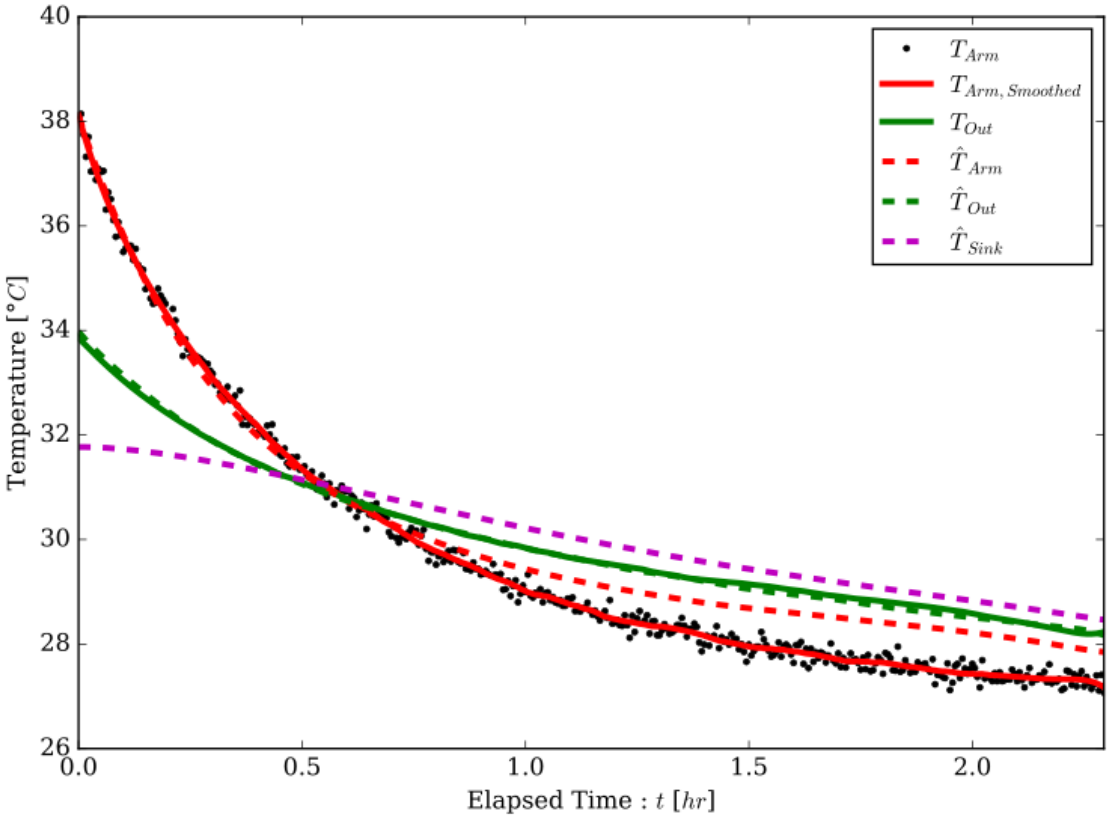

Figure 5.11: Attempted fit of second-order model to reduced flow-rate cool-down sample at 80% fan speed. Fit is good for the first half of the cooling, though deviation occurs in the later half.

5.4 Second-Order Model Validation

5.4.1 Second-Order Modeling of Armature Temperature

Figure 5.13 shows the resultant motor temperature estimation by the second-order modelling approach for a process cycle, as well as the actual armature temperature and the error through the cycle, using the upper values of the heat transfer parameters as discussed in section 5.3.4, and tabulated in table 5.3. In the figure, the measured and estimated armature temperatures (left axis) are compared over the duration of the process-cycle, (y-axis) along with the error between them (right axis). Points

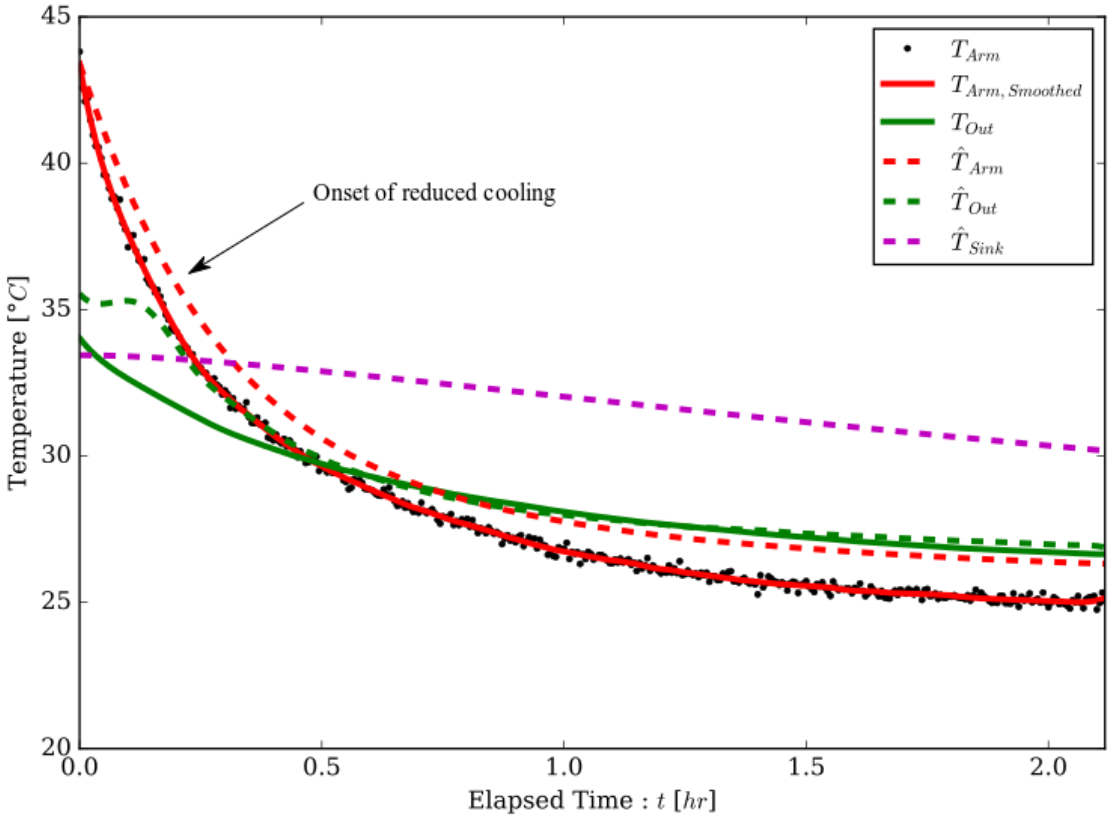

Figure 5.12: Attempted fit of second-order model to reduced flow-rate cool-down sample at 60% fan speed. Good convergeance was not met, as a step-change in the mass-flow rate, and thus HTCs, occurred approximately 20min into the test.

A and B indicate the periods of fast transients in heating and cooling, respectively, similar to that shown for the first-order model in figure 4.8 where they were under-predicted (A) and over-predicted (B). Point C indicates a region where the model accurately predicts the motor's behaviour in both heating and cooling. D indicates a region where the model under-predicts in both heating, operation, and in cooling.

Referring to figure 4.8 for the first-order model and figure 5.13 for the second-order model, the second-order model can be seen to perform much better in the prediction of the armature temperature during rapid and extensive cooling (B), indicating that the attempt to include an additional heat transfer path with a second thermal capacitance

Table 5.3: Model parameters used in second-order model, as determined in section 5.3.4

Parameter	**Value**
C_{Arm}	11.6 $[MJ/°C]$
C_{Sink}	77.6 $[MJ/°C]$
$UA_{Conv,Arm}$	11.4 $[kW/°C]$
$UA_{Conv,Sink}$	14.5 $[kW/°C]$
UA_{Cond}	2.7 $[kW/°C]$
R_E	6.5 $[m\Omega]$

to account for the deficiency in the first-order model produced generally better results.

The maximum and average errors in estimation using the second-order model for the 18 isolated process-cycles, in $°C$, are shown in table 5.4.

Comparing the errors of all 18 process-cycle samples as tabulated in tables 4.2 and 5.4 for both maximum and average errors in $°C$ over the process-cycle estimations, it is found that the second-order model performs better than the first-order model.

It is seen in figure 5.13 that in some case (D) the model under-predicts, while in others it predicts much more accurately (C) despite both of these regions being preceded by similar thermal cycles (heating up quickly, then cooling down gradually). Incorrect heat transfer parameter estimation of would result in globally poor performance, therefore it is likely that the differences are due to the inaccuracy of the assumption that losses in the machine are due to Joule-heating only. Core-losses, which are a function of both input current and motor speed, are therefore believed to contribute significantly to heat generation in the machine. As discussed in section 2.3.1.1, the identification of the parameters involved in the core-loss terms requires specific and methodical testing of the equipment, which was not available in the present study. Additionally, both core-loss terms depend upon the motor speed, which was also not

Table 5.4: Second-Order model validation error for 18 process-cycles

Sample	**Max** $[^{\circ}C]$	**Average** $[^{\circ}C]$
1	6.6	1.7
2	8.6	3.3
3	6.7	1.8
4	6.9	1.7
5	4.7	1.5
6	6.6	1.8
7	6.8	2.1
8	6.8	2.3
9	6.2	2.2
10	5.0	1.8
11	4.1	1.9
12	4.9	1.4
13	6.1	1.6
14	5.9	1.6
15	7.7	2.3
16	7.6	2.0
17	6.5	1.9
18	4.5	1.7
Max	**8.6**	**3.3**

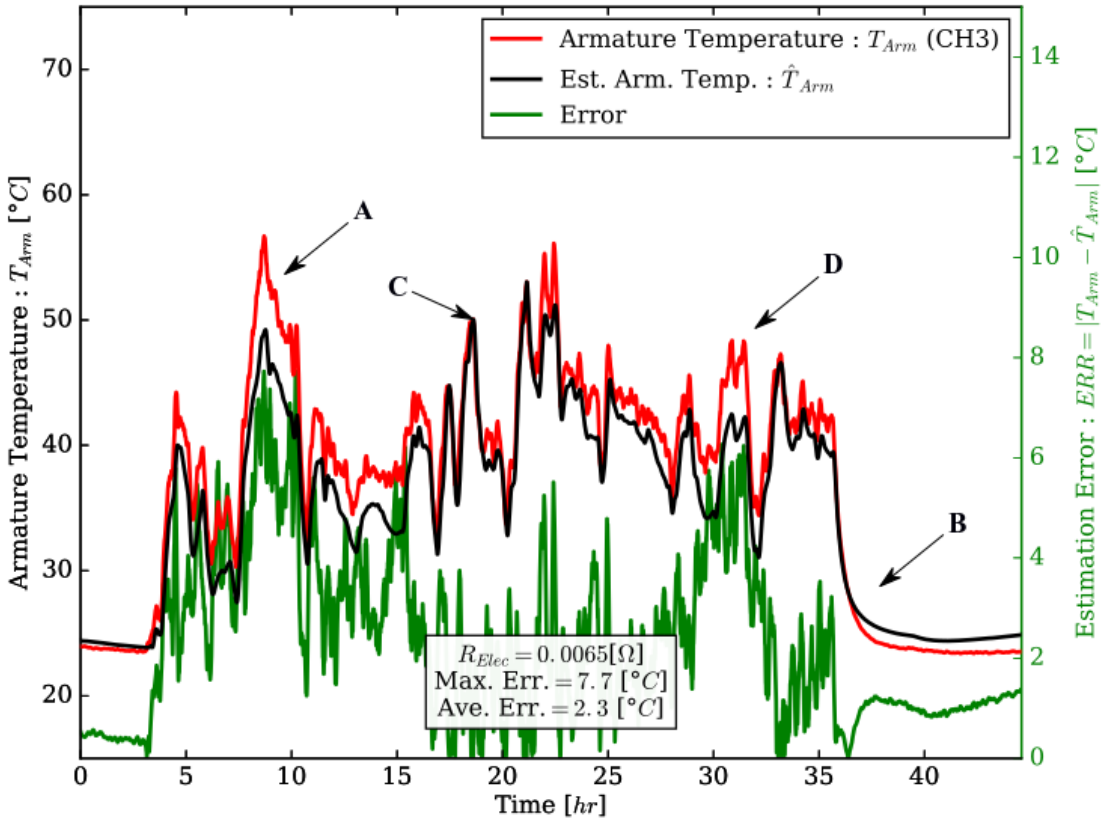

Figure 5.13: Plot of measured and second-order estimated armature temperature (right axis) with estimation error (right axis) for process-cycle sample 15.

captured in this study.

5.4.2 Reduced Cooling Effects in the Second-Order Model

Though the first-order modelling approach was able to provide a good estimate of the motors temperature, the change in the convective HTC could not be determined since there was too much variability in the determined machine time-constant that the effect of reduced cooling on the time-constant could not be determined. Though it was hoped that the inclusion of the additional heat transfer path and thermal capacitance would provide a basis under which some of the skewing effects of the

distributed machine dynamics could be minimized, this was not found to be the case. In the second-order model, it was also found that the presence of non-steady-state starts in the cooling data resulted in a high variance of the determined parameters, especially those concerning the thermal sink.

As described in the section 5.3.4, the true value of the parameters may be estimated by using the upper-limit of the parameter spread, which was found to be a better estimate, as the non-steady-state starting condition in the cooling samples tended to skew the results downwards. However, this approach requires that extensive cooling samples exist in order to establish a well-defined parameter spread. Since the extent of the reduced cooling tests was very limited, as only a single test was performed at each reduced fan speed, the effects of a non-steady-state start condition cannot be accounted for at this time, as it is possible and likely that the values determined at reduced flow-rates shown in figure 5.9 and figure 5.10 under-predict the actual trend due to the tests being sensitive to the initial condition of the machine at the start of the test. It is worth noting that these observations hold true for both the first- and second-order modelling methods, thus given sufficiently extensive reduction tests, or cooling tests where the machine is truly at a steady state at the onset of the cooling, both first and second-order models have potential to be used as machine temperature monitoring methods under reduced cooling air flow-rates.

Chapter 6

Conclusions and Future Recommendations

6.1 Conclusions

The objective of this study was to develop an on-line modelling methodology in order to model the thermal behaviour of large, through-ventilated DC machines used in industry. The motivation for the development of this model was its implementation in the control of the machines cooling rate for energy conservation through the monitoring of the machines critical temperature. The key limitations to the modelling of machines used exclusively in industrial processes is that opportunities for controlled testing are limited, as any time taken for these tests results in production down-time, thus the costs due to lost productivity are immense. As such, the development of the model identification methodology required that the only inputs be those which can be captured during normal machine operation. This presents a departure from most of the literature, which focuses on results of well-characterized controlled testing.

The methodology presented in this work takes the form of a bottom-up analysis,

where physics are initially proposed, and the model is then refined to a higher-order based on the performance of the simpler model. In this case, this takes the form of an initially assumed first-order system. From the performance of this simple model, and from an understanding of fundamental heat transfer phenomena, a second-order model and identification methodology was proposed.

The first-order model was identified by fitting the model's single parameter, UA, to process-cycle data using only the temporal measurements of the cooling air properties and the machine temperature as validation. This model was able to be independent of the machines input, requiring only cooling-air data to be implemented after the model has been identified. Though the effect of reduced cooling on the model could be more easily determined by performing whole process-cycles at reduced cooling loads, performing the model fit and correlating the change to the reduction in air-flow, this would present potentially high risk to the machine, as the extent of the effects of reduced cooling is unknown. As such, an attempt was made to identify the effect of reduced cooling air flow rate during cool-down tests. However, it was determined that higher-order machine dynamics resulted in a very wide parameter spread, (as high as $\pm 47\%$ of the median value) which enveloped any effects of the reduced cooling within the uncertainty. Additionally, due to difficulties in scheduling the reduced flow rate tests in the industrial environment, the flow rate was often not reduced until 15-20 minutes past the onset of cooling, which resulted in errors in the fitting process to these samples.

Using the value of UA which minimized the error for a specific process-cycle, the model was found to predict the temperature of the machine within 2-3 $^{\circ}C$ for most of the machine operation in that process-cycle. However, in situations where the machine recently experienced a temperature-rise, the model under-predicted the temperature, while in situations where the machine recently experienced a drop in

temperature, the model over-predicted. This resulted in maximum errors as high as 8.6 $°C$, suggesting that there was an additional heat transfer path to the cooling air through some large thermal capacitance. However, for practical purposes, the value of UA used was required to be accurate to all-process cycles, and therefore the median of the parameter spread was used in the validation of the model. As the variation in UA was as high as $\pm 10\%$, errors in the generalized first-order model as high as 9.0 $°C$ and average errors as high as 4.3 $°C$ occurred. If a correlation could be made which could account for the variation in UA between the cycles, then this error may be reduced, however the underlying deficiencies in heating and cooling would still be present.

Since the system behaviour in cooling is greatly skewed by higher-order effects when the machine is not at steady state at the start of the cooling period due in particular to additional thermal capacitance, it is not possible to determine the effects of reduced cooling air flow on the convective heat transfer of the machine using the given production data. In order for this modelling technique to be used in a cooling control scheme, controlled testing of the machine would be required, where the machine would be brought to a steady-state operation before the cooling tests began. Alternatively, it could be supposed that the time-constant values which are higher in the spread are more accurate estimations of the overall machine time-constant, as a non-steady-state start reduces the apparent time-constant of the machine. However, this would also require that many more reduced cooling tests be performed at each fan speed in order to develop a similar spread from which the reduced heat transfer coefficient could be estimated.

Using the knowledge that an additional heat transfer path and thermal capacitance term were lacking in the first-order model, an additional lumped-node was added to

the first-order model, resulting in the proposed second-order model. In order to simplify the solution, the second-order model required that the fitting be performed over regions exhibiting simpler dynamics, such as machine cool-downs. Process-cycle data including the machine electrical current was required for use in the heat generation term of the model, which was assumed to be due to Joule-losses only. In the analysis performed on cool-down data, the initial condition that the machine was initially at a steady state temperature distribution had to be assumed. However, as in the first-order model, the lack of the steady-state-start condition was found to skew the estimations downwards. It could be concluded that given a large enough population of cool-down data, an upper-limit to the parameter ranges could be identified allowing for a more accurate estimation of the parameters. As a result, in order to determine the effects of reduced cooling on the parameters, more tests of reduced cooling rate would still be required in order to give a sufficiently large population for the limits of the spread to be determined.

The second-order model performed better for all process-cycles than did the first-order. (With maximum errors as high as 8.6 $^{\circ}C$, and average process-cycle errors of 3.3 $^{\circ}C$) A conclusion drawn from the performance of the second-order model was that non-linearities may exist in heat generation term in the machine, suggesting that core-losses are also significant, though their determination requires additional testing as well as the measurement of machine speed.

Although the first-order model was not found to capture all of the dynamics of the machine, it does provide a very simple method of estimating the machines temperature during operation using only the properties of the cooling air flow, allowing for an extremely inexpensive computation. Furthermore, the system identification process is entirely unintrusive, requiring only a few samples of process-cycle temperature data. With the application of a sufficient factor of safety, (10 $^{\circ}C$) this model could be used

for real-time machine temperature monitoring control.

Though the second-order model performance follows the transient behaviour of the machine more closely, the more complex identification scheme is much more sensitive to the effects of the machine not reaching a steady-state temperature distribution at the onset of testing. Without further cool-down tests that either start with a steady state machine no relationship to reduced cooling-load was possible.

6.2 Future Recomendations

The main objective of this work, the development of a modelling approach that may be used for the on-line temperature monitoring of an DC machine with a reduced-cooling strategy. Unfortunately, a comprehensive model could not be met with the given data as inconsistent test data did not allow for the identification of the effects of reduced cooling on the proposed models. In order to quantify these results by the methods outlined in this work, it is required that cool-down tests at all desired intervals of reduced cooling be performed either more consistently, (allowing the machine to reach a steady-state temperature distribution before the cooling is performed) or more extensively (capturing many more tests at each desired flow-reduction so that the upper limit of the spread, which was determined to be a more accurate estimation of the parameter, may be determined). Additionally, it is required that for the reduced cooling tests, the flow-reduction be applied immediately at the onset of cooling in order to achieve more accurate results, especially in the implementation of the second-order model.

Additional sensors may also serve to improve the model performance. The measurement of the temperatures of larger bodies such as the armature spider which are suspected to contribute much of the additional thermal capacitance and heat transfer

path are recommended. This would help to constrain the analysis by eliminating the need for the steady-state assumption in the identification of the second-order model parameters.

In both models presented, it is important to recall that the critical component, the armature, is considered as a lumped body having a uniform temperature, and as such neither is able to capture the hot-spot phenomenon. In the analysis, only one of the seven armature temperatures was used, channel 3, as it represented the temperature which, on average, was the highest to provide the most consistently conservative estimate of the armature temperature. However, channel 7 was found to exhibit higher random temperature spikes, suggesting that it better represents a potential hot-spot. In the application of either model presented in this work, this limitation should be considered in the application of any factor of safety desired by the user. If the specific location of each of the temperature readings in the armature were known, the armature could potentially be modelled as fully distributed or as several lumped bodies to provide a more accurate model of the armature temperature distribution.

Appendix A

Biot Number Calculations for Select Components

In order to assess the validity of the lumped assumption used in this work, the Biot number, Bi, (equation A.1) was calculated for each significant machine component; the stator, the armature windings, the armature spider, and the shaft. Table A.1 summarizes the assumed material and geometry of the component, as well as the thermal conductivity, k, of the material, and the convective heat transfer coefficient of air taken as 25-250 W/m^2K, which is considered as the typical range for the HTC in forced convection of gasses (24). Table A.2 shows the assumed lengths of the components modelled, and table A.3 shows the calculated surface area, A, and volume, V, as appropriate for the modelled geometry, which were also used to calculate the characteristic length, L_C, and finally the identified range of Bi for each component.

$$Bi = \frac{L_C h}{k}, \qquad L_C = \frac{V}{A} \tag{A.1}$$

From table 4.1, it is evident that the validity of the lumped assumption for the

Table A.1: Assumed component material, heat transfer properties (24), and shape.

Component	**Material**	$k[W/m.K]$	$h[W/m^2.K]$	**Modelled Shape**
Stator	Steel	60.5	25-250	Annulus
Armature Windings	Copper	401	25-250	Annulus
Armature Spider	Steel	60.5	25-250	Annulus
Shaft	Steel	60.5	25-250	Cylinder

Table A.2: Estimated component dimensions.

Component	$L[m]$	$D_o[m]$	$D_i[m]$
Stator	1.25	3.74	2.54
Armature Windings	1.25	2.5	2.25
Armature Spider	1.25	2.25	1.00
Shaft	4.30	1.00	N/A

Table A.3: Calculated geometry Area, volume, characteristic length, and Biot number range.

Component	$A[m^2]$	$V[m^3]$	$L_C[m]$	Bi
Stator	67	29	0.44	0.2 - 1.8
Armature Windings	22	4.7	0.2	0.01 - 0.1
Armature Spider	36	16	0.5	0.2 - 1.8
Shaft	14	3.4	0.3	0.1 - 1.0

components depends upon the true heat transfer coefficient between the cooling air and the component. However, it can also be seen that for the whole range of heat transfer coefficient, the armature windings are within the accepted range of Bi ($Bi < 0.1$) where the lumped assumption is considered valid. For the other components, where $Bi > 0.1$, the lumped assumption will be less accurate.

It is important to note that this analysis is based on simple geometries of the components that were able to be determined with the present knowledge of the system. These geometries do not necessarily accurately reflect the more complex shapes and flow paths present in the machine that would reduce the volume and increase the convective surface area of the components, thus lowering their Biot numbers and potentially rendering the assumption more valid.

Appendix B

First-Order Fitting to Raw vs. Smoothed Data

In section 4.3.2, equation 4.10 is fit to the cool-down samples using data smoothed using the Savitsky-Golay filtering method outlined in section 3.4.2. Though the smoothing of the data may cause errors when a function different from that used in the smoothing is fit to the data, it was found that for this data there is no significant difference in the fitting of equation 4.10 to the smoothed cool-down data. Figure B.1, which plots the motor temperature vs. the elapsed cooling time with the fitting of equation 4.10 to the raw experimental data, where the equation of the fitted curve is presented in the figure, as well as the determined time-constant, $\tau = 1919.0$. Figure B.2 shows the same, but with smoothed data, where the fitted equation and the determined time-constant are identical to those found when the raw data was fit in figure B.1.

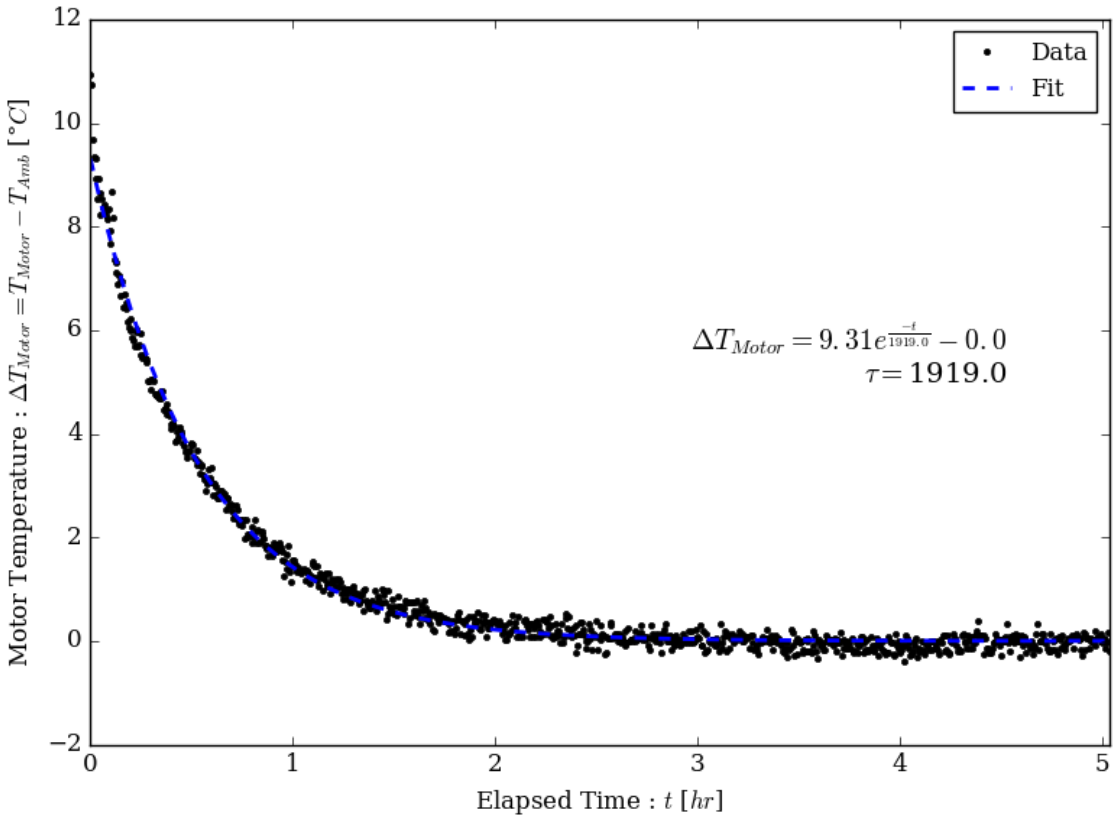

Figure B.1: Motor temperature (channel 3) vs. elapsed cooling time for an example fit of equation 4.10 to a cool-down sample using the raw cool-down data.

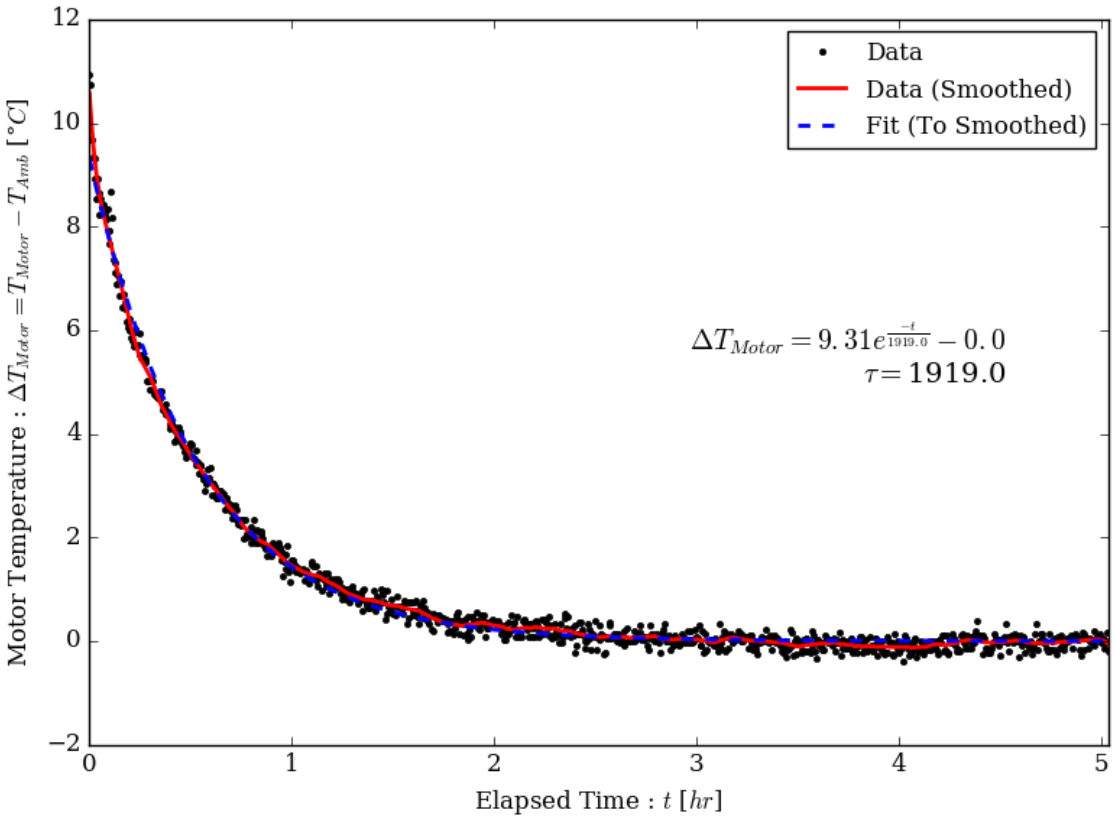

Figure B.2: Motor temperature (channel 3) vs. elapsed cooling time for an example fit of equation 4.10 to a cool-down sample using the smoothed cool-down data.

Appendix C

Second-Order Modelling Analysis

C1 Impacts of the Steady-State-Start Assumption

The efficacy of the steady-state assumption is likely poor, as the extremely dynamic operation of the machine seldom, if ever, truly reaches a steady state condition. However, the effect of a non-steady state condition on the value of the fitted parameters may be easily understood by simulating test data with the given model, to which the same analysis may be applied, both with and without a steady state start condition. To establish a baseline, N cooling tests of random initial armature temperatures were simulated for a system given the parameters found in section 5.3.4 from the upper-limits of the parameter spreads, including the assumption of a steady state start. These parameters are summarized in table C.4.

In order to simulate non-steady-state start conditions, a thermal saturation parameter, γ, was prescribed. This parameter represents how close to the steady-state temperature the thermal sink is relative to the ambient cooling air temperature (lower limit) at the onset of cooling, such that $\gamma = 1$ corresponds to a steady-state start, $\gamma < 1$ corresponds to the case where the thermal sink is cooler than the steady state

Table C.4: Second-order model parameters as determined by initial guesses in SECTION.

Parameter	**Value**
C_{Arm}	10 $[MJ/°C]$
C_{Sink}	100 $[MJ/°C]$
$UA_{Conv,Arm}$	7.6 $[kW/°C]$
UA_{Cond}	7.6 $[kW/°C]$
$UA_{Conv,Arm}$	7.6 $[kW/°]$

case, i.e. the machine was still heating up before the onset of cooling, and $\gamma > 1$ corresponds to the case where the initial sink temperature is higher than the steady state temperature, i.e. the machine originally ran quite hot, but had a second phase of running much cooler before the onset of cooling. The simulated initial thermal sink temperature was then calculated as:

$$T_{Sink_i} = T_{Air,Ave} + \gamma(T_{Sink_{i,SS}} - T_{Air,Ave}) \tag{C.2}$$

Figure C.3 compares the simulated temperatures of the second-order model components for cool-downs where $\gamma = 1$ (solid lines) and $\gamma = 0.5$ (dashed lines), where the component temperatures are plotted against elapsed cooling time. Though the simulated armature temperatures do not vary greatly between the $\gamma = 1$ and $\gamma = 0.5$ cases, the outlet air temperature and the sink temperatures vary more significantly by approximately $2°C$. Figure C.3 shows the heat flows of the second order model, as drawn in figure 5.1, during the cooling of the simulated cool-down shown in figure C.3 for the $\gamma = 1$ (solid lines) and $\gamma = 0.5$ (dashed lines) cases. From this figure, it can be seen that the armature convective and the conductive heat flows are not

significantly affected by the change in γ, however the sink convective heat flow is affected by approximately 10 kW, or about 17% of the maximum sink convective heat flow rate. The effect that the change in γ has when these cool downs are analyzed using the parameter estimation method outlined in section 5.3 is shown in figure C.5, where the estimated capacitances and HTC's of the model, assuming that $\gamma = 1$, are shown by the black circles ($\gamma = 1$) and red squares ($\gamma = 0.5$). It is clear from figure C.5 that when the analyzed data has $\gamma < 1$, the second order model parameters are all under-estimated by the scheme which assumes that $\gamma = 1$.

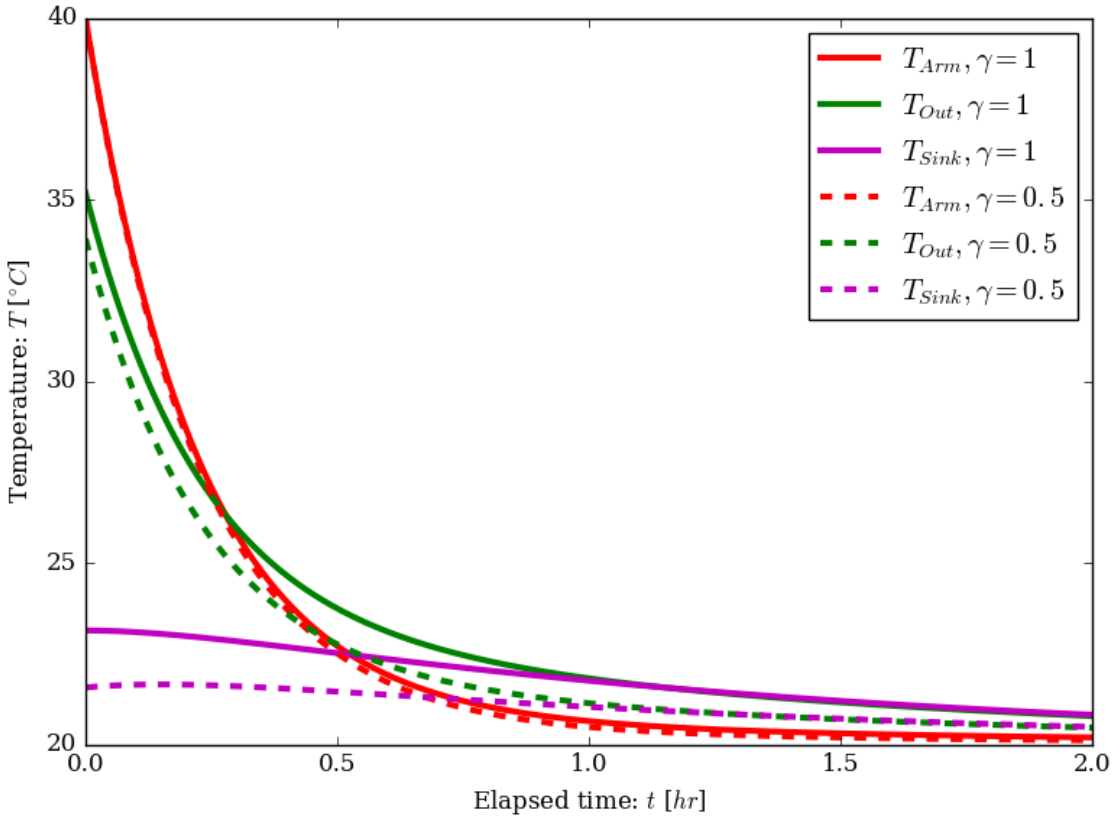

Figure C.3: Plot of temperature vs. elapsed time for simulated cool-downs having $\gamma = 1$ (solid) and $\gamma = 0.5$ (dashed).

These simulated results are extended by generating a large simulated sample of cool-downs, $N = 200$, from the second-order model with both steady state start ($\gamma =$

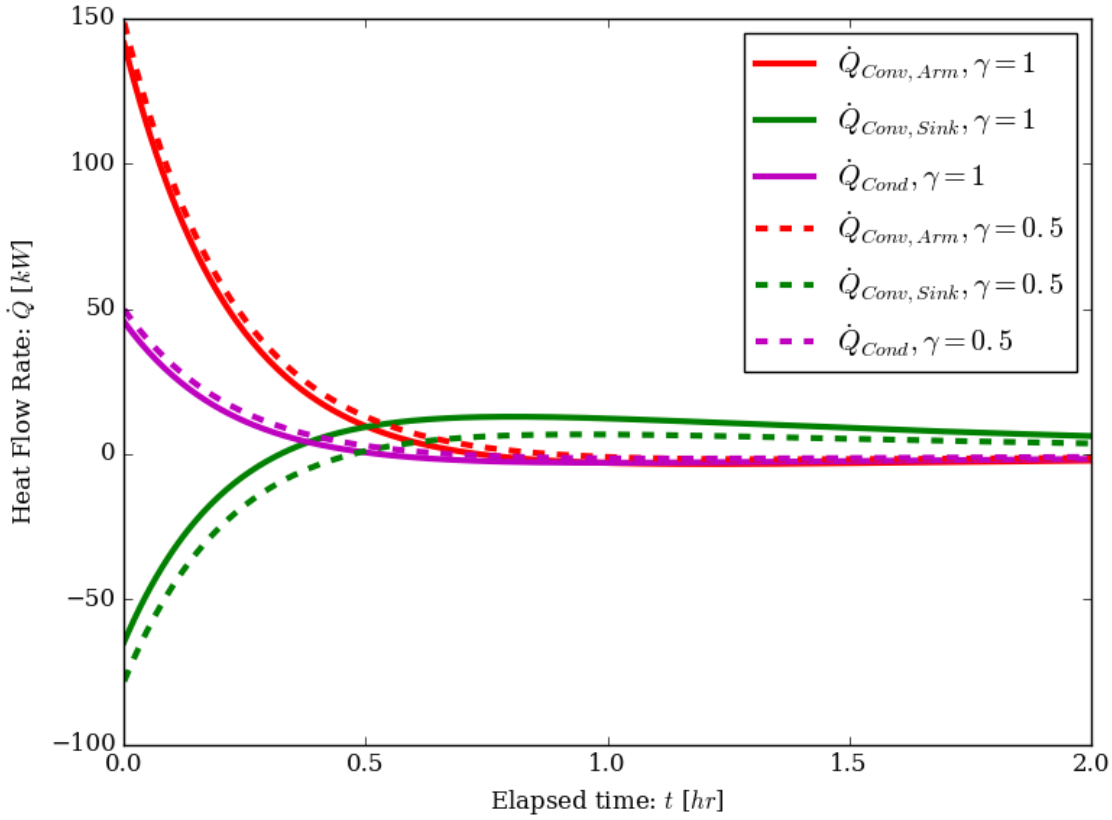

Figure C.4: Plot of heat-flow vs. elapsed time for simulated cool-downs having $\gamma = 1$ (solid) and $\gamma = 0.5$ (dashed).

1) and non-steady state start ($\gamma < 1$) assumptions, and analyzing them in the method outlined in section 5.3, as shown in figures C.6 and C.7 (ss start) and in figures C.8 and C.9 (non-SS start). For the non-steady-state start condition simulations, a value of γ was randomly generated for each sample between 0 and 1. From these figures, it can be seen that when the steady-state-start condition is not met, the variance of each estimated parameter increases, especially in the case of the thermal sink convective HTC and capacitance. It is also of note that the variance does not increase symmetrically, but is entirely downwards with respect to the actual parameter value. As a result, it is concluded that the presence of non-steady-state start conditions in the cooling data is the reason for the parameters determined in section 5.3.4 to have

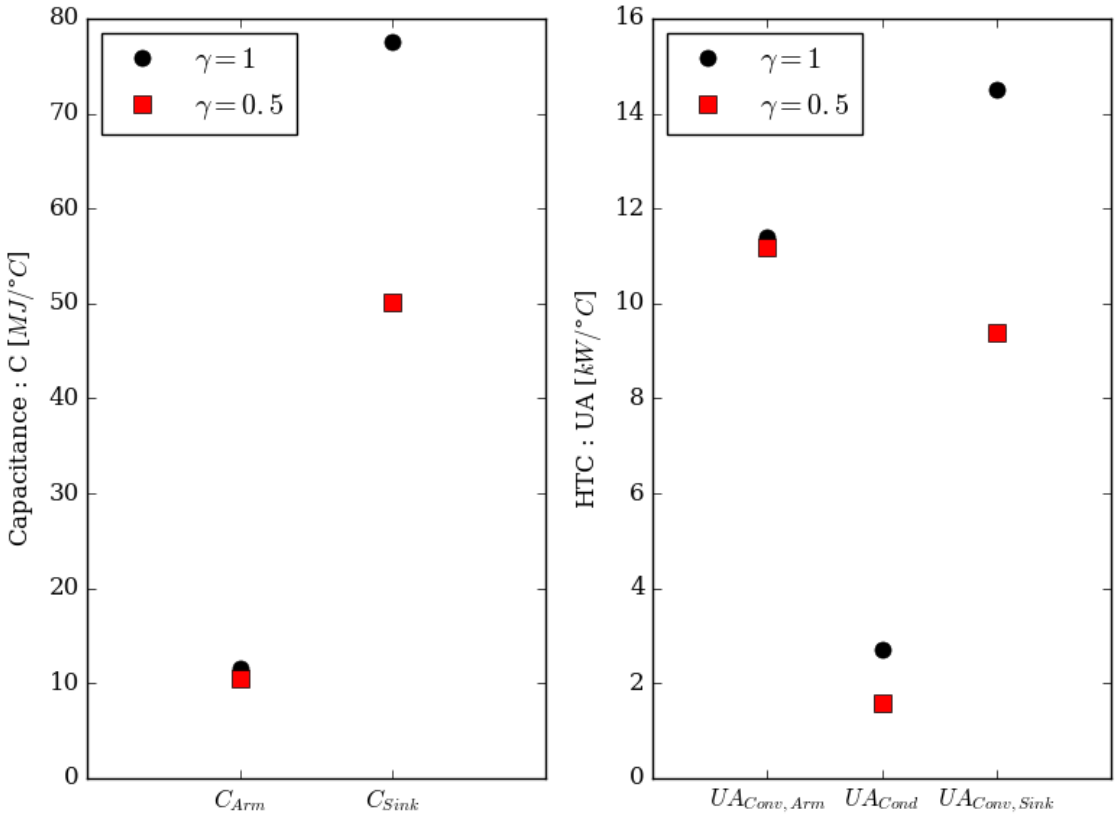

Figure C.5: Second-order capacitances and HTC's found from optimization of second-order model to simulated cool-downs with $\gamma = 1$ (circles) and $\gamma = 0.5$ (squares). For $\gamma = 1$, the values are predicted exactly, while for $\gamma = 0.5$ the values are under-predicted.

a wide variance, and that the better estimation of the parameters true values is the upper limit of the parameter spread.

C2 Second-Order Model Fitting Convergence Behaviour

In performing the fits of the second-order model to the data, it was often found that a single iteration of the process was not enough to achieve acceptable levels of error,

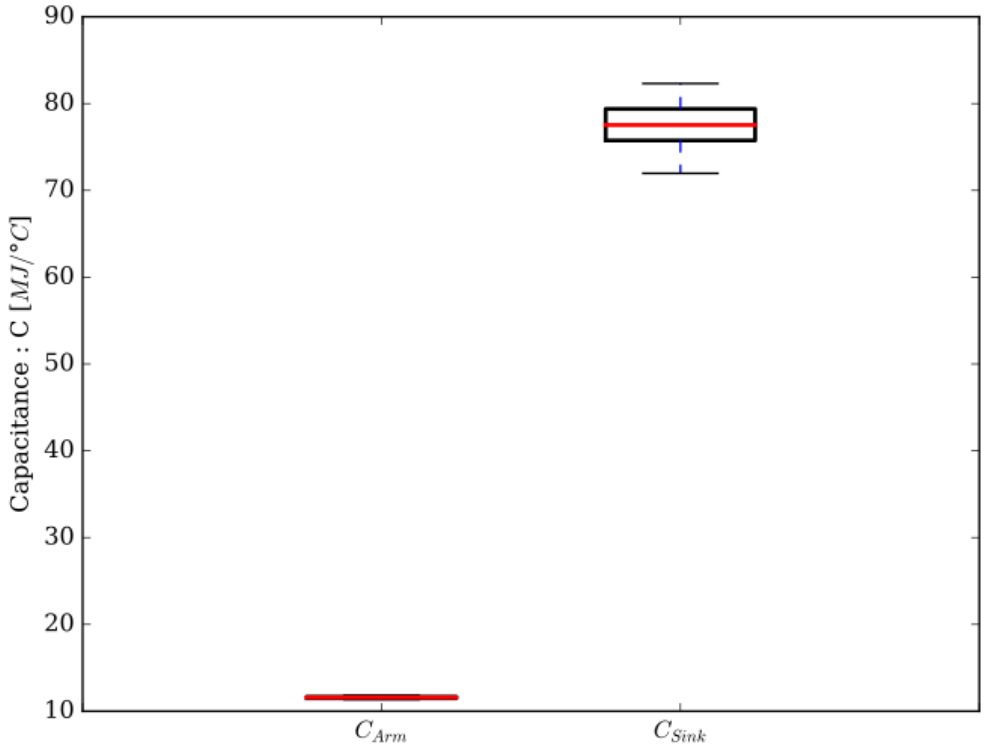

Figure C.6: Second-order capacitances found from optimization of second-order model to simulated cool-downs with the steady-state start assumption. Boxplots are used to visually represent the spread of the data.

so the algorithm was set to iterate several times in an attempt to force convergence. Very mixed results were observed: in some cases the fit improved monotonically, while in others the error fluctuated through the iterations or grew even larger. This is believed to be the result of a wavy solution space to the objective function, where many local minima exist, thus when the algorithm attempts to minimize the error, it may become stuck in these local minima, and un-stuck by numerical errors. Because of this, the parameters determined in the iteration with the least error in the objective function was chosen as the final fit parameter for that sample. Though this increased computational costs, it was found to be the best method of insuring that good fits to

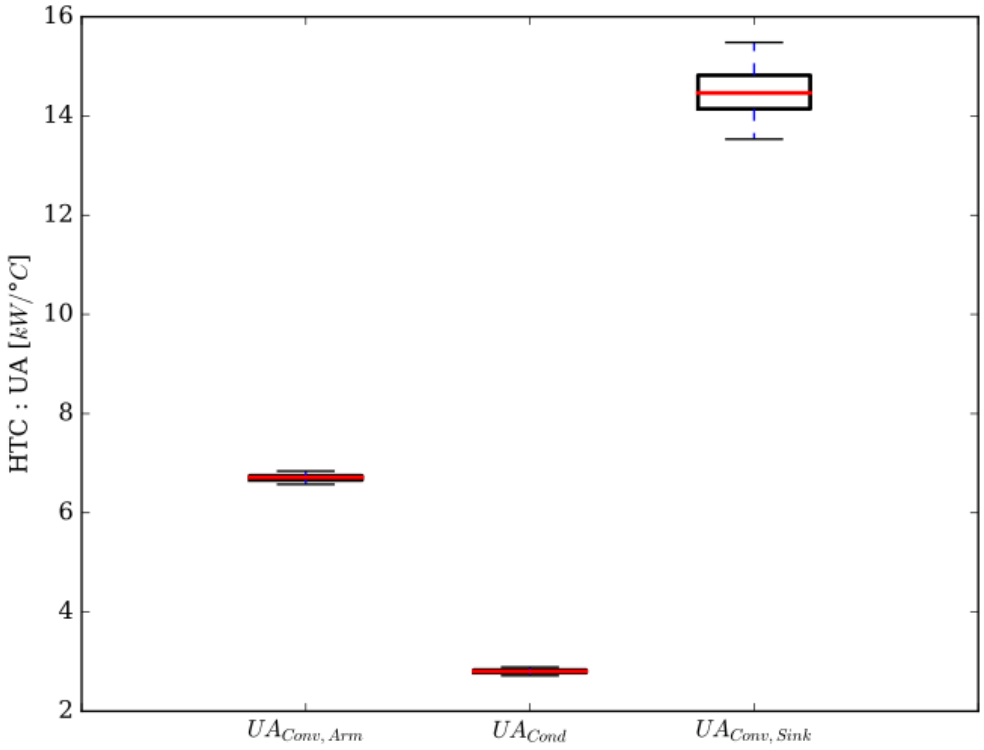

Figure C.7: Second-order HTC's found from optimization of second-order model to simulated cool-downs with the steady-state start assumption. Boxplots are used to visually represent the spread of the data.

the data were achieved.

Figure C.10 and C.11 show the convergence behaviour of the iteration of the algorithm for sample cool-downs from the data, plotting the maximum error in the fit against the iteration number. These convergence plots refer specifically to the fits of the cool-downs as shown in figure C.12 and C.13, respectively.

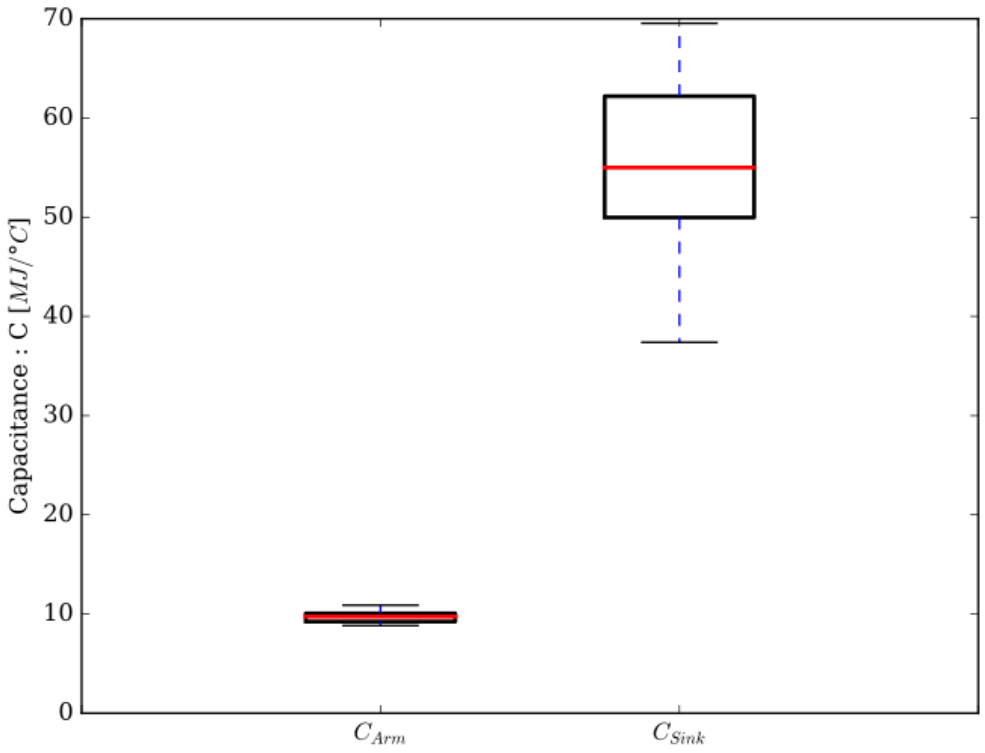

Figure C.8: Second-order capacitances found from optimization of second-order model to simulated cool-downs without the steady-state start assumption. Boxplots are used to visually represent the spread of the data.

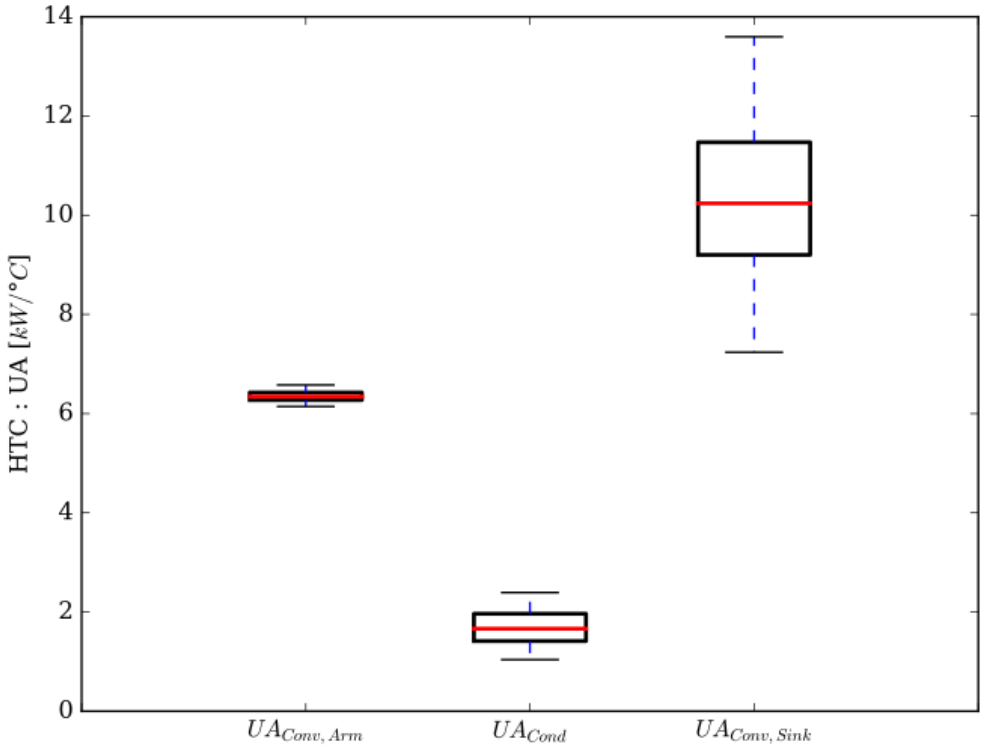

Figure C.9: Second-order HTC's found from optimization of second-order model to simulated cool-downs without the steady-state start assumption. Boxplots are used to visually represent the spread of the data.

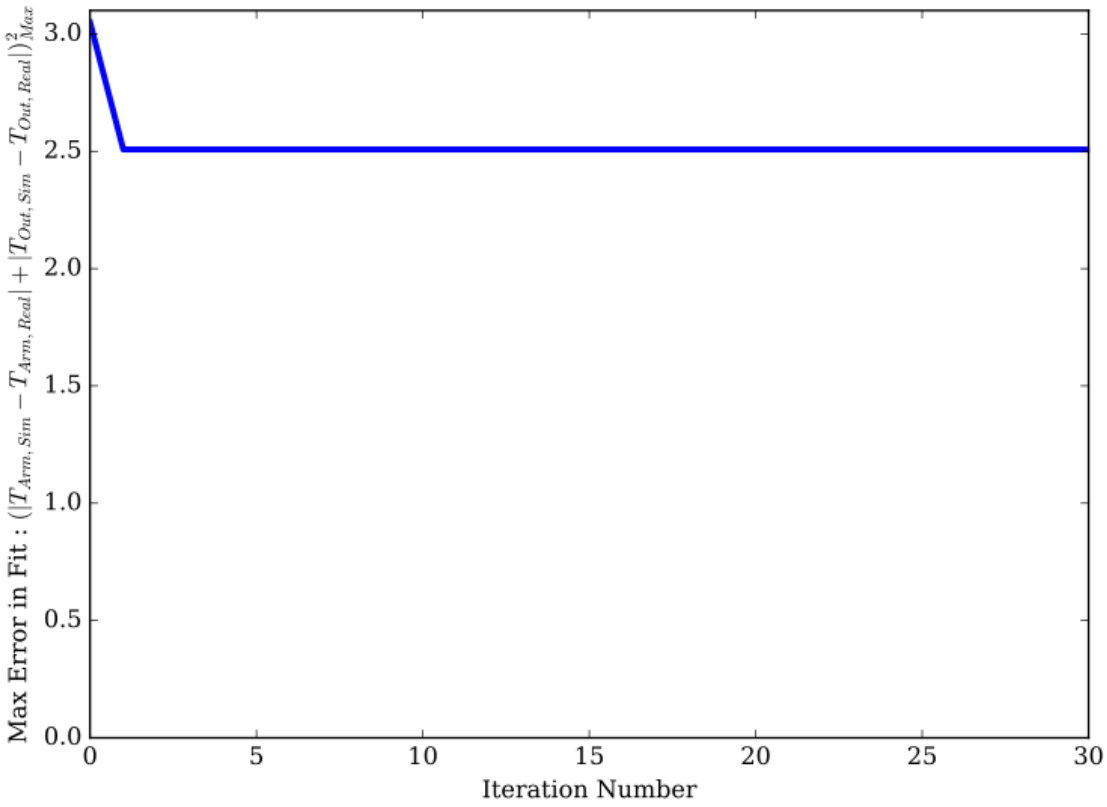

Figure C.10: Second-order model fit convergence behaviour for a sample cool-down (figure C.12) where no further improvement is achieved after the first iteration of the optimization algorithm.

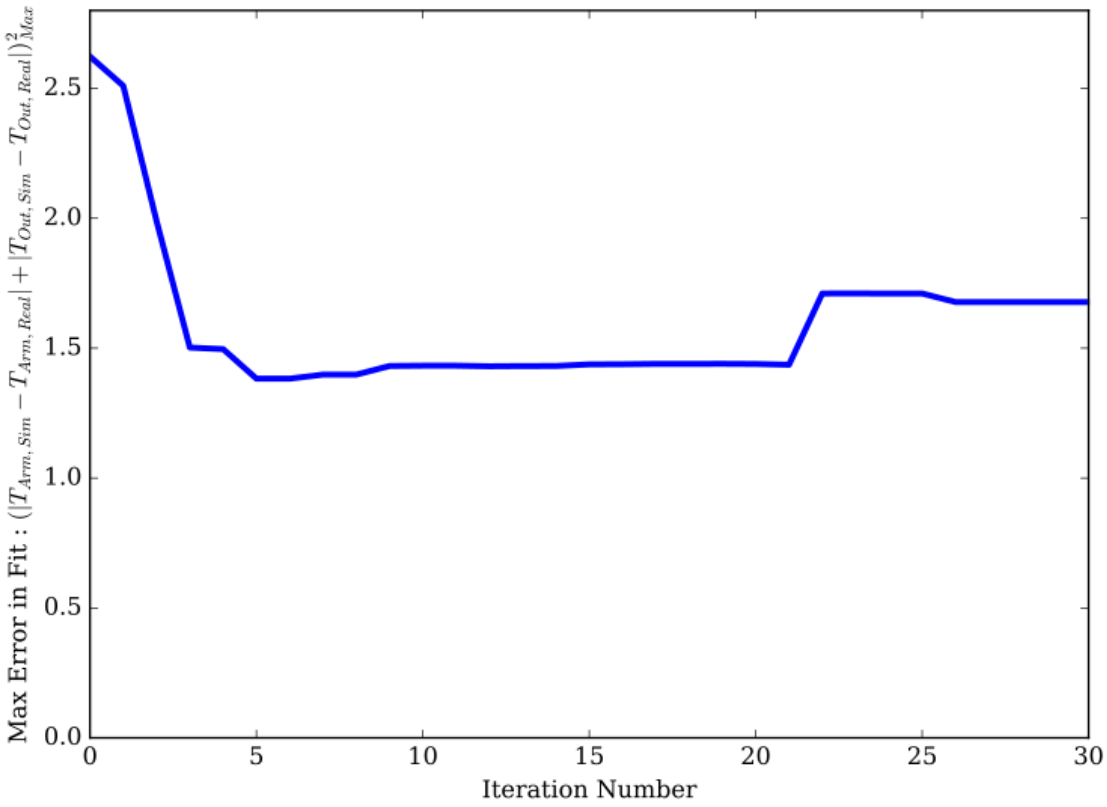

Figure C.11: Second-order model fit to a sample cool-down (figure C.13) where the fit improves, initially, with additional algorithm iterations. The sudden increase in error suggests that the solution is not stable.

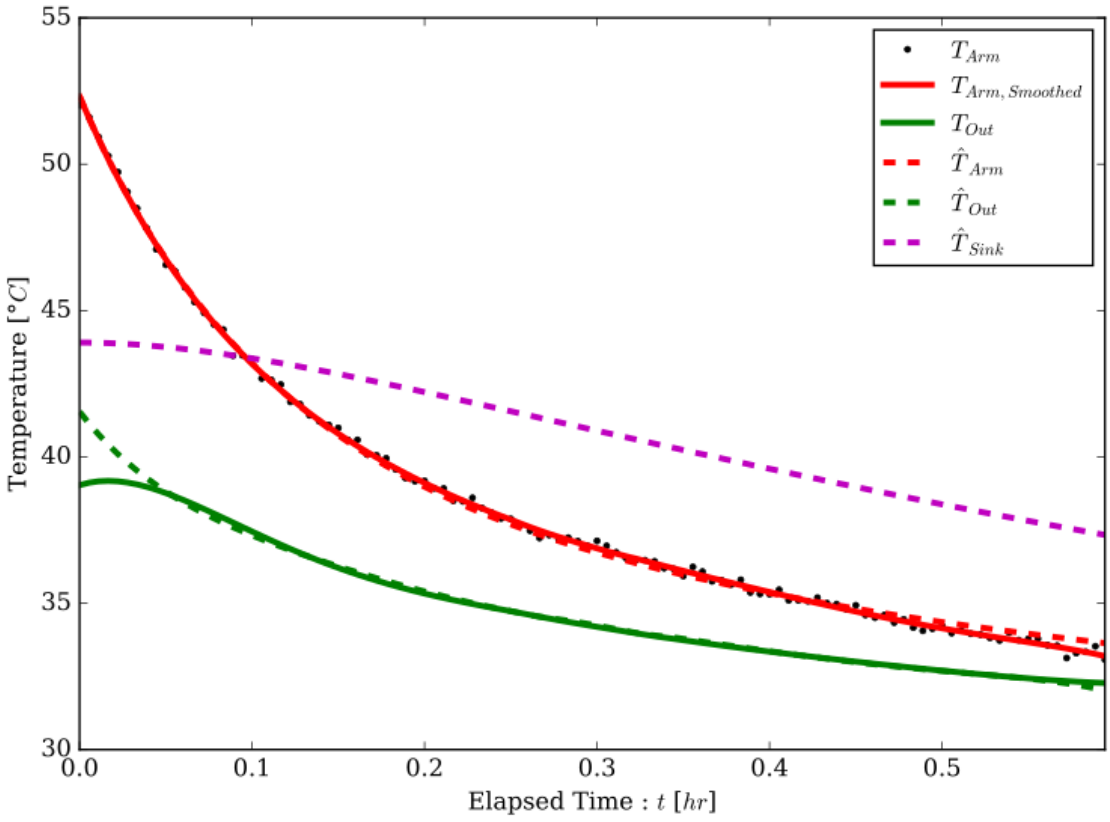

Figure C.12: Second-order model fit to a sample cool-down. Convergence behaviour for this fit is shown in figure C.10

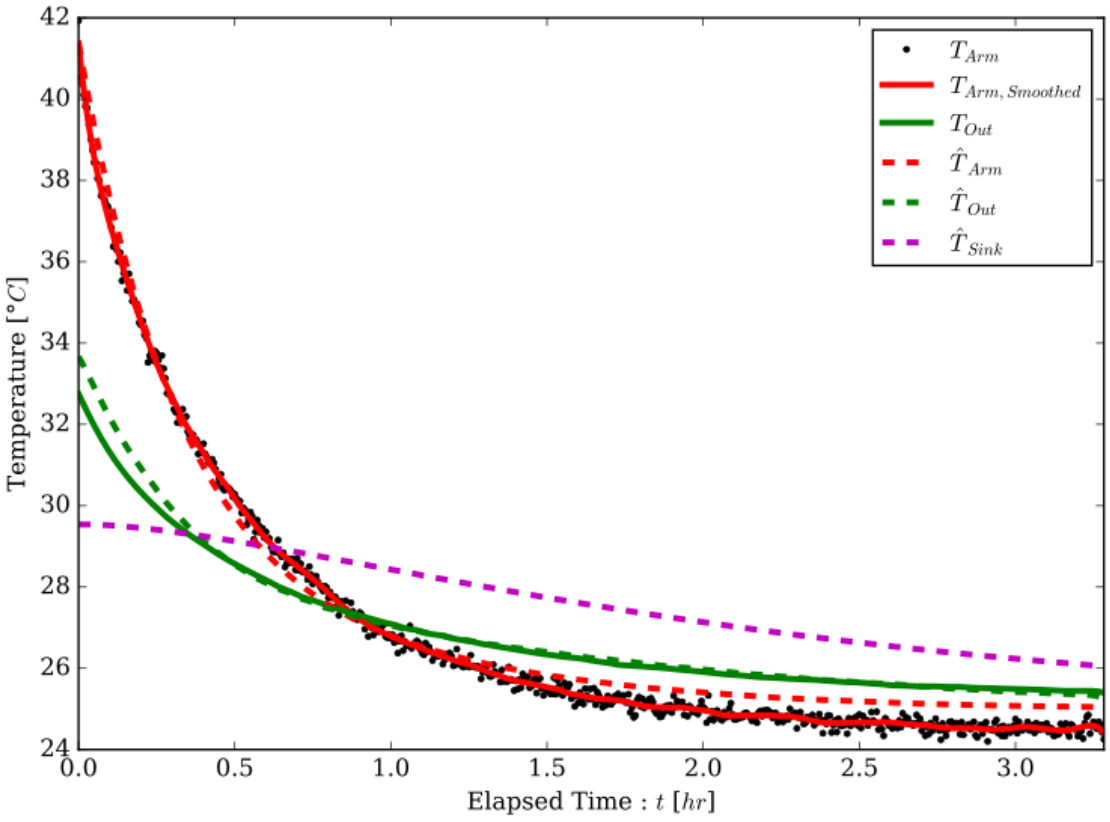

Figure C.13: Second-order model fit to a sample cool-down. Convergence behaviour for this fit is shown in figure C.11

Bibliography

[1] "Technical Paper on the Federal Carbon Pricing Backstop," *Environment and Climate Change Canada*, p. 26, 2017.

[2] A. Morrow, "Why does Ontario's electricity cost so much? A reality check," 2017. [Online]. Available: https://www.theglobeandmail.com/news/national/why-does-electricity-cost-so-much-in-ontario/article33453270/ [Accessed: 2018-11-04]

[3] StatsCAN, "CANSIM." [Online]. Available: http://www5.statcan.gc.ca/cansim/a01?lang=eng [Accessed: 2018-05-04]

[4] I. Nishimura, "Trends in Electricity Conservation Measures: Focusing on Responses by Industry Groups and Companies," *Japan Labor Review*, vol. 9, no. 4, pp. 22–41, 2012.

[5] A. T. de Almeida, P. Fonseca, and P. Bertoldi, "Energy-efficient motor systems in the industrial and in the services sectors in the European Union: Characterisation, potentials, barriers and policies," *Energy*, vol. 28, no. 7, pp. 673–690, 2003.

[6] TMEIC, "Metals Industry Energy Savings," Toshiba Mitsubishi-Electric Industrial Systems Corporation, Tech. Rep., 2011.

[7] "Variable frequency drives: Energy efficiency reference guide," CEATI International, Tech. Rep., 2009.

[8] "Defining Ontario's Typical Electricity Customer (EB-2016-0153)," Ontario Energy Board, Tech. Rep., 2016.

[9] T. Macnair, "Industry 4.0 is here: What are we doing about it?" 2018. [Online]. Available: http://usa.arcelormittal.com/news-and-media/blog/2018/jan/01-22-2017 [Accessed: 2018-11-04]

[10] S. J. Chapman, *Electric Machinery Fundamentals*, 3rd ed. McGraw Hill Companies, 1998.

[11] H. A. Toliyat and G. B. Kliman, "Handbook of Electric Motors," in *Handbook of Electrical Motors*, 2nd ed. New York: Marcel Dekker, 2004, p. 850.

[12] W. Pawlus, J. T. Birkeland, H. Van Khang, and M. R. Hansen, "Identification and Experimental Validation of an Induction Motor Thermal Model for Improved Drivetrain Design," *IEEE Transactions on Industry Applications*, vol. 53, no. 5, pp. 4288–4297, 2017.

[13] D. R. Boothman, E. C. Elgar, R. H. Rehder, and R. J. Woodall, "Thermal Tracking - A Rational Approach to Motor Protection," *IEEE Transactions on Power Engineering Systems*, pp. 1335–1344, 1974.

[14] P. H. Mellor and D. R. Turner, "Real Time Prediction of Temperatures in an Induction Motor Using a Microprocessor," *Electric Machines & Power Systems*, vol. 15, no. 4-5, pp. 333–352, 1988.

[15] C. Wang, H. Liu, X. Liu, X. Zhang, and Z. Chen, "A Sensor-less Method for Online Thermal Monitoring of Switched Reluctance Machine," *18th International*

Conference on Electrical Machines and Systems (ICEMS), 2015, pp. 1709–1715, 2015.

[16] A. M. U. Emadi, *Advanced Electric Drive Vehicles*. CRC Press, 2015.

[17] *IEEE Standard Test Procedure for Polyphase Induction Motors and*. IEEE Machinery Committee, 2004, vol. 2004, no. November.

[18] J. Puranen, "Induction Motor versus Permanent Magnet Synchronous Motor in Motion Control," Ph.D. dissertation, Lappeenranta University of Technology, 2006.

[19] M. S. Rajagopal, "Transient Thermal Analysis of Induction Motors," *IEEE Transactions on Energy Conversion*, vol. 13, no. 1, pp. 62–69, 1998.

[20] D. Biswas, M. Ishizuka, and H. Iwasaki, "Three-dimensional thermo fluid analysis of large scale electric motor," *International Journal of Rotating Machinery*, vol. 6, no. 6, pp. 433–444, 2000.

[21] J. F. Trigeol, Y. Bertin, and P. Lagonotte, "Thermal modeling of an induction machine through the association of two numerical approaches," *IEEE Transactions on Energy Conversion*, vol. 21, no. 2, pp. 314–323, 2006.

[22] Z. Rehman and K. Seong, "Three-D numerical thermal analysis of electric motor with cooling jacket," *Energies*, vol. 11, no. 1, 2018.

[23] D. A. Staton, "Thermal computer aided design-advancing the revolution in compact motors," in *IEMDC 2001 - IEEE International Electric Machines and Drives Conference*, Cambridge, Massachusetts, 2001, pp. 858–863.

[24] F. P. Incropera, T. L. Bergman, A. S. Lavine, and D. P. DeWitt, *Fundamentals of Heat and Mass Transfer*, 7th ed. John Wiley & Sons, Inc., 2011.

[25] S. Noodleman and B. R. Patel, "Duty Cycle Characteristics for DC Servo Motors," *IEEE Transactions on Industry Applications*, vol. IA-9, no. 5, 1973.

[26] W. Pawlus, J. T. Birkeland, H. Van Khang, and M. R. Hansen, "Identification and Experimental Validation of an Induction Motor Thermal Model for Improved Drivetrain Design," *IEEE Transactions on Industry Applications*, vol. 53, no. 5, pp. 4288–4297, 2017.

[27] B. Venkataraman, B. G. Black, V. Corporation, and W. P. Ge, "Fundamentals of a Motor Thermal Model and Its Applications in Motor Protection," *Motor Thermal Model Protection Applications*, pp. 127–144, 2005.

[28] Z. Gao, "Sensorless Stator Winding Temperature Estimation for Induction Machines," Ph.D. dissertation, Georgia Institute of Technology, 2006.

[29] J. Moreno, F. Hidalgo, and M. Martinez, "Realisation of tests to determine the parameters of the thermal model of an induction machine," *IEE Proceedings - Electric Power Applications*, vol. 148, p. 393, 2001.

[30] P. Milanfar, "Failure monitoring in small permanent-magnet synchronous motors," Ph.D. dissertation, University of California at Berkeley, 1988.

[31] P. Milanfar and J. H. Lang, "Monitoring the thermal condition of permanent-magnet synchronous motors," pp. 1421–1429, 1996.

[32] A. Boglietti, E. Carpaneto, M. Cossale, and S. Vaschetto, "Stator-Winding Thermal Models for Short-Time Thermal Transients: Definition and Validation," *IEEE Transactions on Industrial Electronics*, vol. 63, no. 5, pp. 2713–2721, 2016.

[33] I. J. Perez and J. G. Kassakian, "A stationary thermal model for smooth air-gap

rotating electric machines," *Electric Machines and Power Systems*, vol. 3, no. 3-4, pp. 285–303, 1979.

[34] a. Boglietti, a. Cavagnino, M. Lazzari, and a. Pastorelli, "A simplified thermal model for variable speed self cooled industrial induction motor," *Conference Record of the 2002 IEEE Industry Applications Conference. 37th IAS Annual Meeting (Cat. No.02CH37344)*, vol. 2, no. 4, pp. 945–952, 2002.

[35] A. Boglietti, A. Cavagnino, and D. Staton, "TEFC induction motors thermal models: a parameter sensitivity analysis," in *Conference Record of the 2004 IEEE Industry Applications Conference, 2004. 39th IAS Annual Meeting.*, vol. 4, no. 3, Seattle, WA, 2005, pp. 2469–2476.

[36] A. Boglietti, S. Member, A. Cavagnino, and D. Staton, "Machine Thermal Models," *IEEE Transactions on Industry Applications*, vol. 44, no. 4, pp. 1150–1159, 2008.

[37] A. Boglietti, A. Cavagnino, D. Staton, M. Shanel, M. Mueller, and C. Mejuto, "Evolution and modern approaches for thermal analysis of electrical machines," *IEEE Transactions on Industrial Electronics*, vol. 56, no. 3, pp. 871–882, 2009.

[38] "DC Motor Brush Life White Paper." [Online]. Available: http://industrialelectricalco.com/wp-content/uploads/2014/01/DC-Motor-Brush-Life-White-Paper.pdf [Accessed: 2018-04-13]

[39] I. Bell, J. Wronski, S. Quoilin, and V. Lemort, "Pure and Pseudo-pure Fluid Thermophysical Property Evaluation and the Open-Source Thermophysical Property Library CoolProp," pp. 2498–2508, 2014. [Online]. Available: http://pubs.acs.org/doi/abs/10.1021/ie4033999http://www.coolprop.org/ [Accessed: 2018-04-13]

[40] M. Newville, T. Stensitzki, D. B. Allen, and A. Ingargiola, "LMFIT: Non-Linear Least-Square Minimization and Curve-Fitting for Python¶," sep 2014. [Online]. Available: https://zenodo.org/record/11813 [Accessed: 2018-04-09]